The Assimilation of Infrared Satellite Radiances into a Limited-Area NWP Model

DISSERTATION

zur Erlangung des akademischen Grades eines
Doktors der Naturwissenschaften
am Fachbereich für Geowissenschaften
der Freien Universität Berlin

vorgelegt von

MARTIN STENGEL

Berlin, Januar 2011

1. Gutachter: Prof. Dr. Jürgen Fischer

2. Gutachter: Prof. Dr. Ralf Bennartz

Tag der Disputation: 27. Mai 2011

Selbstständigkeitserklärung

Hiermit erkläre ich, Martin Stengel, an Eides Statt, dass ich die vorliegende Arbeit selbstständig und ohne fremde Hilfe angefertigt, keine anderen als die angegebenen Quellen und Hilfsmittel benutzt und die den benutzten Quellen wörtlich oder inhaltlich entnommenen Stellen als solche kenntlich gemacht habe. Diese Arbeit hat in gleicher oder ähnlicher Form noch keiner Prüfungsbehörde vorgelegen.

Berlin, 17.01.2011

Abstract

The potential benefit of geostationary satellite radiance observations, taken in clear-sky and cloudy atmospheric conditions, on the analysis and forecast accuracy of a numerical weather prediction (NWP) model was investigated. The NWP model used is the High Resolution Limited Area Model (HIRLAM) which provides with its state-of-the-art four-dimensional variational data assimilation (4D-Var) scheme an optimal framework to exploit spatio-temporal highly resolved geostationary infrared radiance observations such as measured by the Spinning Enhanced Visible and InfraRed Imager (SEVIRI) on-board the METEOSAT Second Generation satellite series.

In the framework of this work the assimilation scheme has firstly been modified to enable the SEVIRI radiance observations being used as additional observation type, and secondly, it has been equipped with a observation operator for satellite radiances particularly designed for those radiances significantly affected by clouds. For the latter, a simplified moist physics scheme was implemented to diagnose the cloudiness from the NWP background state valid at the time of the observation. Sophisticated observation screening procedures have additionally been developed and implemented to provide both the identification of cloud-unaffected radiances in clear-sky regions and low-level cloud regimes, and the identification of usable cloud-affected radiances by matching of modelled and observed cloudiness.

Further, the developed extended assimilation scheme has been tested and evaluated in various comprehensive assimilation and forecast experiments. The forecast accuracy was assessed by comparison with standard conventional observations, which were valid at the same time, as reference. The geostationary satellite observations in clear-sky regions were found to have a small positive impact on the HIRLAM forecast accuracy, in particular on the upper air values of temperature, relative humidity, geopotential height and wind. Adding radiance observations in the presence of low-level clouds further improves the accuracy mostly for geopotential height and precipitation. Cloud-affected radiances assimilated on top of the clear-sky radiances also alter the analysis fields. Corresponding forecasts were characterized by improvements in the mid and upper troposphere. Minor, but visible degradations for temperature and humidity forecasts were found in the lower troposphere. Overall, the impact of assimilated cloud-affected radiances on the forecast quality, given the described framework, is judged to be slightly positive.

The results clearly indicate the positive impact that geostationary satellite observations of SEVIRI-like instruments can have on the accuracy of a limited-area NWP model with the given framework. In particular the inclusion of the time dimension in the 4D-Var system might be the key to fully explore such high-frequent satellite observations. The developed framework further provides a tool to employ satellite observations, also from other sensors, in nearly all atmospheric conditions. The full potential will be revealed when applied on global scale.

Zusammenfassung

Der potentielle Einfluss von geostationären Satellitenbeobachtungen in unbewölkten und bewölkten Beobachtungsszenen auf die Qualität der Analyse und Vorhersage eines Modells zur numerischen Wettervorhersage (NWV) wurde untersucht. Benutzt wurde das *High Resolution Limited Area Model* (HIRLAM), das mit seinem modernen vier-dimensionalen variationellen (4D-Var) Assimilationsschema einen optimalen Rahmen bietet, um die Benutzung räumlich und zeitlich hochaufgelöster geostationärer Infrarot-Strahldichtemessungen zu untersuchen. Diese werden z.B. mit dem *Spinning Enhanced Visible and InfraRed Imager* (SEVIRI), welches auf den METEOSAT *Second Generation* Satelliten installiert ist, gemessen.

Im Rahmen dieser Arbeit wurde das Assimilationsschema zunächst so modifiziert, dass geostationäre Strahldichtemessungen als weiterer Observationstyp benutzt werden können. Zweitens wurde das Schema mit einem Observationsoperator ausgestattet, der speziell für solche Messungen entwickelt wurde, die signifikant von Wolken beeinflusst sind. Dafür wurde ein spezielles, vereinfachtes Wolkenschema in den Observationsoperator eingebunden, um die Bewölkung anhand der NWV-Felder zu diagnostizieren. Dieser erweiterte Operator wurde detailliert hinsichtlich der realistischen Modellierung von Bewölkung und hinsichtlich seiner Linearität im Strahldichteraum getestet. Zusätzlich wurden spezielle Observationsfilterprozeduren definiert und implementiert, sodass erstens eine Identifikation von wolken-unbeeinflussten Strahldichten in Gebieten mit keiner oder mit tiefer Bewölkung erfolgen kann, und zweitens eine Identifikation von geeigneten wolkenbeeinflussten Strahldichten durch einen zusätzlichen Abgleich von beobachteter und modellierter Bewölkung möglich ist.

Das erweiterte Assimilationsschema wurde in verschiedenen Vorhersageexperimenten getestet und evaluiert. Die Vorhersagegenauigkeit wurde durch Vergleiche mit konventionellen Observationen, die als Referenz dienten, ermittelt. Es wurde gezeigt, dass die Satellitenobservationen in wolkenfreien Regionen einen kleinen positiven Effekt auf die Genauigkeit der HIRLAM-Prognosen haben, insbesondere auf Temperatur, Relative Feuchte, geopotentielle Höhe und Wind in den troposphärischen Schichten. Die zusätzliche Benutzung von Strahldichten aus Gebieten mit tiefer Bewölkung führt zu einer weiteren Verbesserung der Genauigkeit, speziell für geopotentielle Höhe und Niederschlag. Der Effekt von zusätzlich assimilierten wolkenbeeinflussten Observationen wird insgesamt

ebenfalls positiv beurteilt. Während ein leichter negativer Effekt auf de Genauigkeit der Vorhersage der atmosphärischen Parametern in den unteren troposphärischen Schichten festgestellt wurde, zeigte sich in der mittleren und oberen Troposphäre eine deutliche Verbesserung der Vorhersagegenauigkeit.

Diese Resultate unterstreichen, dass SEVIRI oder ähnliche geostationäre Satelliteninstrumente im Allgemeinen Potenzial besitzen, die Analyse- und Vorhersagegenauigkeit von numerischen Wettervorhersagemodellen zu verbessern. Insbesondere unterstützt das Einbeziehen der zeitlichen Entwicklung atmophärischer Prozesse in 4D-Var-Schemen die Nutzung der zeitlich und räumich hochaufgelösten geostationären Satellitedaten. Zusätzliche Entwicklungsarbeit ist jedoch nötig, um die Assimilationsmethoden und die Verwendung von Satellitendaten, speziell in bewölkten Regionen, weiter zu verbessern.

Contents

1 Introduction

Numerical weather prediction (NWP) models are in general believed to be the best source of reliable information about the development of weather-related atmospheric processes for forecast ranges of a few hours to numerous days. The forecast quality of NWP systems has significantly been improved during the last decades. This has been achieved firstly by the more accurate physical description of atmospheric processes in the analysis and forecast systems, which has partly been enabled by increased computational performances. Secondly, the initial atmospheric state can nowadays be described much more accurately due to a multiplication of available meteorological observations and due to the developed sophisticated analysis techniques, which are able to more effectively incorporate these new observations. A common and very successful analysis technique to assimilate the observations is based on the so-called variational approach (section 1.1), which is the basis for further research at many weather centres all over the world nowadays.

The initial atmospheric state in NWP systems can be seen as a three-dimensional analysis of variables affecting weather-related atmospheric processes. A commonly used set of variables for describing this state includes temperature, moisture, the wind components (or other variables describing the dynamical fields), and surface pressure. The choice of this subset is done with respect to their importance - more parameters lead to more computational cost - and with respect to the feasibility to analyse these. The latter is strongly dependent on available observations containing a signal of specific atmospheric parameters and a proper background estimate of these. Furthermore, the variational approach is based on Gaussian error characteristics of an unbiased background. Thus, significant violations of this assumption will lead to an sub-optimal analysis.

Typical values of the spatial resolution of NWP systems, including their analysis systems, are 5 to 25 km in the horizontal and 40 to 100 vertical levels spanning levels from the Earth's surface and atmospheric levels with pressures of a few hPa or less. The horizontal resolution during the analysis is often reduced by a factor of 2 to 3. These properties are limited by the computational cost higher resolution is causing. Thus, increasing available computer power has lead to increased spatial resolutions in the NWP models.

As mentioned above, the number of available meteorological observations has amplified a lot. While the number of conventional observations, such as reported from SYNOP and Radiosonde stations, has been more or less constant in the last decades, the number

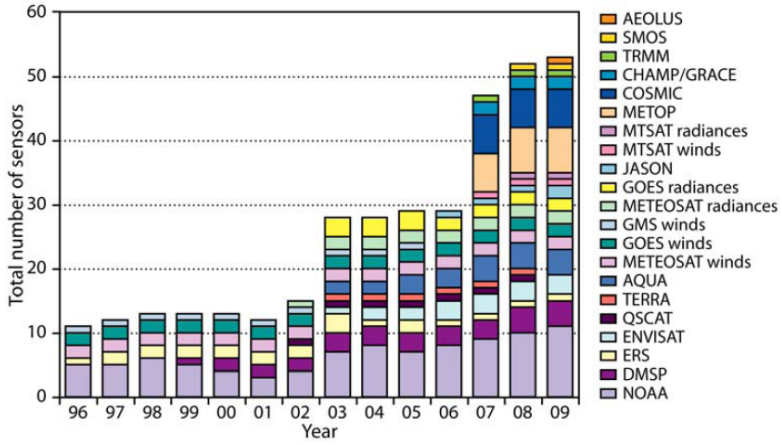

Figure 1.1: Number of satellite sensors with meteorological observations which have been operationally assimilated in the global model of the ECMWF (Kelly and Thépaut, 2007)

of available observations from meteorological satellites has increased significantly. As a consequence, and after successful assimilation experiments (e.g. Andersson et al., 1994), the assimilation of satellite observations has become operational at many weather centres and their numbers have increased dramatically (Figure 1.1). These observations are so-called top-of-atmosphere (TOA) radiances which are defined as "the flux (measured on a surface normal to the beam) per unit solid angle travelling in a particular direction" (Petty, 2004), where the term flux refers to the flux of radiation. On the other hand, the term radiance is often also used for brightness temperature, which is the temperature a body with an emissivity of 1 must have to emit the measured radiance.

Depending on the satellite instrument, the observations are taken in different parts of the electro-magnetic spectrum, thus contain informations about different atmospheric properties. While the emphasis in NWP systems is still placed on radiances measured on polar-orbiting instruments, due to their extended vertical sounding capabilities, geo-stationary radiances, which are especially characterized by a high spatial and temporal resolution, have also been included into NWP systems in the recent past (e.g. Köpken et al., 2004; Szyndel et al., 2005).

Considering instruments measuring radiation in the infrared, the main focus has been placed on clear radiances, i.e. radiances which can be assumed to be unaffected by any clouds, while cloud-affected radiances have almost been completely rejected from the assimilation process. However, the utilization of clear radiances only is a major under-exploitation of the very-high-cost satellite instruments, and has the potential to bias the atmospheric analysis towards specific atmospheric condition which are characterized by clear sky (McNally, 2002). Further, there is a strong indication that cloudy areas are meteorologically sensitive areas in nature as well as in the model. Supporting the

atmospheric analysis by additional observations in these regions will limit corresponding forecast-error growth.

1.1 Variational data assimilation in NWP systems

The variational approach is the most commonly used approach in NWP assimilation systems nowadays. Such systems analysing the three-dimensional atmospheric state have been implemented in global NWP models for example at ECMWF (Courtier et al., 1998), UK MetOffice (Lorenc et al., 2000), Environment Canada (Gauthier et al., 1999), Japan (Takeuchi and Tsuyuki, 2002). The variational approach is based on the minimization of the so-called *cost function* (Equation 1.1). This function measures the distance of a certain atmospheric state $\mathbf{x}$, defined by specific atmospheric parameters at all horizontal and vertical grid points (also called: *state vector* or *control vector*), firstly to the temporarily collocated observations (J^o term), and secondly to an a-priori provided estimation of the atmospheric state, which is usually referred to as background (J^b term). The cost function is often complemented by an initialisation part which is formulated as a weak digital filter constraint.

$$J = J^o + J^b \tag{1.1}$$

$$J^o = \frac{1}{2}(\mathbf{y} - H(\mathbf{x}))^T \mathbf{R}^{-1} (\mathbf{y} - H(\mathbf{x})) \tag{1.2}$$

$$J^b = \frac{1}{2}(\mathbf{x} - \mathbf{x}_0)^T \mathbf{B}^{-1} (\mathbf{x} - \mathbf{x}_0) \tag{1.3}$$

$\mathbf{x}_0$ in the J^b term (Equation 1.3) is the background state, which is usually provided by the forecast data based on the previous analysis cycle, which is valid at the same time as the analysis to be done. $\mathbf{B}$ and $\mathbf{R}$ are the error covariance matrices for the background and the observations, respectively. The observational part of the cost function (Equation 1.2), is defined in observation space. This is, in case of a satellite measurements, the radiance (or brightness temperature) space. To express the distance of the state vector to these observations, collocated profiles of those state vector parameter, that influence the radiative transfer (RT) calculation, have to be transferred into radiance space. This is done by radiative transfer models (in this context often called: forward operator or observation operator H), which is described in more detail in section 1.5.

In four-dimensional variational data assimilation (4D-Var) frameworks the state vector is not only considered at one point in time but at several, each with a certain time window

(observation window) of representativeness. The entire window which is spanned by all observation windows is usually called assimilation window, which normally covers 6 to 12 hours. In the 4D-Var formulation of the cost function, the J^o term becomes the sum over all observation windows. The background part of the cost function in 4D-Var contains the state vector at the beginning of the assimilation window, while the the output of the linearised forecast model, starting at the beginning of the assimilation window, is used as background temporally collocated to the observations within the assimilation window. Several global NWP models have been equipped with such 4D-Var systems in the recent past, for example at UK Met-Office (Rawlins et al., 2007), ECMWF: (Rabier et al., 2000; Mahfouf and Rabier, 2000), Environment Canada (Gauthier et al., 2007), NCEP (Zou et al., 2001)).

During the 4D-Var analysis the cost function is minimized by iteratively modifying the analysis state vector. This minimization is using the calculated gradient of the cost function. For this both the linearised forecast model, providing the changing distance to the background with varying state vector, and the linearised observation operator, providing the changing distance to the observations with changing state vector, are employed. Under normal circumstances the minimization of the cost function is ended when the slope of the cost function reaches a pre-defined limit.

4D-Var frameworks are ideal tools to assimilate satellite observations which are often also available at times different from commonly used analysis time such as 00 and 12 UTC. An example of the impact of satellite observations on the ECMWF forecast accuracy using a 4D-Var system is shown in Figure 1.2. There, the most important contribution for forecast accuracy is coming from satellite observations in the experiment results shown, especially in the Southern Hemisphere. Often, the positive impact of satellite observations on the NWP accuracy can be linked to channels being mainly sensitive to temperature variations, while the impact of assimilated moisture channels is often still questionable. However, Andersson et al. (2007) showed the positive impact of these channels in the ECMWF 4D-Var system. Reasons for the, in general, smaller impact of moisture channels can be related to the fact of the significant non-Gaussian error characteristics of the commonly used moisture control variables due to limitation at 0 and at moisture saturation. Further, the moisture information in the NWP analysis does not last very long in the subsequent forecast. Thus, smaller impact on the prediction accuracy can be expected from assimilated moisture observations.

1.2 Satellite data assimilation in limited area models

Besides global models, also limited area NWP models include 3D and 4D-Var assimilation systems. In the literature, examples for 3D-Var implementations can be found for

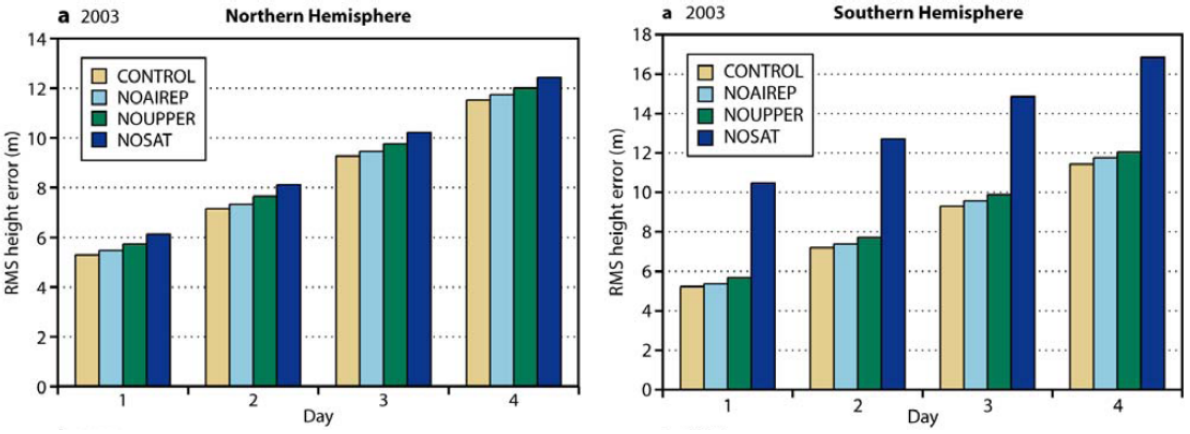

Figure 1.2: Impact of different observation types on the ECMWF 500 hPa geopotential height forecast accuracy for forecast lengths of 1 to 4 days in 2003. CONTROL: all observation types used; NOAIREP: All aircraft measurements (wind and temperature) removed; NOUPPER: All TEMP, PILOT and PROFILER reports removed; NOSAT: All satellite data removed (from Kelly and Thépaut, 2007). Left panel shows the scores for the Northern Hemisphere and right panel for the Southern Hemisphere. TEMP, PILOT, and PROFILER refer to measurements from radiosondes, balloons, and wind profilers.

ALADIN (Fischer et al., 2005), MM5 (Barker et al., 2004), HIRLAM (Gustafsson et al., 2001; Lindskog et al., 2001), and for 4D-Var implementations for the WRF model (Huang et al., 2009) and HIRLAM (Huang et al., 2002; Gustafsson, 2006).

Proving the positive impacts of satellite radiances in limited area NWP models is more difficult. There are several reasons for this: (1) the relative small number of available satellite observations within the model domain (in particular for polar-orbiting satellite instruments), (2) the constraints to the model forecast at the boundaries due to the inserted host model information, (3) limited areas models, which are, for example, placed over Europe, usually benefit already from the relative dense network of conventional observations e.g. SYNOP, balloon and aircraft measurements, while significant improvements can mainly be expected in data sparse regions, such as southern hemispheric oceans, and (4) the length of the operationally performed forecast of limited area model does usually not exceed 3 days. All these points support the conclusion that smaller impacts of additionally assimilated satellite observations on the analyses of limited area models can be expected.

1.3 The assimilation of cloud-affected radiance observations

In many NWP assimilation systems radiances which are significantly affected by clouds are not considered. This means, when assuming that on average 2/3 of the globe are cloud covered, that the majority of all available satellite observations are not used in these sys-

tems. This is due to the fact that the assimilation of these radiances is characterized by some complications as discussed in more details in sections 3.1 and 4.1. Besides the under-exploitation of the satellite data, it can be assumed that by the assimilation of clear-sky radiances only the analysed atmospheric state and the corresponding forecast might systematically be driven towards the atmospheric conditions occurring in cloud-free areas (McNally, 2002). This motivates further research in this particular field. Different approaches and results have recently been published. Most approaches favour the determination of RT-relevant cloud parameters prior to the 3D/4D-Var analysis. These parameters are then used either to constrain the RT calculations or to filter out significantly cloud-affected channels (e.g. Pavelin et al., 2008; Pangaud et al., 2009). This methodology has recently be extended towards the inclusion of basic cloud parameters in a locally extended control vector, where the prior-determined values serve as first guess (McNally, 2009).

A different strategy was proposed in Chevallier et al. (2004). This strategy favours an extended observation operator which temporarily diagnoses the cloudiness in itself rather than using prescribed cloud properties such as cloud top height or cloud cover. A float chart summarizing this strategy is shown in Figure 1.3. Using this methodology, the information of assimilated cloud-affected radiances is projected onto the commonly used control vector variables for temperature and moisture. In 4D-Var also analysis increments in the wind fields can occur through the 4D-Var effect, where sequences of observations can force the analysis model to alter the dynamical fields. This has the advantage that no further cloud variables with non-Gaussian error characteristics have to be introduced into the control vector. Another advantage is that multi-level clouds can be handled, which is superior to all other approaches.

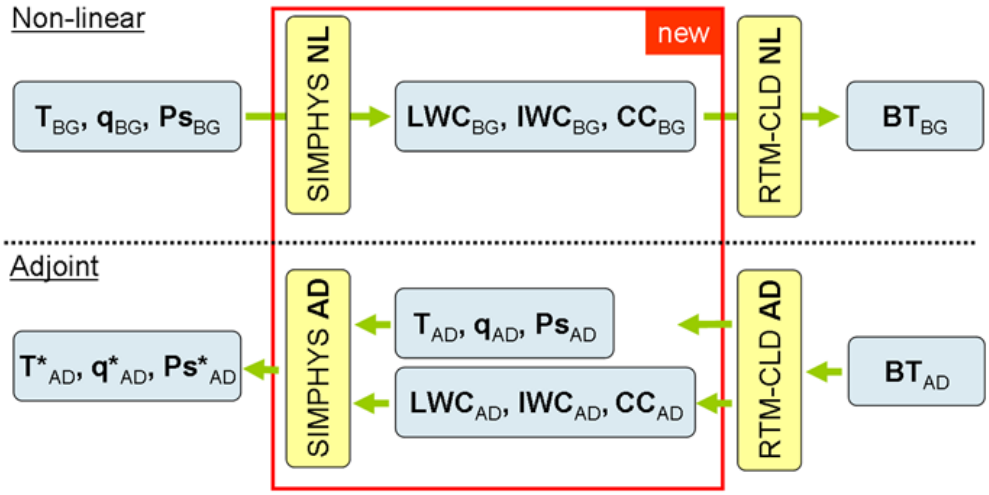

Figure 1.3: Schematic picture of the extension of the non-linear (NL) and adjoint (AD) part of a typical observation operator for satellite radiances in NWP systems. T, q, Ps refer to the control vector variables of temperature, moisture and surface pressure, while LWC, IWC and CC refer to the temporarily existing cloud variables of liquid water content, ice water content and cloud cover. The superscripts BG and AD stand for background and adjoint, respectively. The extension, compared with a usual observation operator, is marked with a red rectangle and describes the inclusion of a simplifies moist physics module (SIMPHYS) which complements the application of a radiative transfer model (RTM-CLD).

Figure 1.4: Pseudo-RGB image from MSG-1 measurements for the entire visible Earth's disk.

1.4 The SEVIRI instrument and its capabilities in NWP assimilation frameworks

The Spinning Enhanced Visible and Infrared Imager (SEVIRI) is the main payload of the Meteosat Second Generation (MSG) series, the latest generation of European geostationary meteorological satellites. With SEVIRI, which is a 12 channel imaging radiometer, the primary mission of MSG, the continuous observation of the Earth's full disk, is achieved (Schmetz et al., 2002). An example of the Earth's disk as observable from Meteosat-8 (MSG-1) is shown in Figure 1.4.

1.4.1 Instrument properties

Spectral properties

As mentioned above, SEVIRI is measuring radiation with 12 channels in different spectral bands. Three channels are located in the visible spectral region. Two of them cover rather narrow bands around 635 nm and 810 nm. The third visible channel, called High Resolution Visible (HRV), is characterized by a broader spectral response function covering about 400 nm to 1.1 μm. Another channel is centred at 1.6 μm in the transition from the visible to the infrared part of the electromagnetic spectrum. The remaining 8 channels

are spectrally located in the infrared and are characterized by the following central wave lengths: 3.9 μm, 6.25 μm, 7.35 μm, 8.70 μm, 9.66 μm, 10.8 μm, 12.0 μm, and 13.4 μm. Hereafter the IR channels will be referred to as IR039, WV062, WV073, IR087, IR097, IR108, IR120 and IR134. Their spectral locations are shown in Figure 1.5 in comparison to the spectral dependence of the total atmospheric transmissivity and the main gaseous contributions, simulated for the US standard atmosphere. The atmospheric signal measured in each channel can be summarized as follows: IR120, IR108, IR087, IR039 are window channels, which means that only a slight interaction of the radiation with the cloud free atmosphere occurs in these spectral bands (slight CO_2-absorption in IR039 and slight water vapour continuum absorption in IR120, IR108 and IR087). IR134 lies at the edge of a strong CO_2 absorption band centred around 14 μm. Due to the relative well mixed and more or less constant CO_2 content in the atmosphere, this channel contains significant information about the tropospheric temperature. IR097 is located in a ozone absorption band, therefore mainly sensitive to changes in ozone and temperature in the stratosphere. WV062 and WV073, which are also called water vapour channels, cover the dip and the edge of a strong water vapour absorption band making these channels being sensitive to water vapour and temperature in the mid and upper troposphere. Due to the strong interaction of infrared radiation with both liquid and solid cloud particles, all channels show a significant sensitivity to clouds if occurring. However, due to the vertical location of their sensitivity function, low-level clouds are not detectable in the two water vapour channels, in particular in the WV062.

Imaging properties

The MSG satellites are spin-stabilized and the nominal spin rate is 100 revolutions min^{-1}. The rotation axis is nominally parallel to the north-south axis of the earth. The imaging is done by combining the satellite spin, leading to an East-West scan of the Earth, and a stepping of the scan mirror, shifting the East-West scan north after each each satellite rotation. One single East-West scan consists of three neighbouring scan lines, since three detectors are used at once for 11 of the 12 spectral channels. Nine detectors are use for the HRV. The scan mirror runs through 1250 subsequent scan positions. For that reason the final observed image contains 3712 scan lines with also 3712 pixels per line. As an exception, the HRV channels covers only half of the full disk in E-W direction and therefore a complete HRV image consists of 11136x5568 pixels. The full disk imaging is completed after about 12 minutes. After that, SEVIRI's IR channels undergo an on-board calibration. This is done by inserting a black body into the optical path of the instrument.

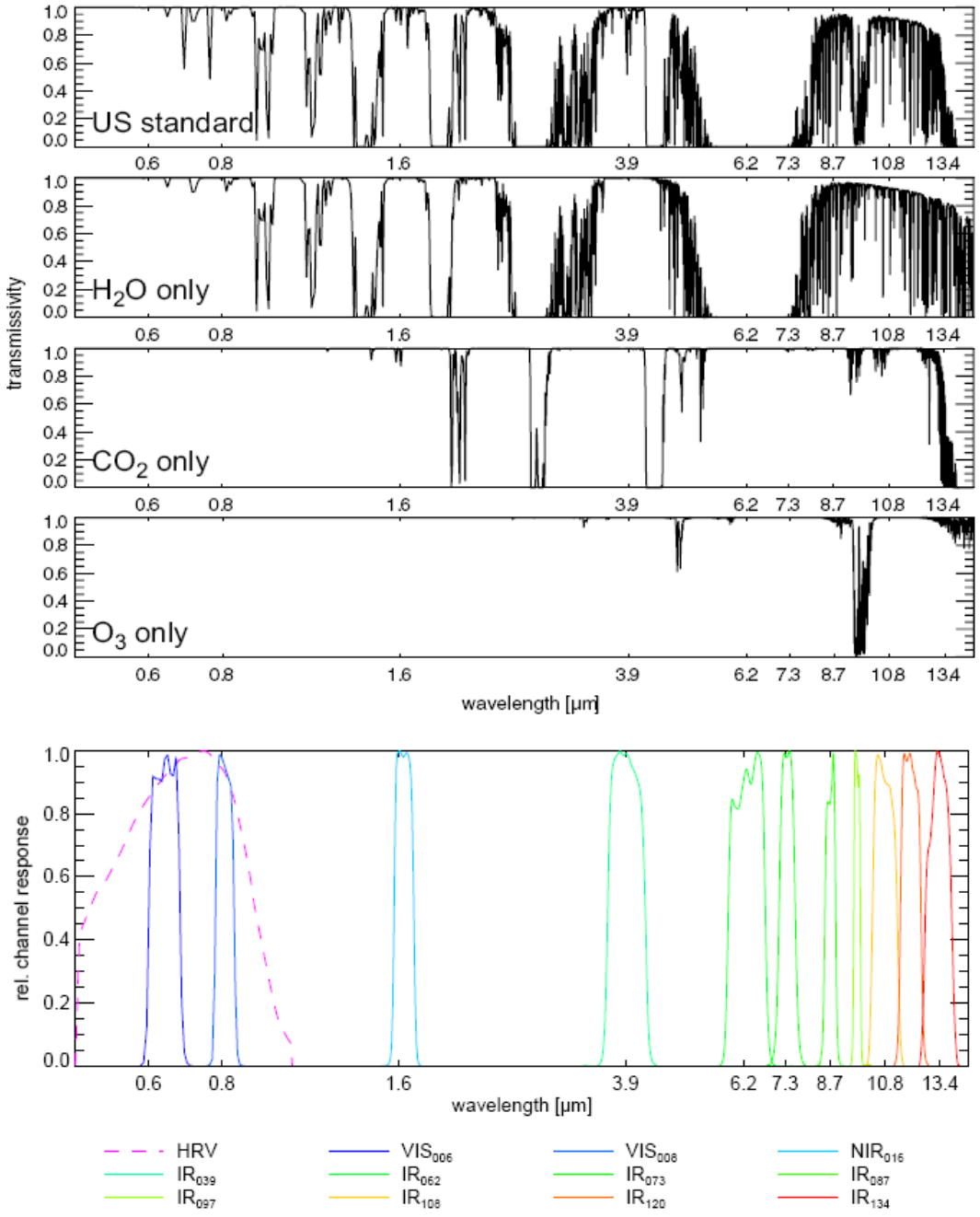

Figure 1.5: Upper three panels: Total transmissivity of the Earth's atmosphere and some of its important gaseous constituents for radiative transfer in visible and infrared spectral regions (from Stengel, 2005). The data was inferred from line-by-line simulations for clear-sky atmospheric conditions given in the US-Standard-Atmosphere shown for the visible and IR part of the electro-magnetic spectrum. Lower panel: Spectral locations of the SEVIRI channels in the same spectral range (from Reuter, 2005).

1.4.2 The use of SEVIRI in NWP assimilation frameworks

Due to SEVIRI's spectral characteristic, which are limited in comparison to sounding instruments on-board polar-orbiting satellites, it capabilities to distinguish the signal from different atmospheric layers is small. In other words, when considering a measurement in a single footprint, SEVIRI contains less information about the atmospheric conditions than sounding instruments, as for example the Atmospheric Infrared Sounder (AIRS) and the Infrared Atmospheric Sounding Interferometer (IASI). The information of SEVIRI's measurements about the vertical structure of atmospheric parameters in clear-sky conditions is limited to: (1) water vapour and temperature in two broad layers in the middle and upper troposphere, provided by its two water vapour channels, (2) a mean tropospheric temperature information, provided by the IR134 channel, and (3) water vapour (by continuum absorption) in lower tropospheric layers in channels IR087, IR108, IR120, IR134. The latter is very difficult to exploit, since the mentioned channels are very sensitive to the surface temperature and surface emissivity. Uncertainties in estimated surface emissivities, which are large for land surfaces, often limit, for example, the water vapour signal extractable from these channels.

However, SEVIRI is characterized by a very high spatial resolution of approximately 3 km for its IR channels at the sub-satellite point and approximately 5 km over Europe. Together with its fast imaging cycle, its spatial coverage capabilities are superior to any other operational geostationary satellite as well as any instrument on-board polar-orbiting satellites. Thus, its information content usable in NWP systems might be comparable to sounding instruments, in particular in a limited-area model, for which the amount of available satellite information from polar-orbiting instruments depends on the time offset between analysis and satellite overpass. The latter depends very much on the size and location of the model domain. SEVIRI's high spatial resolution is also of advantage in cloudy scenes, for which SEVIRI allows to detect many small scale features. The full exploitation of satellite observations, taken in cloudy regions, in NWP assimilation systems in the future, will significantly be supported by such imaging properties.

A few studies have been carried out in the past to assess the potential of impact of SEVIRI-like instruments on the NWP analysis and forecast accuracy. It has been shown that the measurements of geostationary satellite instruments can be beneficial for the quality of NWP systems on a global scale. This is for example documented in Munro et al. (2004); Köpken et al. (2004) for METEOSAT-7. Szyndel et al. (2005) investigated the impact of SEVIRI on the ECMWF system.

Due to SEVIRI fast measurement repetition rate it can be assumed that also limited area model may benefit, since the provision of observations of polar-orbiting sounder instruments are usually very variable in time. This is, as mentioned above, due to the

usually small domain size, which is not always covered by those observations. In this context, Montmerle et al. (2007) investigated the impact of polar-orbiting and geostationary radiances on the ALADIN/France model, using a 3D-Var system. They found a positive impact of assimilated SEVIRI radiances on the very short range forecast, which resulted in reduced background departures of moisture sensitive channels of the High Resolution Infrared Radiation Sounder (HIRS) and the Advanced Microwave Sounding Unit-B (AMSU-B) and in better accuracy of short-range precipitation forecasts.

1.5 Radiative transfer calculations

The calculation of radiative transfer (RT) for satellite applications in NWP framework is usually performed using specific fast RT models such as the Radiative Transfer Model for TOVS (RTTOV: Eyre, 1991; Saunders et al., 1999). These models were specifically made to decrease computational cost in order to enable the processing of very high number of available satellite observations in a very short time. To achieve this, the RT calculations in RTTOV are performed using channel-specific transmittances and emission functions, which were convolved with respect to the spectral characteristics of each channel. The approximate form of the atmospheric RT equation, neglecting scattering effects, used in RTTOV is given in Equation 1.4 (Saunders and Brunel, 2005), where $L(\nu, \theta)$ is the top of the atmosphere upwelling radiance at a frequency ν and viewing angle θ from zenith at the surface.

$$L(\nu, \theta) = (1 - N)L^{Clr}(\nu, \theta) + NL^{Cld}(\nu, \theta) \tag{1.4}$$

The two right hand terms of the equation described the sum of the clear-sky and fully cloudy top of atmosphere (TOA) upwelling radiances $L^{Clr}(\nu, \theta)$ and $L^{Cld}(\nu, \theta)$ scaled by the fractional cloud cover N. The clear-sky term can be written as

$$L^{Clr}(\nu, \theta) = \tau_S(\nu, \theta)\varepsilon_S(\nu, \theta)B(\nu, T_S) + \int_{\tau_S}^{1} B(\nu, T)d\tau \tag{1.5}$$

$$+(1 - \varepsilon_S(\nu, \theta))\tau_S^2(\nu, \theta) \int_{\tau_S}^{1} \frac{B(\nu, T)}{\tau^2} d\tau \tag{1.6}$$

with $B(\nu, T)$ as the Planck function depending on frequency ν and temperature T, τ as the transmittance, T_S as the surface temperature, τ_S and ε_S as the surface to space transmittance and surface emissivity, respectively.

The cloud contribution to the TOA radiance is described in Equation 1.7 for a single layer black, opaque cloud, with $\tau_{Cld}(\nu, \theta)$ being the cloud top to space transmittance and

T_{Cld} the cloud-top temperature.

$$L^{Cld}(\nu,\theta) = \tau_{Cld}(\nu,\theta)B(\nu,T_{Cld}) + \int_{\tau_{Cld}}^{1} B(\nu,T)d\tau \tag{1.7}$$

RTTOV also provides an interface to calculate cloudy radiances for grey, multi-level clouds by means of incorporating profiles of liquid water content, ice water content and cloud cover (Saunders et al., 2005). In general, the calculated and measured radiances are converted to brightness temperatures (TB), which is the theoretical temperature of a black body, with an unity emissivity, would have to emit that radiance.

Figure 1.6 shows a comparison of observed SEVIRI radiances and equivalent radiance simulations based on radiosonde measurements. In general, good agreement is found between the observations and the simulations with the smallest deviations found for WV072 and IR134, while largest deviations are found for the window channels. This latter is due to the errors in the input surface temperatures, which were just taken from the lowest radiosonde measurement level. Largest systematic deviations are found for WV062. Another example is shown in Figure 1.7 where the observations in two SEVIRI channels are compared with the equivalent radiance simulations based NWP data. As in the previous comparison, a significant systematic deviation to warmer brightness temperatures in the simulations is found compared to the observations in the WV062 channel.

As an important feature of RTTOV (or similar models), it also provides the partial derivatives of the TOA radiances with respect to the control vector variables, also called Jacobians. The Jacobians provide the necessary information to the assimilation system to successfully adjust the control vector to match the radiances and to correctly distribute the assimilated radiance information in the vertical. The Jacobians are scene- and angle-dependent and are usually re-calculated for each observation. Examples are shown in Figure 2.2 for clear-sky conditions, and in Figures 3.3 to 3.6 for cloudy scenes.

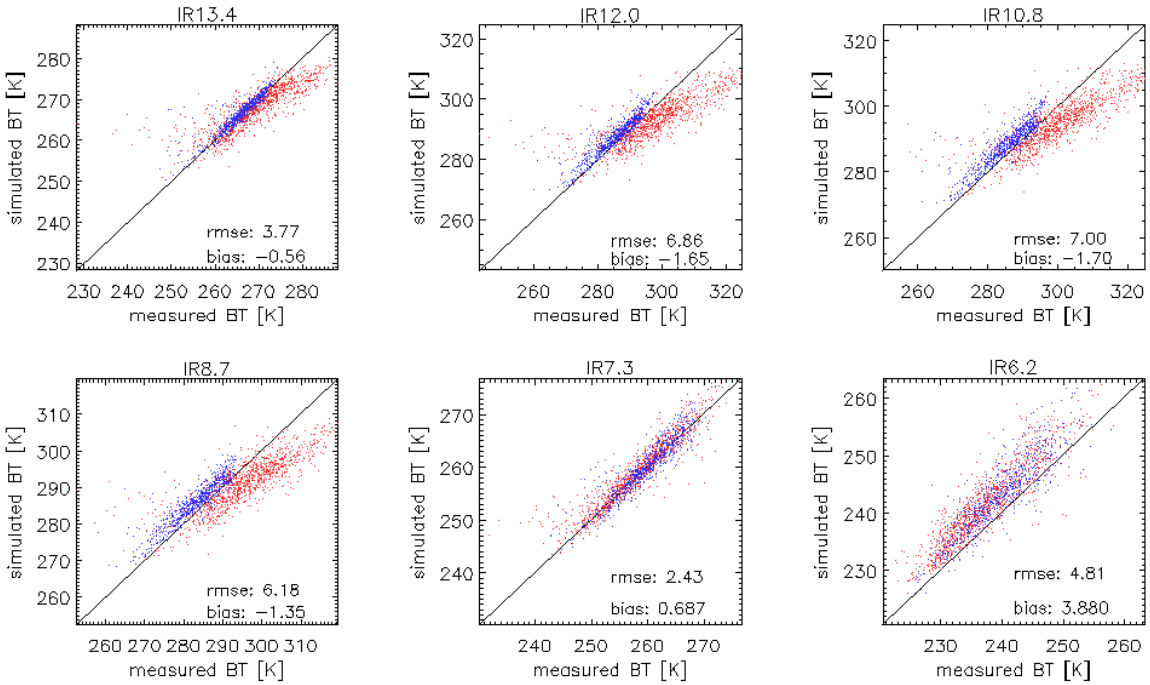

Figure 1.6: Simulated and measured SEVIRI brightness temperatures (BT) based on radiosonde atmospheric profiles. Blue dots mark 00 UTC and red dots mark 12 UTC radiosonde launch times.

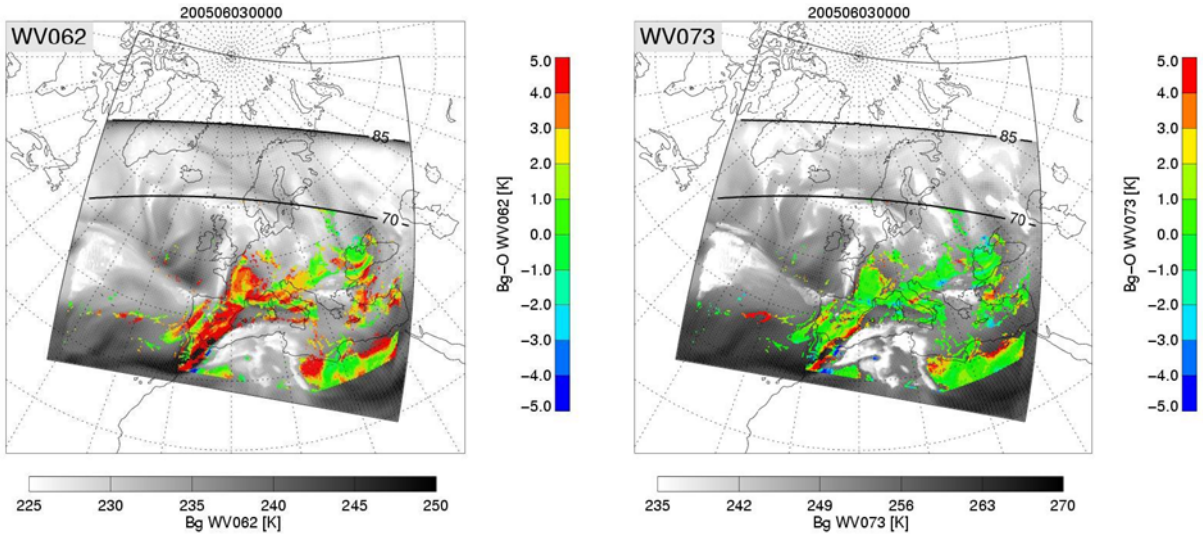

Figure 1.7: Differences between observed (O) and simulated brightness temperatures (Bg) of two SEVIRI channels in clear-sky regions (coloured areas). The simulations are based on the atmospheric profiles taken from HIRLAM 6 h forecast fields. In cloudy regions the simulated brightness temperatures are shown in grey-scale.

1.6 Overview over this dissertation

This dissertation assesses several aspects of the assimilation of SEVIRI IR radiances into a limited area NWP model. Chapter 2 reports about the introduction of these radiances as a new observation type into the HIRLAM assimilation scheme providing, among all other used observations, another piece of valuable information about the atmospheric state. The impact of the radiances in clear sky regions is investigated in assimilation and forecast experiments. Chapter 3 comprehensively describes the definition of an extended observation operator for satellite radiances in the HIRLAM 4D-Var system, which enables the inclusion and proper treatment of cloud-affected satellite radiances. The operator's performance is investigated with respect to the simulation of cloud-affected satellite radiances, the provision of proper cloudy Jacobians and their validity in the vicinity of the background state when cloud processes are involved. Further, a 4D-Var case study including the operator and corresponding results are presented. In Chapter 4 this new framework is applied in long-term assimilation experiments with subsequent forecast runs. This served as a reference to judge the potential impact of cloud-affected satellite radiances on the HIRLAM forecast accuracy, which is assessed by validation of the results against reference model runs and independent in-situ observations. The work presented in this dissertation is summarized in chapter 5, which also gives some generic outlook tackling important aspects to improve the assimilation of satellite observations in clear-sky and cloudy conditions.

2 Assimilation of SEVIRI infrared radiances with HIRLAM 4D-Var

Authors: M. Stengel[1], P. Undén[1], M. Lindskog[1], P. Dahlgren[1], N. Gustafsson[1], R. Bennartz[2]

Article published in *Quarterly Journal of the Royal Meteorological Society Volume 135, Issue 645, October 2009 Part B, Pages: 2100-2109* (`http://dx.doi.org/10.1002/qj.501`)

Abstract

Four-dimensional variational data assimilation (4D-Var) systems are ideally suited to obtain the best possible initial model state by utilizing information about the dynamical evolution of the atmospheric state from observations, such as satellite measurements, distributed over a certain period of time. In recent years, 4D-Var systems have been developed for several global and limited-area models. At the same time, spatially and temporally highly resolved satellite observations, as for example performed by the Spinning Enhanced Visible and InfraRed Imager (SEVIRI) on-board the Meteosat Second Generation satellites, have become available.

Here we demonstrate the benefit of a regional NWP model's analyses and forecasts gained by the assimilation of those radiances. The 4D-Var system of the HIgh Resolution Limited-Area Model (HIRLAM) has been adjusted to utilize three of SEVIRI's infrared channels (located around 6.2 μm, 7.3 μm, and 13.4 μm, respectively) under clear-sky and low-level cloud conditions. Extended assimilation and forecast experiments show that the main direct impact of assimilated SEVIRI radiances on the atmospheric analysis were additional tropospheric humidity and wind increments. Forecast verification reveals a positive impact for almost all upper-air variables throughout the troposphere. Largest improvements are found for humidity and geopotential height in the middle troposphere. The observations in regions of low-level clouds provide especially beneficial information

[1]Swedish Meteorological and Hydrological Institute, Folkborgsvägen 1, Norrköping, Sweden
[2]Atmospheric and Oceanic Sciences Department, University of Wisconsin, Madison, Wisconsin, USA

to the NWP system, which highlights the importance of satellite observations in cloudy areas for further improvements in the accuracy of weather forecasts.

2.1 Introduction

Since the first usage of satellite observations in Numerical Weather Prediction (NWP) systems, which focused on the TIROS Operational Vertical Sounder (TOVS), this type of observations has become increasingly important for atmospheric analyses and weather forecasting (Kelly and Thépaut, 2007). The introduction of variational data assimilation and the development of fast radiative transfer models and their adjoints have enabled the direct assimilation of satellite radiances into NWP systems (e.g. Andersson et al. (1994)). This approach provides a more efficient and less time-consuming use of satellite observations by avoiding preceding retrievals of atmospheric parameters, which can be subject to additional errors.

For global NWP models, satellite data nowadays contribute an amount of information to the atmospheric analysis which is comparable to radiosondes (Kelly and Thépaut, 2007). The main focus in recent years has been on polar-orbiting satellites carrying sounding instruments such as the Advanced Microwave Sounding Unit (AMSU), the Atmospheric Infrared Sounder (AIRS), or the Infrared Atmospheric Sounding Interferometer (IASI). Their spatial coverage is high compared to ground-based measurements. In remote and data sparse regions, like the Tropics or the Southern Hemisphere, satellite data have become the single most important source of observational data and the biggest analysis increments are usually found there. These regions also show the largest increase in forecast accuracy due to the satellite data. In the Northern Hemisphere, which is characterised by denser ground-based measurements, positive impacts of these observations are mostly found in the medium- and long-range forecasts, after an integration time of a few days.

Besides polar-orbiting satellites, geostationary instruments, such as the Meteosat Visible and InfraRed Imager (MVIRI) and the Spinning Enhanced Visible and InfraRed Imager (SEVIRI), on-board the Meteosat satellites were also found to be a valuable source of information and were introduced to data assimilation successfully in recent years. On the one hand, those instruments have for the time being lower spectral resolution, and therefore less capabilities in terms of vertical sounding of the atmosphere than polar-orbiting instruments. On the other hand, geostationary instruments provide a comprehensive and almost continuous picture of the evolution of weather phenomena due to their high spatial and temporal resolution. Studies highlighting the impact of the geostationary radiances on the European Centre for Medium-Range Weather Forecasts (ECMWF) model are for example documented in Köpken et al. (2004) for MVIRI on-board Meteosat-7 and Szyndel et al. (2005) for SEVIRI on-board Meteosat-8.

Evaluating the benefit of satellite observations for regional NWP models is somewhat harder than for global models, since model domains are usually much smaller and the integration time is typically not longer than two or three days. The impact of assimilated satellite data on regional NWP models might further strongly depend on the region where the model is run. Operational limited area models in Europe and North-America usually also benefit strongly from the dense upper-air observation network of radiosondes and aircraft measurements and are constrained by the host model's accuracy at the boundaries.

Nonetheless, studies in recent years have shown that satellite data can also be valuable on a regional scale. For example, Montmerle et al. (2007) investigated the impact of polar-orbiting and geostationary satellite radiances in the Aladin/France model, using a 3D-Var system. One result was that SEVIRI radiances have a positive impact on the very short range forecast, resulting in decreased background departures of moisture sensitive channels of HIRS and AMSU-B. Furthermore, they found an increased accuracy of short-range precipitation forecasts.

In this paper we investigate the benefit of assimilating SEVIRI radiances using the 4D-Var system of the HIgh Resolution Limited Area Model (HIRLAM) (Undén et al., 2002b). The assimilation of SEVIRI observations in a 4D-Var system of a limited-area model is fairly new and to our knowledge has not yet been evaluated in the peer-reviewed literature. In our study, SEVIRI data with an hourly resolution, equally distributed over a 6 h assimilation window, were assimilated. In 4D-Var, this results in flow-depended assimilation increments in, for example moisture and temperature fields inferred by additional adjustments of the dynamical control variables, which is complementary to the balances in the background-error structure functions. Furthermore, we introduced a sophisticated procedure to identify useful SEVIRI observations in the presence of low-level clouds. Evaluating their impact on forecast accuracy compared to the observations in clear-sky conditions is another central point of our study.

In the following section we describe the experimental framework of our studies, giving an overview of the HIRLAM model and its assimilation system, SEVIRI observations and their processing for our studies, and describing the experiment series we performed. The impact of SEVIRI on the analysis is discussed in section 3. Furthermore, we present forecast-error verifications for the conducted experiments in section 4.

2.2 Experimental framework

2.2.1 The HIRLAM model and its 4D-Var system

The HIRLAM model is a limited-area NWP model, which is used operationally at SMHI as well as in other countries participating in the HIRLAM project. The hydrostatic

model is in our studies specified with a horizontal resolution of around 22 km and with 60 vertical levels. The model domain is shown in Figure 2.1. The HIRLAM model contains a variational data assimilation system (HIRVDA). A description of the 3D-Var specifications and initial tests can be found in Gustafsson et al. (2001) and Lindskog et al. (2001), respectively. Its current 4D-Var system is largely along the lines of Huang et al. (2002) and Gustafsson (2006). In our studies, two sequenced cost function minimizations were performed with a model resolution of 66 km during the first and 44 km during the second minimization process. The cost function J is formulated as in Equation (2.1) as the sum of the background part (J^b), the initialisation part (J^c), and the observational part (J^o).

$$J = J^b + J^c + J^o \tag{2.1}$$

The background part is described in Equation (2.2), where $\mathbf{B}$ denotes the background error covariance matrix and $\delta\mathbf{x}_0$ the increment in model space with respect to background $\mathbf{x}_0^b$ at the beginning of the assimilation window.

$$J^b = \frac{1}{2}(\delta\mathbf{x}_0)^T\mathbf{B}^{-1}\delta\mathbf{x}_0 \tag{2.2}$$

The initialization part of the cost function is formulated as a weak digital filter constraint following Gustafsson (1992) and Gauthier and Thépaut (2001). The observational part of the cost function is shown in Equation (2.3), which is formulated as the sum over all K observations window contributions.

$$J^o = \frac{1}{2}\sum_{i=0}^{K}\{(\mathbf{d}_i + \mathbf{H}(\delta\mathbf{x}_i))^T\mathbf{R}^{-1}(\mathbf{d}_i + \mathbf{H}(\delta\mathbf{x}_i))\} \tag{2.3}$$

$\mathbf{R}$ represents the observation-error covariance matrix, which accounts for errors in the observations as well as in the forward modeling. $\delta\mathbf{x}_i$ is the increment in model space propagated forward in time from the beginning of the assimilation window to each observation window i using the tangent-linear forecast model. The difference vector $\mathbf{d}_i$ is formulated as

$$\mathbf{d}_i = H(\mathbf{x}_i^b) - \mathbf{y}_i^o \tag{2.4}$$

and stands for the innovations between the observations $\mathbf{y}_i$ and the modelled radiances $H(\mathbf{x}_i^b)$.

$\mathbf{H}$ represents the tangent-linear of the observation operator H, which is, in case of satellite radiances, the widely-used fast Radiative Transfer Model for TOVS (RTTOV) (Eyre, 1991; Saunders et al., 1999). Version 8_7 of RTTOV was used in our studies.

The RTTOV model computes radiances for passive infrared and microwave satellite instruments. It is very time-efficient by using the polychromatic approximation of the radiative transfer equation. In this approximation the radiative transfer calculation is performed using transmittances and Planck functions convolved with respect to the spectral response function of each channel. This is in contrast to the convolution of radiances inferred from line-by-line calculations. An important feature of RTTOV is that it also computes the gradient of the radiances with respect to the state vector variables, which is crucial for the direct assimilation of satellite radiances in NWP systems.

The state vector variables in HIRVDA are surface pressure and upper-air values of the wind components in the x- and y-directions, temperature and moisture. Specific humidity has recently been replaced by a pseudo-relative humidity (Holm et al., 2002) as moisture variable. This induces a flow-dependency of the background-error humidity correlations. In addition, large areas of strong super-saturation are avoided due to the near-Gaussian error characteristics. In general, Gaussian error characteristics of the background fields as well as of the observations are assumed in the present formulation of the cost function and are needed to obtain the optimal analysis results.

The background-error statistics for the state vector variables were derived, as proposed in Parrish and Derber (1992), from differences between 36-hour and 12-hour forecasts valid at the same time, utilizing a statistical balance operator (Berre, 1997; Derber and Bouttier, 1999).

The 4D-Var assimilation window was specified with 6 h covering the time period of -3.5 until +2.5 h relative to the analysis time.

In our studies the HIRLAM forecast model is characterized by a semi-Lagrangian advection scheme, physical parametrisations for radiation (Savijärvi, 1990) and for convection and large-scale condensation processes (Rasch and Kristjánsson, 1998; Kain, 2004), a moist conserved turbulence scheme (Cuxart et al., 2000), and the ISBA (Interaction Soil Biosphere Atmosphere) land surface scheme (Noilhan and Mahfouf, 1996). ECMWF forecasts (6 to 12 h old) were provided as lateral boundaries with a 3 h interval.

2.2.2 SEVIRI radiances and used cloud products

The SEVIRI instrument (Schmetz et al., 2002) is the main payload of the Meteosat Second Generation (MSG) satellite series. The first of this series, Meteosat-8 (MSG-1), became operational in January 2004. Since April 2007 Meteosat-9 (MSG-2), the second satellite of this series, has been the prime satellite. SEVIRI provides continuous observations for the full Earth's disc with an imaging cycle of 15 min. Eight of its 12 channels are located in the infrared, one in the near-infrared and three in the visible part of the electromagnetic spectrum. The central wave lengths of the infrared channels are 3.90 μm, 6.25 μm, 7.35 μm, 8.70 μm, 9.66 μm, 10.80 μm, 12.00 μm and 13.40 μm. The spatial

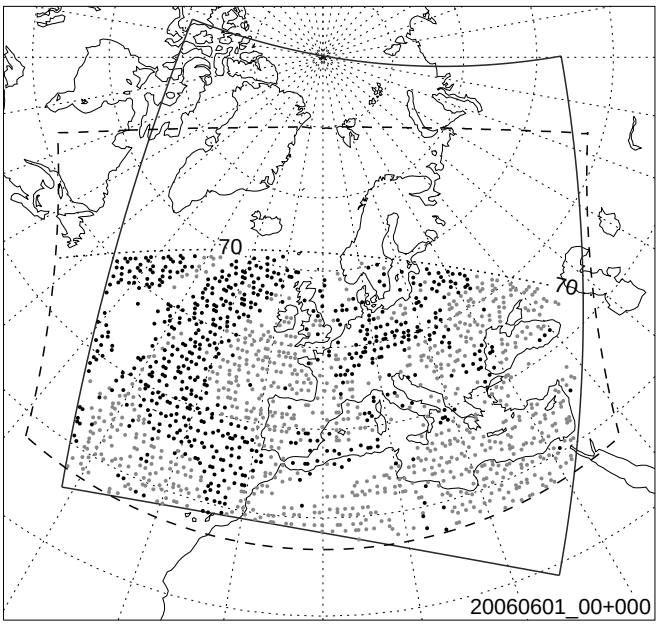

Figure 2.1: Locations of screened clear-sky (CLS, black dots) and low-level cloud (LLC, grey dots) observations after data selection for 0000 UTC on 1 June 2006. The black line and grey dashed line border the HIRLAM/SMHI-C22 domain and the MSG sub-area as currently processed at SMHI. The black dotted line marks the SEVIRI 70° zenith angle.

resolution of the IR channels is about 3 km at the sub-satellite point and $\approx 4-5$ km over Central Europe. For practical reasons, the SEVIRI data processing in our studies was limited to a sub-area of the entire disk, which covers approximately 2/3 of the chosen model domain (Figure 2.1). However, after rejecting measurements with scan angles exceeding 70°, the covered part of the model domain is reduced to approximately the southern half. To identify cloud-contaminated pixels, a cloud mask (Derrien and Le Gléau, 2005) is utilized, which is part of a software package (Le Gleau and Derrien, 2002), developed by the EUMETSAT Satellite Application Facility on Nowcasting and Very Short Range Forecasting (SAFNWC). This packages provides a pixel-based distinction into three classes: completely cloud-filled, partly cloud-filled, or clear-sky. Using this information, all clear-sky observations are identified in a first step. In a second step, radiances in completely cloud-filled pixels undergo a local test to identify channel radiances which are not or only slightly affected by the cloud. Here, a cloud top pressure (CTP) estimation, documented as PGE03 in Le Gleau and Derrien (2002), is used. A detailed description of this procedure is given in the following section. For simplicity all partly cloud-covered pixels were generally rejected in our studies.

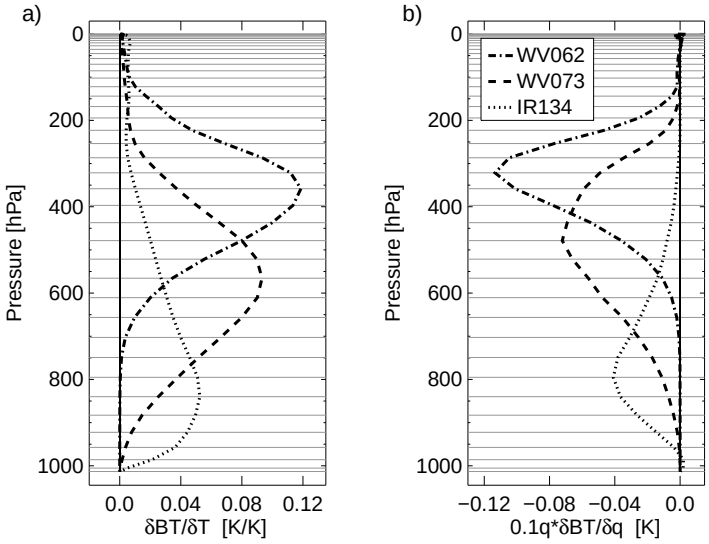

Figure 2.2: Mean Jacobians with respect to (a) temperature and (b) specific humidity. The humidity Jacobians were scaled at each level by 10% of the corresponding background specific humidity value before averaging.

Observation selection

For the time being, we have focused on the assimilation of the two water vapour channels (WV062 and WV073 hereafter), located at 6.2 μm and 7.3 μm, and the CO_2 channel (IR134 hereafter), which is placed around 13.4 μm within a wing of a strong CO_2 absorption band. The modelled sensitivity of these radiances with respect to temperature and moisture (Jacobians) in the absence of radiance-affecting clouds are displayed in Figure 2.2. The shown profiles were generated using RTTOV and averaged over approximately 150 summer cases over Europe. Due to their spectral location, the water vapour radiances comprise mainly information about moisture and temperature in the middle and upper troposphere. Their temperature Jacobians peak on average around 600 hPa (WV073) and around 350 hPa (WV062), respectively. The profile for IR134 shows a moderate temperature sensitivity throughout the troposphere with a maximum amplitude around 850 Pa. Its radiance is also affected by the water vapour continuum absorption in the lower troposphere. Furthermore, this radiance is usually affected by surface emissions. Due to this the IR134 channel is only used over ocean. There, background sea surface temperatures and sea surface emissivities, calculated internally in RTTOV, are of proper quality in the forward modelling.

Due to an insufficient treatment of clouds in our current observation operator, we blacklisted all radiances that were significantly affected by clouds. In the following we describe two classes of retained observations which were used within the assimilation. The first

class is composed by selecting all observations in cloud-free pixels according to the cloud mask. In the following the abbreviation 'CLS' for clear-sky will be used for this class of observations.

Furthermore, we define a second class of observations, which contains observations under mainly low-level cloud conditions, hereafter referred to as 'LLC'. These observation must fulfil two criteria. All pixels within this class had to be identified as cloud-filled by the cloud mask and the CTP estimate for these pixels had to be below a certain height to limit the impact of clouds on the observed radiances. This critical height was determined by the local clear-sky temperature Jacobian (e.g. Figure 2.2) co-located at each observation point. In detail, each Jacobian was integrated from bottom upwards and the critical height was determined to be where the integrated value reached 5% of the total integrated Jacobian. Subsequently, all observations were included in LLC for which the cloud top pressure estimate did not exceed this critical height. This procedure was done for each channel separately. Generally, and when considering an average atmospheric profile as in Figure 2.2, this critical height might lie around 550 hPa for channel WV062 and around 850Pa for the WV073 channel.

In order to provide a spatially optimal and non-redundant set of observations, various preparatory data selection steps were performed. As an initial step, SEVIRI pixels located outside the model domain and pixels with zenith angles greater than 70° were rejected. The zenith angle threshold was chosen as a compromise between the spatial SEVIRI coverage of the model domain and the growing representativeness error of the background profiles for large satellite zenith angles. Additionally, pixels covering mountain regions with altitudes higher than 1 km were rejected. Errors in land surface emissivities and temperatures would increase simulation errors in cases of high-altitude land regions. Furthermore, a data thinning was performed and only one pixel out of each 10×10 pixel-box was kept for further usage, which led at this stage to an average spatial sampling of about 50 km over central Europe. Subsequently, a background check was done, filtering all observations with innovations exceeding the limit of 4 K. These observations were assumed to be affected by gross errors. The final spatial thinning, removing possible spatial error correlations in the observations, had a thinning length of approximately 90 km. This value was chosen with respect to the length-scale of the background-error structure functions. One example of retained SEVIRI pixels after all preparation steps is show in Figure 2.1 for 0000 UTC on 01 June 2006.

Bias investigation and correction

Initially, the background equivalents in radiance observation space ($H(\mathbf{x}^b)$), which were simulated every 6 h using HIRLAM 6 h forecast fields, were monitored against co-located observations ($\mathbf{y}^o$) for a 2-months period in summer 2005 (not shown). The calculated

error statistics of the innovations ($(H(\mathbf{x}^b) - \mathbf{y}^o)$) showed a permanent bias in the WV062 channel remaining during the investigated time period. The background appeared to be much warmer for this channel than the observations. The mean bias was calculated to be 2.6 K. This value is a bit larger than the 1.7 K which were found by Szyndel et al. (2005). This bias might originate from systematic deviations in the upper troposphere in the NWP fields, which could be too dry and/or too warm. One might also speculate that this is partly caused by slight deviations in the brightness temperature definitions in RTTOV and the SAFNWC software that had been used. Furthermore, a diurnal cycle of the bias was found for all three channels, which was also discovered in Szyndel et al. (2005) for the two water vapour channels. The innovations increased during the night and decreased during the day (Figure 2.3). The reasons for this diurnal oscillation is not fully understood so far, but it may indicate a possible diurnal dependency of the NWP model performance or differences in the cloud mask between daytime and night-time scenes. A possibly increased number of undetected clouds in the observations during night-time would shift the innovation bias towards higher values, which is in line with the observed feature. The amplitude of the diurnal bias variation often reaches 1 K. This behaviour would have to be taken into account when applying advanced bias correction schemes such as proposed by Harris and Kelly (2001). For the time being, a flat bias correction was applied to the WV062 channel by means of adding a fixed offset of 2.6 K to the observations. A possible scan-angle dependence was not considered here because of the fairly small variation of scan-angle within the model domain. The channels WV073 and IR134 were not bias-corrected due to a relatively small bias in the investigated period.

2.2.3 Experiment specifications

Three different data assimilation and forecast experiments were conducted (CNTRL, SEVCLS and SEVLLC hereafter). The specifications of the assimilation system as well as of the forecast model were identical. Differences were only in the assimilated observation types, which were specified as follows:

- CNTRL: Conventional observations only
- SEVCLS: Conventional and CLS observations
- SEVLLC: Conventional, CLS and LLC observations

The conventional observations comprise surface station (SYNOP), radiosonde, and pilot-balloon reports, as well as measurements from ships, aircraft and buoys. These data, which were retrieved from the Meteorological Archival and Retrieval System (MARS) at ECMWF, were the same in each experiment. The term SEVIRI experiments will in the following stand for both SEVCLS and SEVLLC.

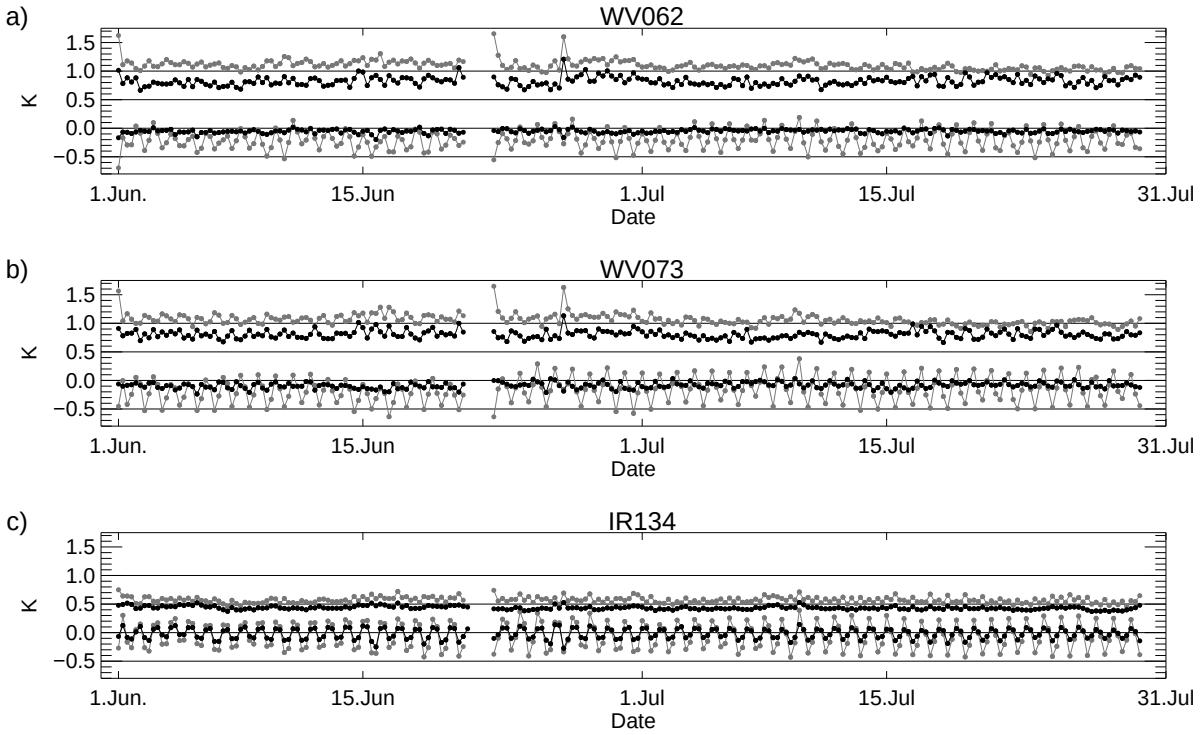

Figure 2.3: Monitoring of biases and RMS errors of CLS observation departures for background (grey dots) and analysis (black dots) for the SEVCLS experiment and channels (a) WV062, (b) WV073, and (c) IR134. The displayed data were time-averaged within each assimilation cycle resulting in a resolution of 6 h. Gaps in the graphs indicate cycles with no SEVIRI data available.

In both SEVIRI experiments, observations from 6 SEVIRI time slots, which were equally distributed over the 6 h assimilation window, were used, resulting in an effective temporal resolution of 1 h. This temporal thinning is based on assimilation characteristics of the HIRLAM model, which assumes the provided observations to be in the centre of each 1 h observation window. Higher temporal resolutions could therefore introduce persistence errors in the current model version due to misrepresentation of the time of the observations. The data preparation as mentioned above was done separately for each SEVIRI time slot. The observation errors were specified higher than SEVIRI's radiometric noise to account for forward modelling errors, and to avoid SEVIRI observations to be too dominant during the assimilation process. The chosen value for both water vapour channels was 2 K in both SEVIRI experiments. The IR134 observations were assigned to have an error of 1.5 K. The period of the assimilation experiments covers almost two full months from 1 June 2006 until 28 July 2006. An assimilation cycle was performed every 6 h, utilizing new observations, and subsequently the forecast model was run until 48 h integration time.

Bias and RMS error statistics of the observation departures for background and analysis fields for the SEVCLS experiment are monitored in Figure 2.3, including all CLS observations used in the minimization. The corresponding values for SEVLLC are very similar and are not shown.

2.3 Analysis increments

Generally speaking, the largest impacts on the analyses, when assimilating SEVIRI, were found in the moisture and wind fields. The moisture was mainly changed in the mid- and upper troposphere, whereas noticeable wind increments were also found in the lower troposphere. The other upper-air fields as well as surface pressure were also affected but to a smaller extent.

In the following the analysis impact of one particular assimilation cycle (1 June 2006 at 0000 UTC) is discussed, in which all three experiments used the same background state conditions. Figure 2.4 shows the differences in the analysed relative humidity at 500 hPa. The increments of SEVCLS and SEVLLC, each compared to CNTRL, correspond to the location of the selected observations as displayed in Figure 2.1. For relative humidity, many small-scale features are found within the range of ± 20%. In a few locations, even higher values are found. The deflection, if drying or moistening, at this pressure level is in general in line with the innovations for channel WV073. A similar relation is found between moisture at higher levels and the WV062 channel. A comparison between the humidity analyses of the SEVIRI experiments (Figure 2.4) reveals some small-scale features in the difference patterns but also the amplification and attenuation of moisture

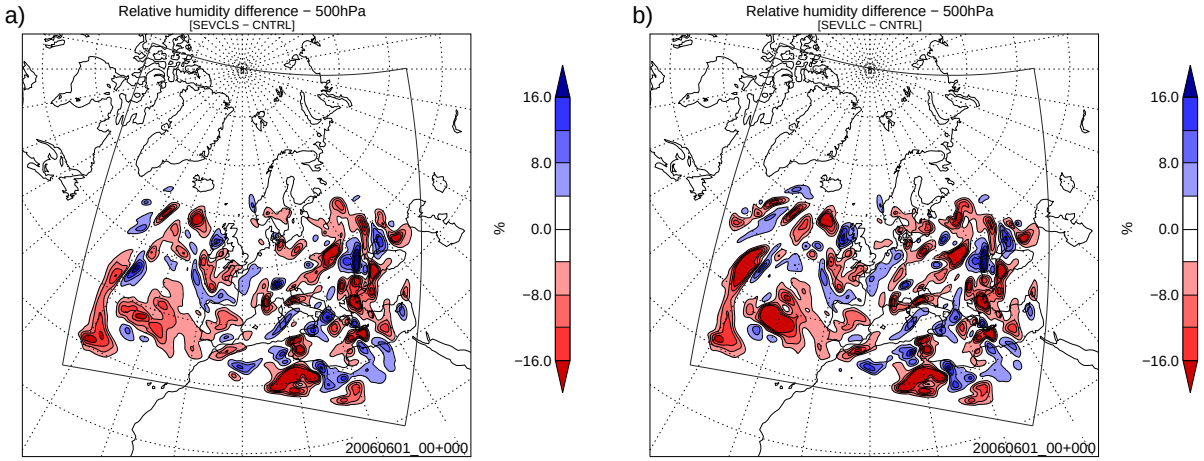

Figure 2.4: Difference in analysed relative humidity at 500 hPa for (a) SEVCLS minus CNTRL and for (b) SEVLLC minus CNTRL. An horizontal smoothing was applied to the data.

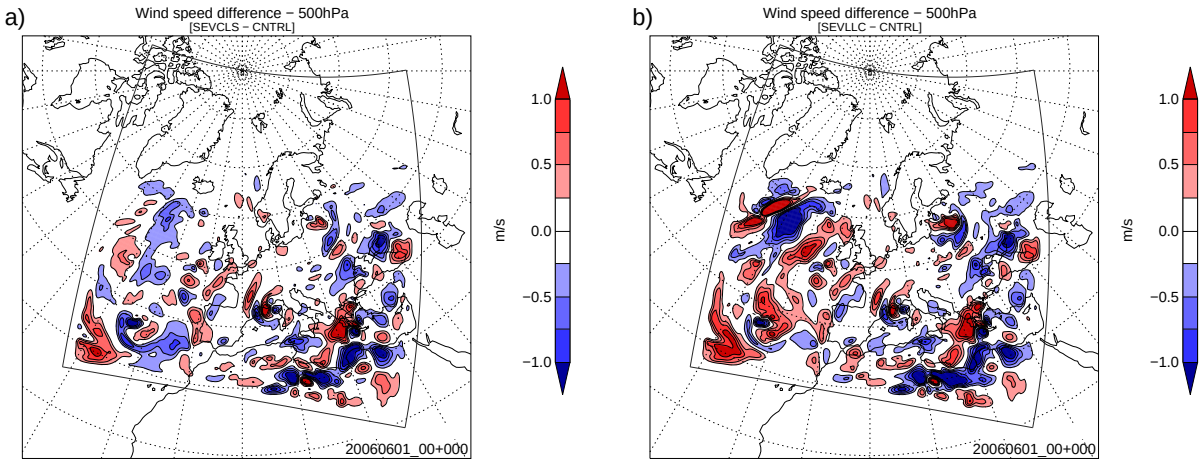

Figure 2.5: As Figure 4, but for wind speed.

increments. Those differences in SEVLLC compared to SEVCLS are again more or less directly co-located to the additional LLC observations in SEVLLC (Figure 2.1).

The wind fields at 500 hPa in Figure 2.5 show small increments over Central Europe and larger increments over the Atlantic Ocean, in the eastern Mediterranean Sea, and parts of Northern Africa. The small impact over land might be due to the conventional observations being dominant for wind in those regions and/or the agreement of those with the satellite observations. Similarl to relative humidity, we find also for wind relatively large differences between SEVCLS-CNTRL and SEVLLC-CNTRL, which are also co-located with the region of additional LLC observations in SEVLLC.

Comparative 3D-Var experiments for this case were conducted to study the difference between 3D-Var and 4D-Var. In 3D-Var, SEVIRI data from only one time slot were assim-

ilated. In general, the 3D-Var experiments exhibit much smaller changes in the moisture increments (not shown). Changes in wind increments in 3D-Var were also significantly smaller than in 4D-Var and almost not noticeable.

An additional statistical investigation of the 4D-Var wind analysis increments over the full domain and for the entire experiment period show clearly the impact of SEVIRI observation on the wind fields, especially in the upper troposphere (not shown). The differences are more pronounced for SEVLLC than for SEVCLS. The standard deviations of the increments in the SEVIRI experiments are in general increased over ocean and decreased over land compare to the control run.

Generally, our results suggest that additional dynamical information were incorporated by assimilating SEVIRI with 4D-Var.

Furthermore, we calculated observation fit statistics of the 4D-Var analyses against radiosondes for the entire period of the experiments. These statistics highlight a slightly increased deviation in both SEVIRI experiments compared to the control run. This behaviour is found for all upper-air parameters in the upper troposphere except geopotential height. The maximum of this deviation is found for relative humidity at 300 hPa. It is also visible in Figure 2.7 at 500 hPa (0 h forecast length), but to a smaller extent.

2.4 Impact on short-range forecast

Radiosoundings and SYNOP reports, which were selected according to the stations list established by the European Working Group on Limited Area Modelling, were used to verify the short-range forecasts. Co-located profiles were extracted from the forecast fields for all three experiments. Based on this dataset, we calculated the root mean square (RMS) and mean errors for various parameters for all three experiment series at 12, 24, 36 and 48 h forecast.

2.4.1 Impact on upper-air variables

Figure 2.6 displays the time-averaged scores for the upper-air parameters temperature, relative humidity, geopotential height and wind speed. Here, the RMS and mean errors are averaged over all forecast lengths.

Generally, the RMS error values of the temperature forecast are very similar in all three experiments. At 500 hPa the values are slightly reduced for SEVCLS and SEVLLC. We found furthermore a slight degradation of forecast accuracy for temperature at 300 hPa for the 24 and 36 h forecasts (not shown). The mean errors for temperatures for SEVCLS and SEVLLC seem to be increased a bit in the lower troposphere. In Figure 2.7(a) the temperature forecast errors at 500 hPa are show as a function of forecast lengths.

A larger positive impact is visible for relative humidity with the biggest change at 300 and 500 hPa. At 500 hPa the forecast error is reduced by $\approx 1\%$ relative humidity for both SEVIRI experiments, which is a relative error reduction of $4-5\%$. The largest impact is found for the 12 hour forecast and then decreasing with forecast time afterwards (Figure 2.7(b)). A general slight drying throughout the troposphere is found, when assimilating SEVIRI.

The change in the geopotential height scores is also characterized by an RMS error reduction. Here, the positive impact is visible throughout the entire troposphere. The RMS errors of SEVLLC are estimated to be 0.5 to 1 m ($\approx 3-5\%$) smaller at 500 and 300 hPa than the corresponding values of CNTRL. The impact in SEVCLS is smaller for this parameter, but still slightly positive at most levels. In general, the positive effect appears to be increasing towards forecast lengths of 36 and 48 hours for both SEVIRI experiments (Figure 2.7(c)).

The error values for wind speed are quite similar to those for geopotential height. Here, we also found decreased forecast errors with the largest extent at 300 and 500 hPa. Furthermore SEVLLC performs better than SEVCLS. The same can be observed in Figure 2.7(d), where SEVLLC shows the lowest RMS errors for wind at 500 Pa at all considered forecast lengths. The mean error values for this variable show only minimal changes.

2.4.2 Impact on surface variables

For many investigated surface variables, the forecast errors in the SEVIRI experiments are nearly identical to the control experiment. However, small positive effects are found for surface pressure, where the error is reduced for forecast lengths from 36 to 48 h (Figure 2.8(a)). Furthermore we found a slight positive impact on precipitation scores for both SEVIRI experiments and all considered forecast lengths (not shown). Here, RMS errors are reduced by up to 5% in SEVCLS and slightly less in SEVLLC compared to CNTRL. A similar picture shows the frequency distribution of the clustered rain amounts (Figure 2.8(b)). For five of the six shown precipitation bins, the values for SEVLLC are closer to the observation values than the CNTRL. For SEVCLS this applies for four of the six bins.

2.5 Summary and discussion

This paper presents a study investigating the impact of assimilated geostationary IR radiances on analyses and forecasts of the limited-area model HIRLAM using a four-dimensional data assimilation framework. For this purpose radiances measured by SEVIRI were converted to brightness temperatures and corresponding cloud products (a cloud

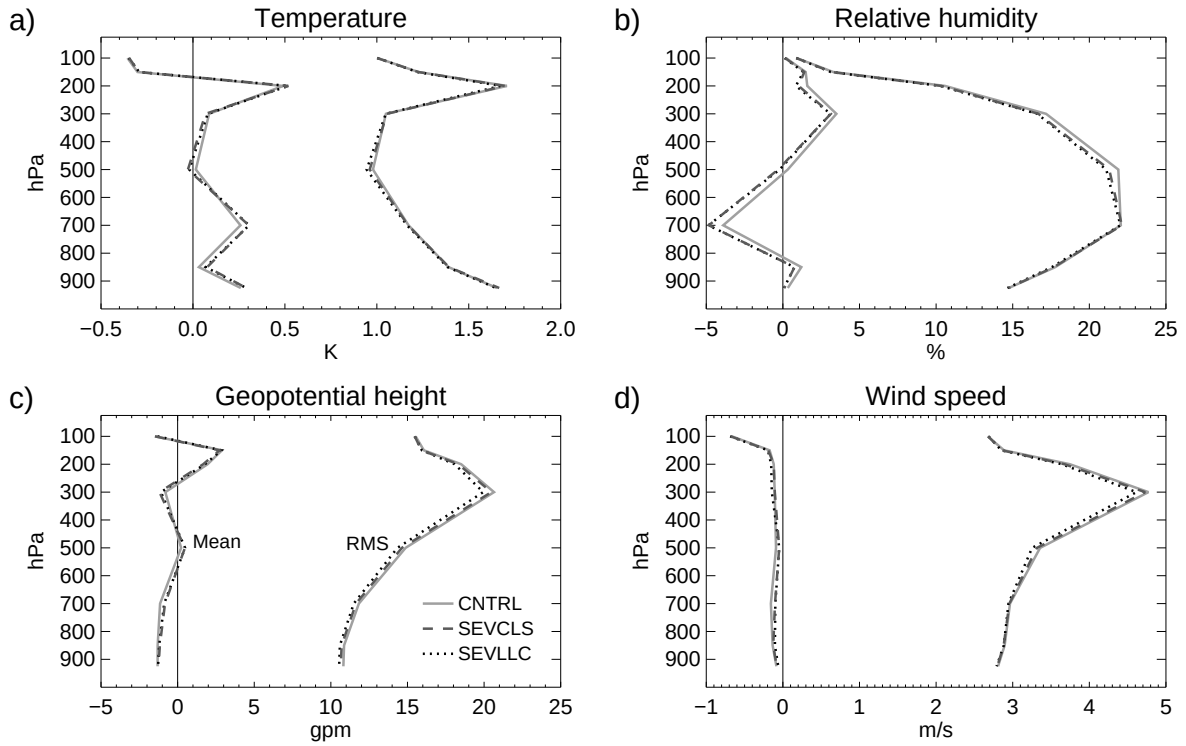

Figure 2.6: Profiles of RMS and mean forecast errors based on 0000 UTC and 1200 UTC analyses, time-averaged over forecast lengths 12, 24, 36, and 48 h.

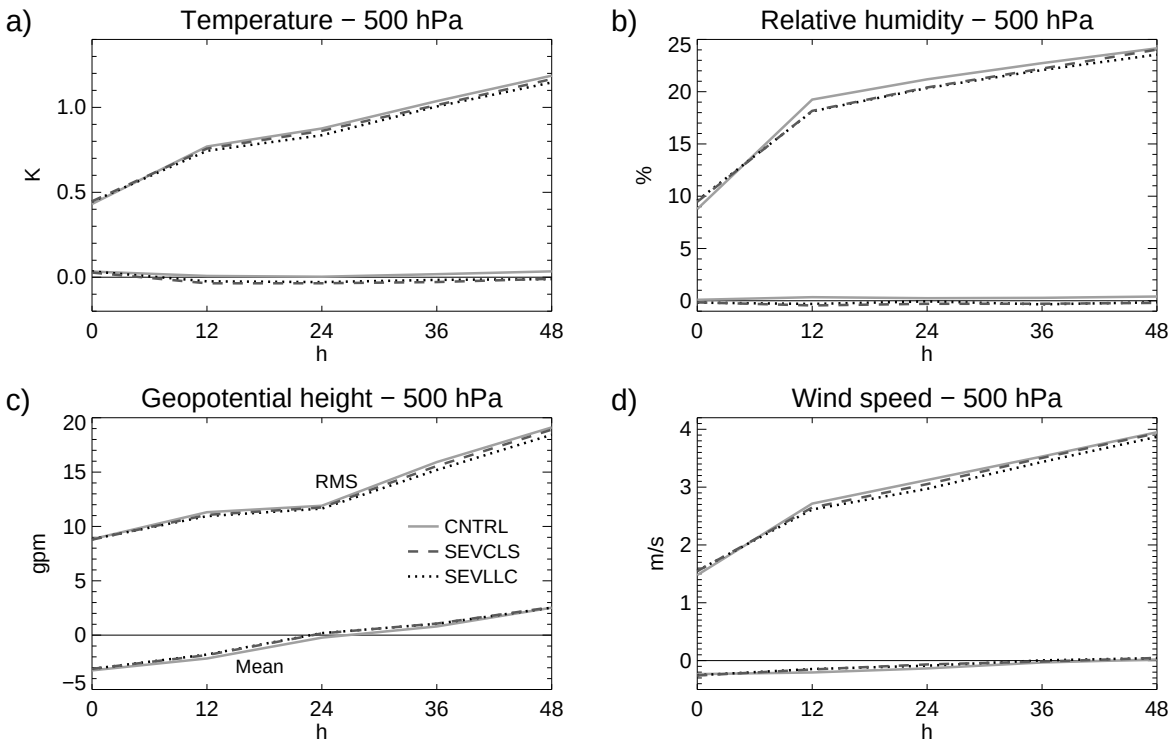

Figure 2.7: RMS and mean forecast errors based on 0000 UTC and 1200 UTC analyses, as a function of forecast lengths 00, 12, 24, 36, and 48 h.

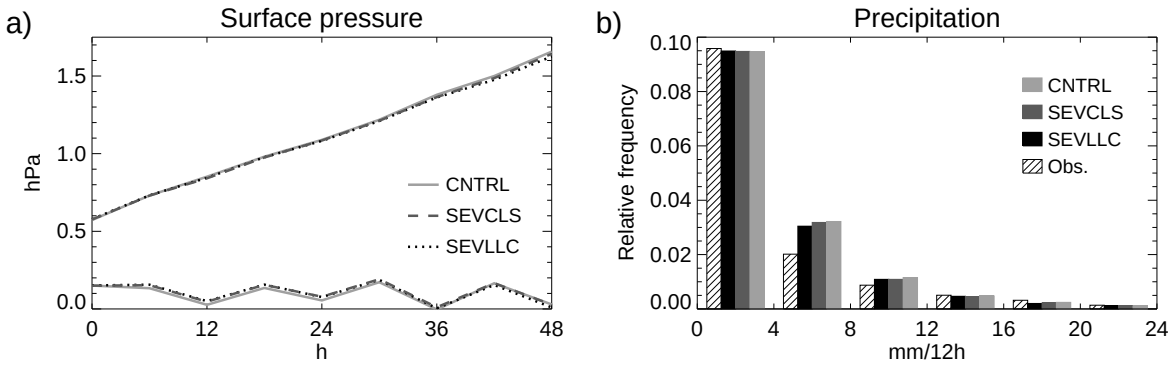

Figure 2.8: (a) RMS and mean forecast errors of surface pressure. (b) Relative frequency distribution for precipitation. The bin sizes are shown on the x-axis. The values of the lowest bin are scaled by 0.1.

mask and a CTP retrieval) were processed. The channels considered in our study were the two water vapour channels (6.2 μm and 7.3 μm) and the 13.4 μm channel. Due to its surface sensitivity, the 13.4 μm channel was not used for land surfaces. Several data preparation steps were defined and, together with the actual data handling, implemented into the variational data assimilation system of the HIRLAM model. Three independent experiments were carried out over a time period of almost two months. These experiments only differ in the types of satellite observations that were assimilated. Besides a control run using conventional observations only, one SEVIRI experiment made use of SEVIRI radiances in clear-sky conditions on top of the conventional observations. A second SEVIRI experiment additionally used the two water vapour channels in low-level cloud conditions, where the radiances were not affected by the cloud.

The major differences in the analysis increments of the SEVIRI experiments compared to CNTRL were found for humidity and the wind components in the mid- and upper troposphere. The differences for wind were smaller in regions with denser radiosonde coverage, due to the constraints of these observations. In a comparison experiment using a 3D-Var technique, these wind increments could not be found.

Generally, these results suggest that additional dynamical information was extracted from the assimilated temporally highly resolved SEVIRI radiances. And that the characteristic trait of 4D-Var systems to gain increments in mass and/or wind fields by 'tracking' certain features in the satellites images, might also be beneficial at regional scales.

The evaluation of the HIRLAM forecast accuracy against radiosondes revealed very encouraging results for the investigated period. The RMS errors of the forecasts for almost all upper-air variables decreased when SEVIRI data were assimilated. The largest positive impacts were found for moisture and geopotential height in the middle and upper troposphere. A slight degradation of the forecast scores was found for temperatures around 300 hPa and forecast lengths of 24 and 36 h. The evaluation of the forecast accuracy for surface variables showed small improvements for surface pressure and precipitation. Both the cloud-free and the low-level cloud SEVIRI experiments were found to perform better than the control run. The best results were achieved for the SEVLLC experiment including observations under low-level cloud conditions.

The results of our study highlight the potential benefit of assimilating SEVIRI observations in a limited-area model using a four-dimensional variational data assimilation system. The results suggest further that the assimilation of observations under low-level cloud conditions provide additionally useful information to the NWP system and highlight the importance of cloudy satellite observations for further improvements in numerical weather forecast.

Acknowledgements

This work was supported by the European Organisation for the Exploitation of Meteorological Satellites (EUMETSAT) in the framework of the Research Fellowship Program and by the Swedish National Space Board (Contract Dnr 105/08:1). The contribution of one of the co-authors (Bennartz) was funded by the U.S. Joint Center for Satellite Data Assimilation (JCSDA). The valuable comments of two anonymous referees are appreciated.

3 An extended observation operator in HIRLAM 4D-VAR for the assimilation of cloud-affected satellite radiances

Authors: M. Stengel[1], M. Lindskog[1], P. Undén[1], N. Gustafsson[1], R. Bennartz[2]

Article published in *Quarterly Journal of the Royal Meteorological Society Volume 136, Issue 649, April 2010 Part B, Pages: 1064-1074* (`http://dx.doi.org/10.1002/qj.621`)

Abstract

An extended observation operator for the direct assimilation of cloud-affected infrared satellite radiances in the HIgh Resolution Limited Area Model (HIRLAM) is examined. The operator includes a simplified moist physics scheme, which enables the diagnosis of cloudiness in itself using background values of temperature, moisture, and surface pressure. Subsequently, a radiative transfer model provides simulated cloud-affected radiances to be used as background equivalents to the satellite observations. The observation operator was evaluated by using infrared observations measured by the Spinning Enhanced Visible and InfraRed Imager (SEVIRI). An observation screening procedure, which incorporates SEVIRI cloud retrieval products, supports an improved selection of usable cloudy scenes leading to good agreements between the observations and background equivalents. The tangent-linear observation operator was verified against finite differences from its non-linear formulation. The increments revealed a near-linear behaviour for the selected channels for a large number of cases. The adjoint observation operator was used to derive brightness temperature sensitivities with respect to temperature and moisture changes in the presence of radiance-affecting clouds. Differences to the clear-sky sensitivities were found in and below clouds. In a four-dimensional variational data assimilation experiment, cloud-affected SEVIRI observations were assimilated resulting in additional increments in both moisture and wind fields. The corresponding analysis fields revealed a reduced deviation from the observations for the majority of all cloudy scenes and a reduced bias

[1]Swedish Meteorological and Hydrological Institute, Folkborgsvägen 1, Norrköping, Sweden
[2]Atmospheric and Oceanic Sciences Department, University of Wisconsin, Madison, Wisconsin, USA

for wind and temperature in the upper troposphere against independent radiosonde observations. Overall, our results highlight the capability of this observation operator in the HIRLAM assimilation system and encourage its application for an extended usage of cloudy satellite observations in numerical weather prediction.

3.1 Introduction

The accuracy of numerical weather prediction (NWP) systems greatly benefits from the assimilation of satellite observations. The number of assimilated satellite observations has significantly increased during the last years providing a comprehensive data source well resolved in space and time (Kelly and Thépaut, 2007). However, the vast majority of utilized satellite observations in NWP systems is located in clear-sky regions while observations in cloudy regions have almost completely been discarded from the assimilation process in the past. This rejection is partly caused by an insufficient treatment of clouds in radiative transfer (RT) models and partly due to general shortcomings in the provision of a proper cloud description in the background fields. Furthermore, the analysed atmospheric state vector in NWP systems does usually not contain any cloud variables. These assimilation limitations are even more significant when infrared (IR) radiances are considered. In this spectral range, the radiation interacts quite heavily with cloud particles, which leads to increased errors in the RT calculations, if clouds are not properly accounted for.

Different techniques have recently been explored to overcome these problems enabling the direct assimilation of cloudy IR radiances. Sophisticated screening procedures rejecting only channels that are actually affected by clouds have been a natural approach. For example Stengel et al. (2009) demonstrated the success of such a method when applying it to infrared radiances of the Spinning Enhanced Visible and Infra-Red Radiances (SEVIRI) resulting in improved short-range forecasts of the HIgh Resolution Limited Area Model (HIRLAM, Undén et al. (2002a)).

Pavelin et al. (2008) used derived estimates of cloud top pressure and effective cloud fraction to constrain a fixed single-layer cloud in their assimilation studies, using simulated and slightly cloud-affected observations from advanced infrared sounders. Their one-dimensional variational data assimilation (1D-Var) results showed clear improvements of the analysis profiles over the first guess. Recently, the direct assimilation of cloud-affected infrared IR radiances was investigated in McNally (2009) using the four-dimensional variational data assimilation (4D-Var) mode of the global NWP model of the European Centre for Medium-Range Weather Forecasts (ECMWF). He introduced two new variables for cloud top pressure and effective cloud fraction (describing a single layer cloud) into the analysis control vector, which were uncoupled to (but simultaneously determined with)

all other control vector variables during the assimilation process.

A different strategy was proposed by Chevallier et al. (2004). They introduced an extended observation operator, which internally diagnoses profiles of cloud cover and cloud condensate from the background values of the model state vector variables. Tangent-linear and adjoint formulations of the observation operator account directly for the interaction between the cloud parameters and the state vector variable increments during the assimilation. Chevallier et al. (2004) investigated the capability of this method with respect to IR radiances from the Advanced InfraRed Sounder (AIRS) and from the Meteosat Visible and InfraRed Imager (MVIRI) and found potential benefits in assimilating the upper-tropospheric channels such as MVIRI's 6.3 μm channel.

Based on these ideas we extended the observation operator for satellite radiances in the limited area NWP model HIRLAM. The operator now contains a diagnostic cloud scheme and a state-of-the-art radiative transfer model. The capability of this observation operator was evaluated using IR radiances from the Spinning Enhanced Visible and InfraRad Imager (SEVIRI). This instrument provides measurements in more spectral bands than its precursor MVIRI and therefore motivates a reapplication of this assimilation strategy to SEVIRI. High quality SEVIRI cloud retrieval products allow furthermore a more detailed assessment of the observation operator performance and enable extended possibilities for improved observation screening procedures.

This paper begins with an overview of the observation operator within the HIRLAM variational data assimilation (Var) system (section 3.2), followed by a brief description of the satellite data used (section 3.3). The observation operator is evaluated in section 3.4. This includes investigations of firstly, simulated cloud-affected radiances and their departures from observations, secondly, radiance increments of the tangent-linear observation operator in the vicinity of the background errors, and thirdly, sensitivities of the simulated radiances with respect to temperature and moisture perturbations in the presence of clouds. Finally, a 4D-Var experiment, using cloud-affected SEVIRI radiances, is presented and discussed in section 3.5.

3.2 The satellite observation operator in HIRLAM Var

The HIRLAM variational data assimilation scheme was initially described and tested in Gustafsson et al. (2001) and Lindskog et al. (2001). The development of its four-dimensional Var (4D-Var) mode is documented in Huang et al. (2002) and Gustafsson (2006). In our study the forecast model is run at a spatial resolution of 22 km. However, the data assimilation system has an incremental formulation and the assimilation increments are applied at an horizontal resolution of 44 km. The reader is referred to Stengel et al. (2009) for further information about other model specifications, which are basically

identical in this study, except for two deviations. Firstly, modifications to the observation operator for satellite radiances have been introduced in the framework of this study, which is described in this section. Secondly, only one outer-loop is applied in 4D-Var due to the extensive computational cost the direct utilization of the tangent-linear (TL) and adjoint (AD) of the observation operator for a large number of satellite observations.

The modified observation operator for satellite radiances consists in our study of two main parts as proposed in Chevallier et al. (2004). The first part is a simplified moist physics scheme (SIMPHYS hereafter). The second part is a fast radiative transfer model. The two parts are described in more detail below. In general and considering the observation operator as a whole, its non-linear (NL) formulation provides simulations of cloud-affected satellite radiances using the model background fields of temperature, moisture and surface pressure, interpolated to the observation location. In the following we will use the notation 'clear-sky observation operator' if SIMPHYS is omitted.

A great advantage of this method is that a near-Gaussian behaviour of the background errors in both model space and radiance observation space can be assumed. Evidence justifying this assumption will be shown in section 3.4.1. An explicit consideration of possible non-Gaussian errors of the intermediate cloud variables can therefore be neglected. Another advantage of this observation operator is the implicit treatment of multi-layer clouds, since the cloud variables are defined at all model levels, which can be used directly in the radiative transfer calculations. Despite these advantages, the modelling of the cloudiness contains errors, which add additional uncertainties and must be regarded as a disadvantage of this method.

3.2.1 SIMPHYS

The SIMPHYS scheme, which was developed at ECMWF, contains two major components. The first component is a simplified convection scheme, which is based on the mass-flux approach. It is largely along the lines of Lopez and Moreau (2005) but with a modified formulation of the entrainment and detrainment, and with a different treatment of shallow convection. The second component of SIMPHYS is a simplified large-scale cloud scheme (Tompkins and Janisková, 2004), which statistically accounts for subgrid-scale variability through a uniform probability density function.

In our study, SIMPHYS is employed to diagnose liquid water content (LWC), ice water content (IWC), and cloud cover (CC) at each individual model level. The background values of temperature, moisture, and surface pressure, which represent a subset of the state vector in the HIRLAM variational assimilation, are used as input variables. The cloud diagnosis is done separately at each observation location. No cloud information is passed forward in time or exchanged between different observation locations. A total cloud fraction was calculated from the cloud cover profiles using a maximum-random

overlap assumption. The diagnosed cloud parameters were found to be very similar to those modelled by the cloud schemes in the operational HIRLAM forecast model, therefore proving the realistic performance of SIMPHYS. The TL and the AD versions of SIMPHYS will hereafter be referred to as SIMPHYS-TL and SIMPHYS-AD, respectively.

3.2.2 Radiative transfer model

To calculate simulated radiances, the Radiative Transfer Model for TOVS (RTTOV, (Eyre, 1991; Saunders et al., 1999)) is employed. RTTOV version 8.5, which was used in our study, and following versions contain an advanced interface (RTTOVCLD, Saunders et al. (2005)) to include profiles for LWC, IWC and CC. These profile values were taken directly from the SIMPHYS output. The calculation of the cloud absorption in RTTOV-8.5 is largely along the lines of Chevallier et al. (2002). Clouds are treated as multi-layer grey bodies and their contribution to the radiance is calculated using their horizontal coverage and their frequency-dependent emissivity. This is done in each NWP model layer, whereas the gas absorption in RTTOV is calculated at 43 fixed levels. Scattering of cloud particles in the IR is not taken into account in the RTTOV version used here.

3.2.3 Tangent-linear and adjoint formulation

In the tangent-linear observation operator, perturbations in cloud variables are produced in SIMPHYS-TL with respect to input perturbations in the state vector variables. All these perturbations are subsequently jointly used as input to the RTTOV-TL. The adjoint formulation of the observation operator employs firstly RTTOV-AD, which delivers increments in the cloud variables as well as in the state vector variables with respect to radiance perturbations. Secondly, the cloud variable increments are converted to additional state vector variable increments within SIMPHYS-AD.

We consider the internal treatment of increments in the cloud variables and the corresponding interactions with the state vector variables in the TL and AD observation operator to be superior to observation operators which only utilize fixed background cloud amounts.

3.3 Satellite observations used

3.3.1 SEVIRI radiances and cloud retrieval products

The SEVIRI instrument (Schmetz et al., 2002), which currently operates on-board the geostationary weather satellites Meteosat-8 and Meteosat-9, is an optical imaging spectrometer measuring top-of-the-atmosphere (TOA) radiances in 12 spectral channels. For this study, three of its eight infrared channels were used, which are spectrally located

around 6.25 μm and 7.35 μm (also referred to as water vapour channels), and around 13.40 μm. In the following the notations WV062, WV073 and IR134 are used for these channels. The spatial resolution of the measurements is approximately 5 km over Central Europe. However, five by five pixel box (quadrant) averages are used in our study. This was chosen with respect to the NWP model resolution and in order to increase the spatial representativeness of the observations. Two SEVIRI cloud retrieval products, namely cloud mask and cloud top pressure (CTP), were processed utilizing a software package (Le Gleau and Derrien, 2002) developed in the framework of the EUMETSAT Satellite Application Facility on Nowcasting & Very Short Range Forecasting. The cloud mask was used to estimate the total cloud fraction by dividing the number of cloud-filled pixels by the total number of pixels in each quadrant. Quadrants with a cloud fraction of 1 were assigned with an average cloud top pressure value. The notation cloud fraction, cloud top pressure and observation (and according acronyms) are in the following used for the representative value assigned to each quadrant. Furthermore, the notation scene will be equivalent to quadrant in this paper.

3.3.2 Initial screening procedure

Useful cloud-affected radiances were identified using observations and simulations by the following criteria. Firstly, only scenes were kept for which both the satellite cloud products and the cloud scheme in the observation operator reported cloudy situations with a total cloud fraction of at least 0.1. Secondly, the effect of the cloud on the radiance had to be greater than 0.5 K, which was inferred from RT simulations with and without cloud information. This was checked for each channel separately.

For quadrants over sea all three channels were considered, while the IR134 channel was rejected for land quadrants. The latter was done with respect to a lack of proper land surface temperature and emissivity knowledge, which would have resulted in additional simulation errors due to a general surface sensitivity of TOA radiances in this channel.

A further partition of the data was made dividing the data into two classes with different cloudy conditions. The first class contained scenes with broken clouds, determined by total cloud fractions between 0.1 and 0.9. The second class contained scenes with full cloud overcast (total cloud fraction of 1.0). For both classes, the cloud fraction criteria had to be fulfilled by the satellite product as well as by the modelled cloudiness. Scenes with cloud fractions between 0.9 and 1 were rejected to avoid strong non-linear processes near cloud saturation as discussed in section 3.4.2.

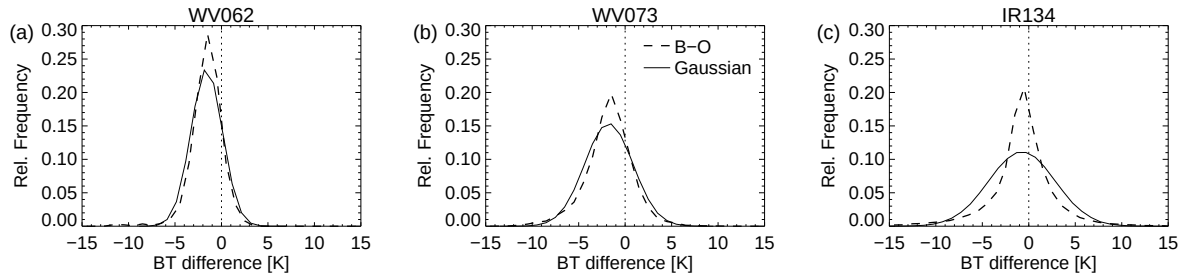

Figure 3.1: Relative frequency distribution of brightness temperature (BT) differences between background and observations (B-O) for scenes with broken cloudiness and SEVIRI channels (a) WV062, (b) WV073, and (c) IR134. The Gaussian distributions with the same error characteristics are also shown.

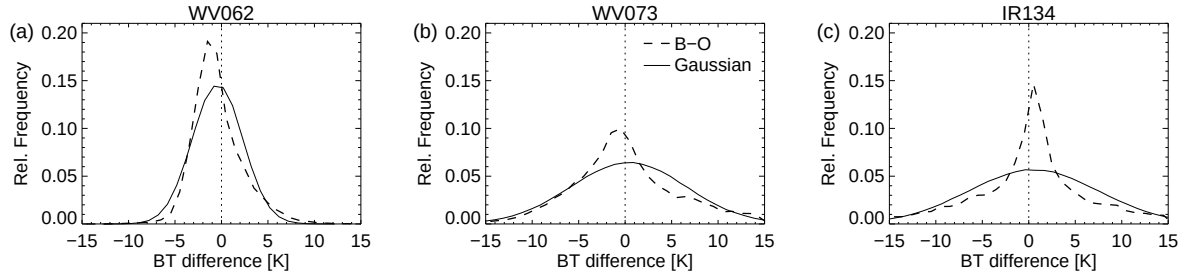

Figure 3.2: Same as Figure 3.1, but for scenes with overcast clouds.

3.4 Evaluation of the observation operator

3.4.1 Background departures in observation space

Embedded in the full HIRLAM 4D-VAR, the observation operator was used to monitor simulated and observed cloudy SEVIRI radiances with an hourly resolution in a two day test period from 00 UTC on 1 June to 18 UTC on 2 June 2006. Assimilation cycles were performed every 6 h using standard in-situ measurements which include surface station, radiosonde and pilot-balloon reports, and observations from ships, aircraft and buoys. Cloudy SEVIRI observations, defined and preselected as described in section 3.3, were kept passive during the minimization and were only sampled with their NWP equivalents. No further quality check was applied at this stage.

The background minus observation (B-O) departures are shown in Figure 3.1 for broken cloud scenes and in Figure 3.2 for overcast scenes, respectively. The departures are characterized by a near-symmetric distribution for broken clouds and overcast cases and for all channels. The largest deviations from a Gaussian distribution with the same error characteristics can be found for the IR134 channel in overcast situations. However, the skewness of the distribution is relative small in all channels considered. This is a clear improvement over radiance simulations using a clear-sky observation operator only. The

Table 3.1: Mean and standard deviation (Std) of background-minus-observation departures (given in Kelvin) for SEVIRI channels WV062, WV073, and IR134. The values are reported for scenes with broken clouds and overcast conditions for the entire data set (all), and for scenes with high clouds only (high) and low clouds only (low). The sample sizes are also reported.

	Broken clouds - all			Overcast - all		
	Mean	Std	Number	Mean	Std	Number
WV062	-1.6	1.7	2915	-0.4	2.7	7426
WV073	-1.8	2.6	10707	0.4	6.2	11877
IR134	-0.7	3.6	21578	0.5	7.1	15958
	Broken clouds - high			Overcast - high		
	Mean	Std	Number	Mean	Std	Number
WV062	-1.6	1.7	2915	-0.4	2.7	7426
WV073	-1.8	2.6	10707	0.3	6.3	11249
IR134	-1.2	4.1	13319	0.2	7.9	11829
	Broken clouds - low			Overcast - low		
	Mean	Std	Number	Mean	Std	Number
WV062	–	–	–	–	–	–
WV073	-1.0	1.9	818	1.8	4.2	628
IR134	0.1	2.3	8259	1.5	3.4	4129

corresponding B-O error distributions are usually characterized by a strong 'warm-tail'. This is due to the on average decreasing effect of clouds on the brightness temperature, which is not accounted for in such an operator.

Table 3.1 reports the calculated mean and standard deviation error values for the data discussed. As already indicated in the figures, the standard deviations under broken cloud conditions are small for WV062 (1.7 K), larger for WV073 (2.6 K) and largest for IR134 (3.6 K), revealing a dependence on the vertical position of the sensitivity functions. The standard deviation values under overcast conditions are considerably higher with 2.7 K, 6.2 K and 7.1 K for WV062, WV073 and IR134, in comparison with broken cloud conditions. Conversely, the mean errors (between -0.4 K and 0.5 K) are clearly smaller for scenes with overcast than in broken cloud scenes (between -1.8 K and -0.7 K), for which the largest values are found for the water vapour channels. As for the skewness of the distributions, the discussed error characteristics reveal improvements over the corresponding results of a clear-sky observation operator.

To assess a possible dependence of the simulation accuracy on the vertical position of the clouds, we additionally calculated the error values separately for scenes with different cloud top heights. A cloud top pressure threshold of 500 hPa was applied to the modelled cloudiness, dividing the data set into groups with high-level clouds and low-level clouds, respectively. The corresponding error characteristics are also reported in Table 3.1. Standard deviation values of 4.2 K and 3.4 K for WV073 and IR134 in overcast scenes with low-level clouds are clearly smaller than in overcast scenes with high-level clouds, where values of 6.3 K and 7.9 K were found. The error standard deviations for broken cloud

scenes with low cloud tops are 1.9 K and 2.3 K for WV073 and IR134, respectively, thus the smallest values found for these two channels. Too few data could be collected for WV062 in low-level cloud scenes preventing calculations of the corresponding error characteristics. Applying the CTP threshold to the satellite-retrieved CTP did not give any clear signal compared to the modelled CTP. However, a further improved matching between background and observations might be reachable, if differences between modelled and retrieved CTP are investigated.

These results prove a good performance of the observation operator in scenes with broken clouds as well as in overcast conditions resulting in acceptable mean and standard deviations of the background brightness temperatures compared to observations. However, the mean errors found highlight the need for a bias correction prior to any assimilation of these observations.

3.4.2 Linearity test

Assimilation increments of the model state vector variables $\delta\mathbf{x}$ from eight consecutive HIRLAM 4D-Var cycles during the 1st and 2nd of June in 2006 were used to passively monitor tangent-linear radiance increments $\mathbf{H}(\delta\mathbf{x})$ and non-linear radiance increments $(H(\mathbf{x}^b + \delta\mathbf{x}) - H(\mathbf{x}^b))$. Cloudy scenes were chosen as described in section 3.3 but with an additional spatial thinning. The agreement between tangent-linear and non-linear radiance increments was compared in terms of correlation coefficients (Table 3.2). A further separation into high clouds and low clouds, using a threshold of 500 hPa for the modelled cloud top pressure, was also done.

The calculated correlation coefficients for all broken cloud scenes are 0.95, 0.89 and 0.82 for channels WV062, WV073 and IR134, respectively. The values for all overcast scenes are lower and lie between 0.88 and 0.66. Additionally splitting the data dependent on the cloud top height reveals particularly increased values for WV073 in low-level cloud scenes. The values for IR134 are similar for low and high clouds in broken cloud scenes, but show a small dependency in overcast scenes. It should be noted that high-level cloud scenes constitute the majority of the considered data set leading to similar correlation coefficients for those cases as for the entire data set. As mentioned in the previous section, too few WV062 data fulfilling the selection criteria could be found for scenes with low-level clouds. Generally, the derived correlation coefficient statistics can help to select channels to be used for assimilation. Chevallier et al. (2004) for example used a correlation coefficient threshold of 0.85 prior to their 1D-Var studies, but channels with even smaller values could potentially be used.

Under the assumption that strongest non-linearities in the data set will occur, if the cloud cover is in the vicinity of 1, we identified a subset of all cases, for which this possible source of non-linearity is avoided. Here, the criterion of cloud cover being between 0.1 and

Table 3.2: Correlation coefficients (R) between tangent-linear and non-linear radiance increments. The values are reported for broken clouds and overcast conditions for the entire data set (all), and for scenes with high clouds only (high) and low clouds only (low). The numbers in the brackets represent a special subset of the data (see text for further explanation). The sample sizes are also reported.

	Broken clouds - all		Overcast - all	
	R	Number	R	Number
WV062	0.95 (0.96)	93998 (86074)	0.88 (0.87)	239446 (197287)
WV073	0.89 (0.92)	345397 (318008)	0.71 (0.72)	383076 (300980)
IR134	0.82 (0.87)	392965 (371095)	0.66 (0.74)	352191 (267125)
	Broken clouds - high		Overcast - high	
	R	Number	R	Number
WV062	0.95 (0.96)	93998 (86074)	0.88 (0.87)	239446 (197287)
WV073	0.89 (0.92)	319157 (294231)	0.70 (0.72)	362837 (288239)
IR134	0.82 (0.87)	244509 (233289)	0.66 (0.74)	241077 (187207)
	Broken clouds - low		Overcast - low	
	R	Number	R	Number
WV062	– (–)	– (–)	– (–)	– (–)
WV073	0.95 (0.96)	26240 (23777)	0.88 (0.94)	20239 (12741)
IR134	0.83 (0.88)	148456 (137806)	0.62 (0.85)	111114 (79918)

0.9 for broken clouds, and being equal to 1 for overcast scenes, had to be fulfilled by the cloudiness diagnosed from $(\mathbf{x}^b + \delta\mathbf{x})$ as well. The corresponding correlation coefficients between the tangent-linear and non-linear increments are given in brackets in Table 3.2, revealing considerably increased correlations for WV073 and IR134. The largest improvements for these channels were found for overcast scenes with low cloud tops. Here, the correlation coefficients changed from 0.88 to 0.94 for WV073 and from 0.62 to 0.85 for IR134. All other scenes were also characterized by larger correlation coefficients for these channels. These numbers suggest that this strategy can additionally be used to reject cases for which strong non-linearities might occur. However, the implementation of such a method applied to $(\mathbf{x}^b + \delta\mathbf{x})$ or a direct TL/NL increment test might be difficult.

One practical approach could be to analyse the cloudiness from $(\mathbf{x}^b + \delta\mathbf{x})$ at each observation location already in the observation preprocessing. However, $\delta\mathbf{x}$ is not known prior to the minimization. For that reason $\delta\mathbf{x}$ could be approximated by a perturbation vector with values in the order of the background errors.

3.4.3 Sensitivity analysis

To calculate the gradient of the observational part of the cost function in variational frameworks, the sensitivities of simulated brightness temperature with respect to the control vector variables, also known as Jacobians, need to be provided. The sensitivities in cloudy scenes differ for many cases significantly from clear-sky scenes. In this section we exemplary analyse these sensitivities which were derived using the adjoint observation

operator and radiance perturbation of 1 K. Four selected cases are discussed in the following. All cases are characterized by different cloudy conditions, which can be summarized as follows:

- Case1: Broken high-level ice cloud above broken low-level water cloud
- Case2: Broken low-level water cloud
- Case3: Overcast of geometrically thick high-level mixed-phase cloud
- Case4: Overcast of geometrically thin low-level water cloud

Figures 3.3-3.6 show the derived sensitivities. In the following, these will be discussed with respect to their clear-sky equivalents, which were derived for the purpose of comparison using the observation operator excluding SIMPHYS. In general, deviations between the cloudy sensitivities and their clear-sky equivalents, occur in all four cases. The deviations depend on the channel and on the vertical position of the clouds. The ice cloud in Case 1 affects all the sensitivities of all three channels with the largest effect for channel IR134. The clear-sky sensitivity for the latter is very small. The sensitivities due to the cloud are visible through the entire cloud layer with increasing amplitude above the maximum cloud cover and decreasing amplitude below. An effect of the lower cloud is only slightly visible for IR134. In Case 2 only the channel IR134 is affected, showing slightly increased sensitivities within the cloud layers. The water vapour channels are not affected due to the low location of the cloud. In Case 3 the sensitivities in all three channels show a relative strong response to the cloud. The response is basically located between the cloud top and the layer with a cloud fraction of 1.0. The sensitivities below that layer quickly drop to zero, which indicates a high cloud optical thickness there. In Case 4, the low-level cloud affects the sensitivities in IR134 and WV073, the latter to a small extent.

Generally, the brightness temperatures sensitivities with respect to temperature and moisture differ considerably from their clear-sky equivalents in the presence of clouds. This is due to the capability of the operator to account for the impact of varying cloudiness on the radiance, and the interaction between the cloudiness and temperature and moisture. In clouds the sensitivities generally decrease (i.e. become more negative compared with clear-sky conditions) for moisture and increase for temperature and have mostly the same sign as the clear-sky equivalents. A simplified explanation is that increased moisture usually leads to more cloudiness via its dependence on relative humidity (RH) in SIMPHYS resulting in lower radiances. This is similar to the effect that increased moisture has on gaseous absorption. Furthermore, increased temperatures lead to less cloudiness, due to decreased RH, resulting in higher radiances. This amplifies the temperature dependent emission of an atmospheric layer for a given layer emissivity. Below cloud layers, the

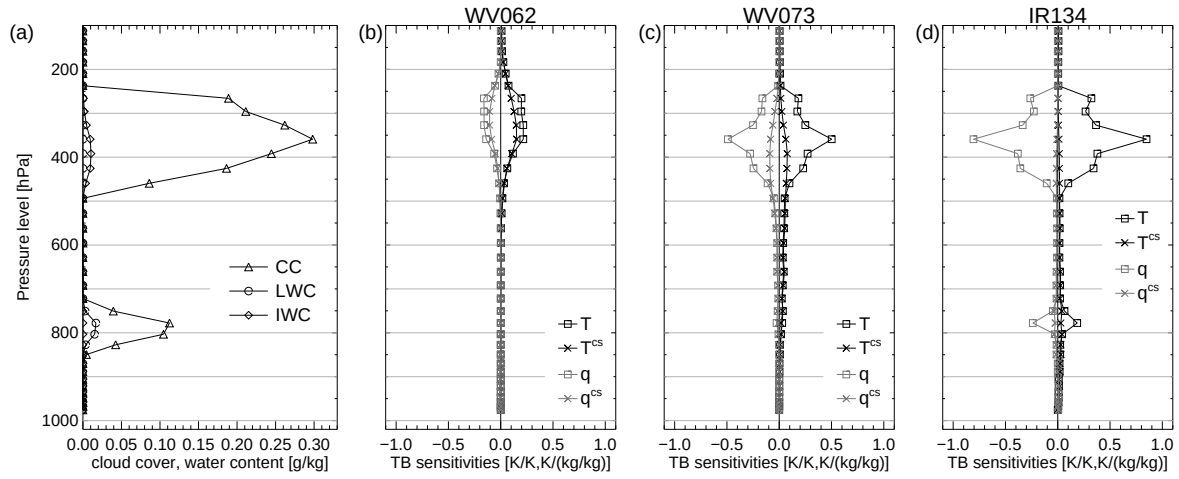

Figure 3.3: (a) Modelled profiles of liquid water content (LWC), ice water content (IWC), and cloud cover (CC) for case 1. (b)-(d) Corresponding brightness temperature (TB) sensitivities with respect to changes in temperature (T, black icons) and specific humidity (q, grey icons). Results from the observation operator without SIMPHYS are marked with the superscript 'cs' for clear-sky conditions. The values for specific humidity were scaled at each level with 10% of the corresponding background specific humidity value.

operator further accounts for the sealing effect of increased optical depth in the overlying cloud layer.

The sensitivity curves are often relatively smooth. Jumps in the curves occasionally occur near the cloud top and near the cloud base, and for in-cloud layers with less cloud fraction than the layers underneath and above, as for example indicated for channel IR134 in Figure 3.5 near 275 hPa. However, analysis increments are usually smooth due to the effect of the background error constraints. The utilization of flow-dependent background error statistics might be an option for further improvements.

3.5 A 4D-Var case study

Building on the investigations and results documented in the previous sections, we conducted two 4D-Var experiments (termed 'CNTRL' and 'SEVCLD') for 3 of June 2006 at 00 UTC, subsequent to the monitoring period as described in section 3.4.1. The experimental setup was the same for both experiments, except that in SEVCLD cloud-affected SEVIRI observations were actively assimilated, while they were kept passive in CNTRL. Both experiments had the same background state conditions. The impact of the assimilated satellite observations is shown and discussed in terms of the analyses differences between SEVCLD and CNTRL, the departure of both analyses from passively monitored radiosonde measurements, and the fit of the SEVCLD analysis to the assimilated satellite observations.

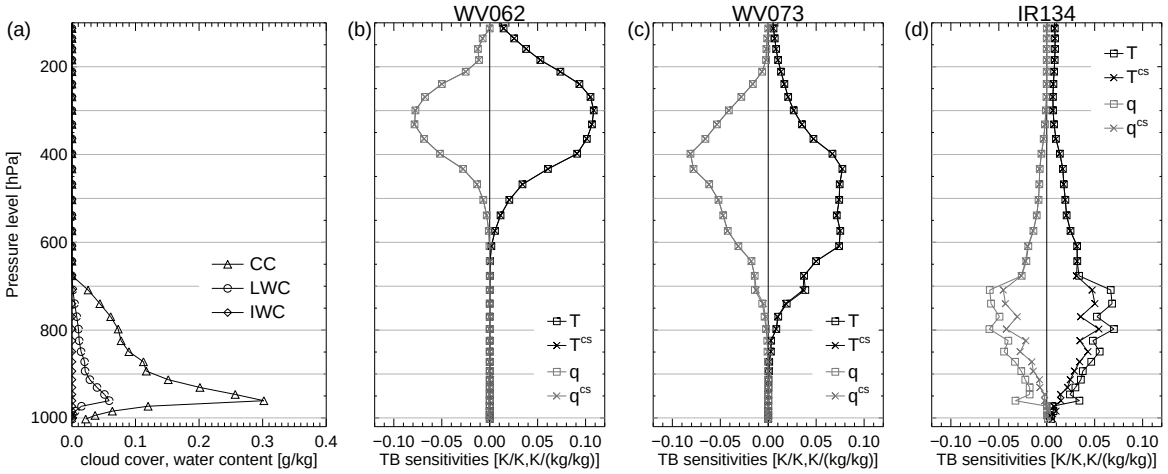

Figure 3.4: Same as Figure 3.3, but for Case 2.

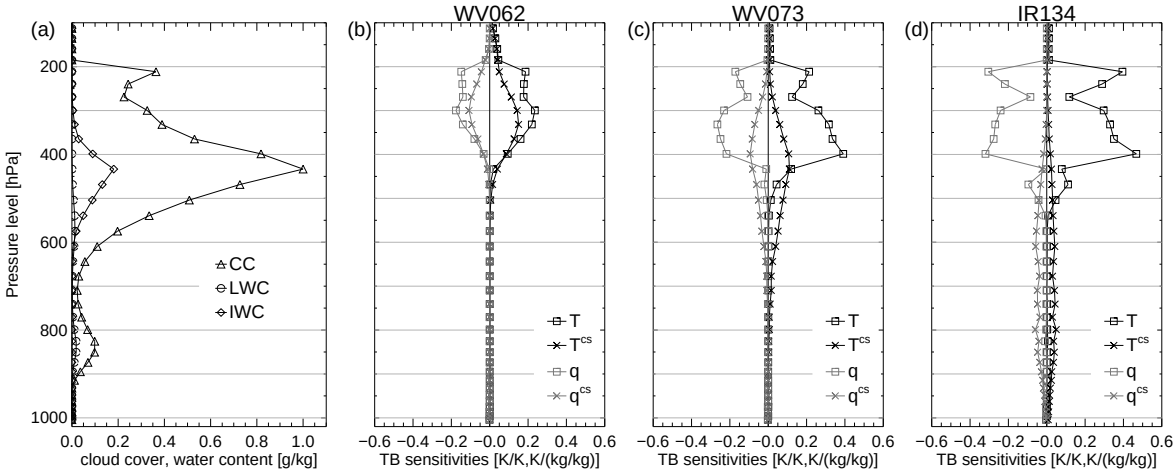

Figure 3.5: Same as Figure 3.3, but for Case 3.

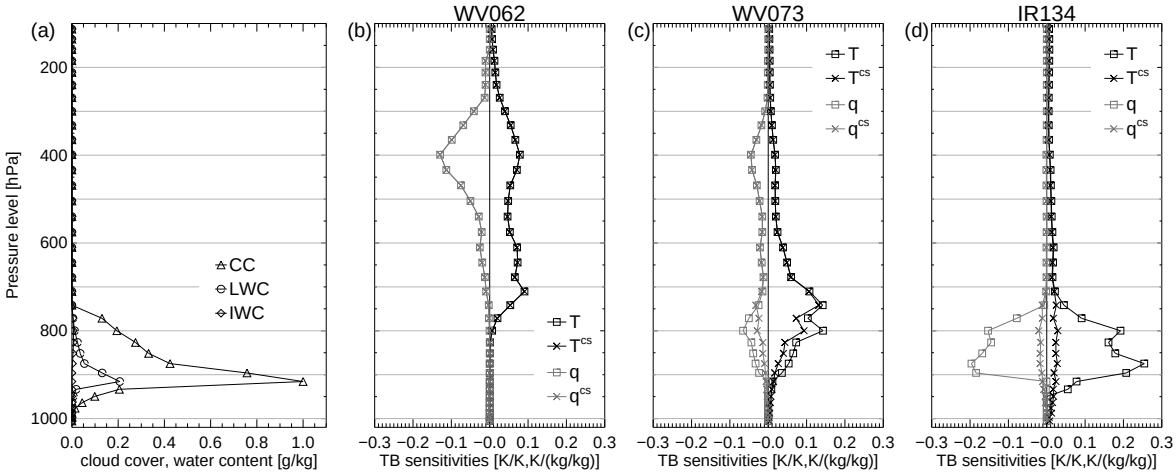

Figure 3.6: Same as Figure 3.3, but for Case 4.

3.5.1 Observation selection and pre-processing

All three channels (WV062, WV073 and IR134) were selected in scenes with broken clouds, while for overcast situations only the WV062 channel and partly the WV073 channels were selected. Due to the low TL/NL increment correlation coefficients (see section 3.4.2), we chose to reject the WV073 channel in overcast scenes with cloud tops above 500 hPa. For the same reason the IR134 channel was not considered in overcast scenes.

All channels were bias corrected, depending on the vertical position of the cloud and the total cloud fraction, by a fixed offset equal to the B-O mean errors for each group as given in Table 3.1. The corresponding calculated standard deviations for each group was used as the observation error standard deviations (σ^o). The background error standard deviations in observation space (σ^b) were arbitrarily assumed to be 1 K. In a quality check, observations with background departures greater than $\sqrt{2(\sigma^{o2} + \sigma^{b2})}$ were rejected. Finally, a spatial thinning with a thinning length scale of 50 km was performed to eliminate the effects of spatial observation-error correlations, which are not taken into account in the minimization. As for the monitoring period, SEVIRI observations are provided at the centre of each of the six observation windows within the 6 h assimilation window. Histograms of bias-corrected background departures for all assimilated observations are shown in Figure 3.9.

3.5.2 Impact on the analysis

The difference field (SEVCLD-CNTRL) of analysed 500 hPa relative humidity in Figure 3.7(b) documents the impact of assimilated cloud-affected SEVIRI observations at

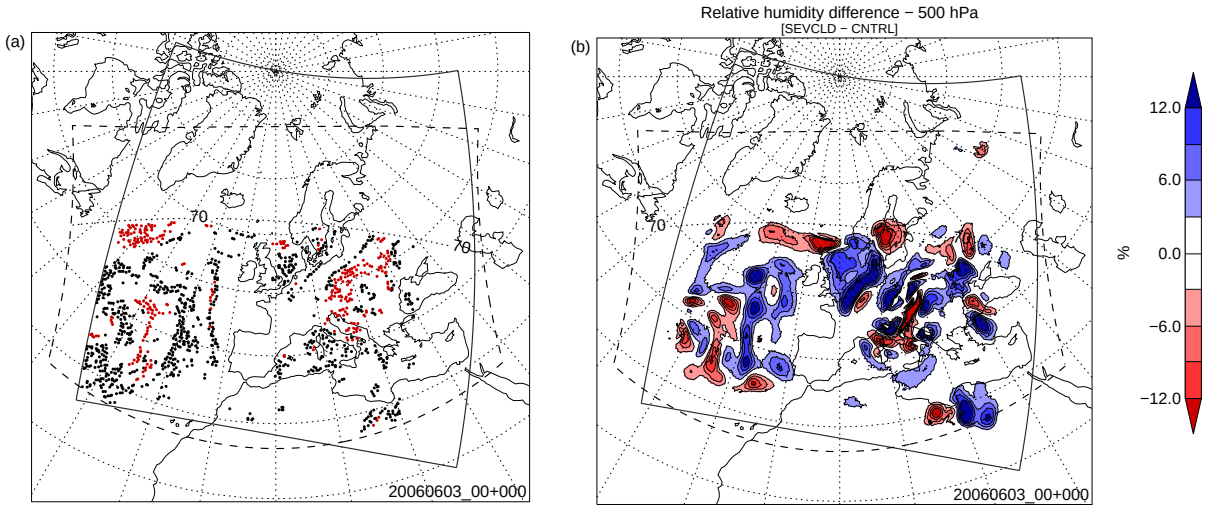

Figure 3.7: (a) Location of assimilated observations at 00 UTC. Black and red dots mark scenes with broken clouds and scenes with overcast, respectively. (b) Difference fields (SEVCLD-CNTRL) of analysed 500 hPa relative humidity at 00 UTC.

00 UTC. The assimilated observations for this point in time are shown in Figure 3.7(a). Roughly speaking, differences in the relative humidity fields are visible in the regions where SEVIRI observations were located and are approximately in the range of ±25 %. The results for wind speed at 500 hPa exhibit a similar behaviour with differences in the order of ±2 m/s (not shown). The increments in the temperature fields are relative small with the largest amplitude below 1 K in a region in the south-west corner of the model domain. It should also be noted that the found analysis increments might be superimposed by additional flow-dependent adjustments in 4D-Var, caused by observations in other observation windows. Generally, the amplitude of the impact for this cycle is comparable to what was shown in Stengel et al. (2009) for a 4D-Var case study with cloud-unaffected SEVIRI observations. The vertical structure of the analysis increments is complex due to the large variety of the assimilated cloudy scenes, and is not discussed in detail in this paper.

Radiosonde observations located south of 60° northern latitude were selected to calculate their analysis departures for both CNTRL and SEVCLD (Figure 3.8). Since these observation were hold passive during the assimilation these comparisons provide an initial performance estimate. In general, small improvements are found for the biases for SEVCLD while the RMS errors are almost identical between CNTRL and SEVCLD. For temperature the bias is slightly improved in the upper troposphere between 200 and 300 hPa. The bias for u-wind shows smaller values for SEVCLD than for CNTRL in the mid- and lower troposphere, while the bias is slightly increased in SEVCLD above 300 hPa. The bias for the v-wind is, similar to temperature, slightly reduced in the up-

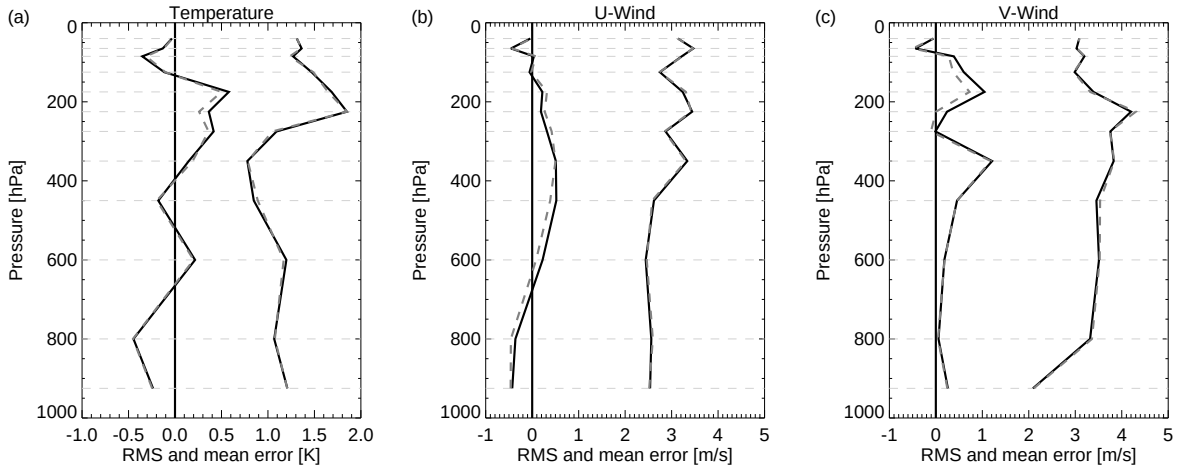

Figure 3.8: Analysis departures of passive radiosonde observations south of 60° northern latitude for (a) temperature, (b) u-wind, and (c) v-wind., for experiments CNTRL (black solid line) and SEVCLD (grey dashed line).

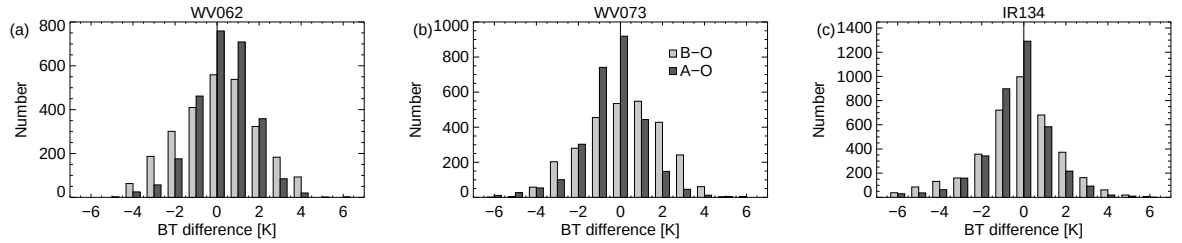

Figure 3.9: Histograms of background (B) and analysis (A) departures of assimilated cloud-affected SEVIRI observations (O) in brightness temperatures (BT) for channels (a) WV062, (b) WV073, and (c) IR134 (1 K bin size).

per troposphere for SEVCLD compared to CNTRL. The differences between CNTRL and SEVCLD were negligible for humidity. Despite the low number of reference radiosondes in these comparisons, they give a first indication of the potential of cloud-affected radiances assimilation. The full potential will have to be assessed by extended forecast verifications based on analyses which include all available observation, which is beyond the scope of this initial study.

Figure 3.9 shows histograms of the observation departures of the analysis, which were recalculated after the assimilation process in SEVCLD. The histograms show a clear improvement of the analysis over the background in terms of their departures from the same cloudy observations for all three channels. A passive monitoring in the CNTRL experiment did not show any significant changes between the analysis and background in this respect. However, a few cases were found in SEVCLD for which the analysis departures were distinctly degraded compared to the corresponding background departures. These

cases could primarily be linked to scenes which were characterized as broken cloud cases in the background and as overcast in the analysis suggesting deficiencies in the tangent-linear assumptions for these cases during the assimilation process.

3.6 Summary and conclusions

In this paper the feasibility of the assimilation of cloud-affected satellite observations in NWP systems is studied. This is approached by extending the HIRLAM observation operator for satellite radiances with a simplified moist physics parametrization scheme. The scheme firstly diagnoses vertical profiles of cloud liquid water, cloud ice water, and cloud cover, and secondly, provides a suitable tool to describe the interaction between the control vector variables and the intermediate cloud variables. This framework is suitable to assimilate cloud-affected radiances avoiding the explicit treatment of cloud variables as a part of the analysis control vector.

The observation operator was applied to three SEVIRI infrared channels WV062, WV073, and IR134. Cloud-affected radiances were selected utilizing also derived SEVIRI cloud products in a data screening procedure. Observation minus background departures were monitored revealing in general a good agreement for all three channels with near-Gaussian error characteristics. The lowest error values were found for the WV062, while the largest errors were found for channel IR134 in the presence of high clouds.

The linearity assumption in the vicinity of the background was investigated for cloudy cases by comparing tangent-linear and non-linear radiance increments. Very high correlations coefficients of about 0.95 were found for channels WV062 and WV073 in the presence of low clouds, while smallest correlation values (0.62) were found for the IR134 channel in overcast situations. Beside scenes with cloud cover values near 1, the tangent-linear observation operator was found to be applicable for most cloudy conditions.

Brightness temperature sensitivities due to changes in temperature and moisture were exemplarily derived and discussed on the basis of four selected cases with different cloudy conditions. Differences to clear-sky equivalents were mainly found in and below clouds with amplitude and shape depending on both the channel and the vertical position of the cloud. The impact of clouds on these sensitivities were found to be properly described by the extended observation operator.

In a preliminary 4D-Var experiment, cloud-affected SEVIRI radiances were actively assimilated with an hourly resolution. The corresponding analysis fields showed additional analysis increments in moisture and wind fields. These increments were mainly located in regions of assimilated cloud-affected satellite observations. The analysis was verified using passively monitored radiosondes which revealed small bias improvements for temperature and wind in the upper troposphere. Furthermore, the analysis departures of the

assimilated cloud-affected radiances were improved against the background proving the consistency of the assimilation approach.

Overall, the discussed extended observation operator is found to provide an appropriate framework for the assimilation of cloud-affected satellite radiances in NWP systems. The performance of the non-linear, tangent-linear and adjoint versions of the operator were found to support the chosen methodology. However, some deficiencies were identified for certain channels in some meteorological situations. The extended observation preprocessing supports an improved observation selection by incorporating satellite derived cloud retrieval products. This can be seen as an additional background check supporting an improved observation selection. It can also be used to reduce the number of problematic cases for which strong non-linearities occur during the minimization. In general it would be of advantage to apply multiple outer-loop iterations, implying a re-linearisation of the cost function. This will be subject to future investigations.

The availability of such an assimilation framework is very encouraging, especially since it can both handle multi-layer clouds and account for the interaction between the cloud properties and analysis control vector elements such as temperature and moisture. Since an explicit inclusion of cloud parameters in the analysis control vector won't be realized in the near future, we believe this framework is worth its application for both research purposes and, if proven to be beneficial for analysis and forecast, in operational frameworks. As a first step we will soon carry out extended assimilation and forecast experiments to assess the full potential of cloud-affected radiances with respect to the forecast accuracy of NWP systems.

Acknowledgements

This work was supported partly by the European Organisation for the Exploitation of Meteorological Satellites (EUMETSAT) in the framework of the Research Fellowship Program and partly by the Swedish National Space Board (Contract Dnr 105/08:1). The contribution of one of the co-authors (Bennartz) was funded by the U.S. Joint Center for Satellite Data Assimilation (JCSDA). The valuable comments of two anonymous referees are appreciated.

4 The impact of cloud-affected IR radiances on forecast accuracy of a limited-area NWP model

Authors: M. Stengel[12], M. Lindskog[1], P. Undén[1]

Manuscript submitted to *Monthly Weather Review* of the *American Meteorological Society* in January 2011

Abstract

The impact of cloud-affected satellite radiances on numerical weather prediction (NWP) accuracy is investigated. The NWP model used is the HIgh Resolution Limited Area Model (HIRLAM). Its four-dimensional variational data assimilation (4D-Var) system was used to assimilate cloud-affected infrared (IR) radiances from the Spinning Enhanced Visible and InfraRed Imager (SEVIRI). Cloud parameters are modelled internally in the observation operator and used in the radiative transfer calculations. The interaction between the cloud parameters and the model state vector variables is incorporated in the adjoint version of the observation operator, which is used to derived cloud-affected Jacobians prior to the inner-loop minimization of the cost function.

This framework supports an extensive usage of satellite observations with spatial coverage extended into cloudy regions which therefore provides additional analysis increments and, if realistic, supports a more accurate description of the atmospheric state. In extended assimilation and forecast experiments the total number of assimilated satellite observations could be increased by approximately 10 %, which was associated with a clear indication of a positive impact of cloud-affected radiances on NWP model forecast accuracy when used used on-top of clear-sky radiance observations. This is shown by reduced forecast errors for upper-air parameters in the mid and upper troposphere in the experiments carried out in this study.

[1]Swedish Meteorological and Hydrological Institute, Folkborgsvägen 1, Norrköping, Sweden
[2]Deutscher Wetterdienst, Frankfurter Str. 135, 63067, Offenbach, Germany

4.1 Introduction

In the past, the measured radiances from various meteorological satellite instruments have been included in the assimilation schemes of numerical weather prediction (NWP) models. These satellite radiances taken under clear-sky conditions were proven to significantly improve the atmospheric analysis and forecast (e.g. Kelly and Thépaut, 2007). The largest impacts are usually found for global NWP models and in regions with spare ground-based observations. Smaller but still noticeable impacts of clear-sky satellite observations can also be found on scales of limited-area models as for example shown in Montmerle et al. (2007) for the ALADIN model, and in Stengel et al. (2009) for the HIgh Resolution Limited Area Model (HIRLAM: Undén et al., 2002b). Stengel et al. (2009) also demonstrated the potential of radiances in the presence of low-level clouds with a negligible effect on the radiance.

Recently, the NWP assimilation schemes at different weather centres have been extended to make use of satellite radiances significantly affected by clouds (e.g. Bauer et al., 2010; Geer et al., 2010; McNally, 2009; Pavelin et al., 2008). These efforts aim at filling the gaps in used satellite coverage which are often left empty due to conducted cloud screening procedures in the assimilation schemes. As a consequence, satellite observations in these weather-active regions, ingested into the NWP system using an appropriate framework, lead to additional analysis increments in these regions. By this, the corresponding atmospheric analysis is, in an ideal case, further drawn towards the true atmospheric state assumed to be subsequently leading to more accurate numerical weather forecast. However, the assimilation of cloud-affected radiances is rather difficult. This is due to the strong interaction of cloud particles with radiation in a wide range of the electromagnetic spectrum, and occurring non-linearities in the cloud processes. Furthermore, the analysis state vector of most operational NWP models does usually not contain any cloud variables. The major reason for the omission of those parameters from the state vector is the significant deviations from Gaussian error characteristics of the first guesses, which will most likely lead to a degraded analysis. One approach to overcome this problem was documented in McNally (2009). Here, the model state vector was locally extended at observation locations only with variables for cloud top pressure and effective cloud fraction. Background values for the cloud parameters were in that work derived from the observed radiances with a least-square procedure. These parameters describe a single-layer cloud and were simultaneously determined with all other control vector variables during the 4D-Var assimilation process. Corresponding impact studies were characterized by small improvements for shorter forecast lengths with the largest extend reported for 700 hPa temperature in the Southern Hemisphere.

A different approach was proposed by Chevallier et al. (2004) with an extended ob-

servation operator for satellite radiances. This operator firstly diagnoses the cloudiness in itself using state vector variables such as temperature and moisture, and secondly accounts for the interaction between these variables and the cloudiness in its linearised and adjoint version. Based on these ideas, an extended observation operator in the HIRLAM had been developed and evaluated (Stengel et al., 2010). The study documented in this article builds on their developments but extends beyond the initial tests by assessing the impact of cloud-affected radiances on HIRLAM analysis and forecast accuracy in extended assimilation and forecast experiments.

For this, spatio-temporal highly resolved geostationary radiances from three infrared (IR) channels of the Spinning Enhanced Visible and InfraRed Imager (SEVIRI: Schmetz et al., 2002) on-board the Meteosat-8 satellite were selected in clear-sky and cloudy conditions as in Stengel et al. (2010). Within a two month period, the impact of the cloud-affected observations on the forecast was quantified by comparing forecast scores against two model runs with different observation selections.

The quantification of the actual impact of cloud-affected satellite radiances on NWP forecast accuracy, using this methodology in a 4D-Var framework, has to our knowledge not been assessed before in the peer-review literature. It provides therefore a valuable information about the benefit of cloud-affected satellite radiances.

In section 2 an overview over the methodology is given including a review of the radiances observation operator and further adaptations done in the course of this work. Section 3 describes the set-up of three assimilation and forecast experiments which were carried out, followed by a discussion of correspondingly introduced changes to the analysis fields and subsequently derived forecast scores in section 4. Section 5 gives a summary and concludes the findings of this study.

4.2 Methodology

4.2.1 The HIRLAM assimilation and forecast system

As described in Stengel et al. (2010) the HIRLAM model was equipped with an extended observation operator for satellite radiances. Included in the observational part of the present form of the cost function in HIRLAM 4D-Var (Equation 4.1), the tangent-linear (TL) formulation of the operator ($\mathbf{H}$) provides the radiance response to increments in the analysis control vector ($\delta\mathbf{x}_i$).

$$J_o = \frac{1}{2}\sum_{i=0}^{K}\{(\mathbf{d}_i + \mathbf{H}(\delta\mathbf{x}_i))^T\mathbf{R}^{-1}(\mathbf{d}_i + \mathbf{H}(\delta\mathbf{x}_i))\} \tag{4.1}$$

In the following, the index i, which denotes each of the K observation windows, will be neglected. The vector $\mathbf{d}$ is defined as the difference (innovation) vector between the observations $\mathbf{y}$ and the modelled radiances $H(\mathbf{x}^b)$, i.e. the background state $\mathbf{x}^b$ projected into radiance space, including the bias correction term $\mathbf{y}^{bc}$:

$$\mathbf{d} = H(\mathbf{x}^b) - \mathbf{y}^o + \mathbf{y}^{bc} \tag{4.2}$$

where H denotes the non-linear observation operator. $\mathbf{x}^b$ is provided at the centre of each observation window by the tangent-linear forecast model which is initialized using a short range forecast of the non-linear model valid at the beginning of the assimilation window. In this study the H term is defined as:

$$H(\mathbf{x}^b) = RT(\mathbf{cl}^b, \mathbf{x}^b) = RT(SP(\mathbf{x}^b), \mathbf{x}^b) \tag{4.3}$$

with RT as the radiative transfer (RT) model and $\mathbf{cl}^b$ symbolizing the modelled cloud profiles of liquid water content (LWC), ice water content (IWC), and cloud cover (CC) diagnosed by a simplified moist physics scheme (SP) (SIMPHYS hereafter). SIMPHYS contains parametrizations for both convection Lopez and Moreau (2005) and large-scale cloud processes (Tompkins and Janisková, 2004). It is applied to the background values, which are collocated profiles of the state vector parameters relevant for the cloud diagnosis and the RT calculation. The reader is referred to Stengel et al. (2010) for more details on SIMPHYS and it s implementation in the HIRLAM system. The RT model used is the Radiative Transfer Model for TOVS (RTTOV: Eyre, 1991; Saunders et al., 1999). Its enhanced cloud module (RTTOVCLD: Saunders et al., 2005) was used, which enables the inclusion profiles of cloud parameters defined at the vertical grid of the NWP model. Important for ice clouds, the absorption coefficient for ice clouds is calculated with respect to aggregate crystals (Saunders et al., 2005) and the effective diameter is diagnosed as in Wyser (1998).

Deviating from Stengel et al. (2010) we replaced the direct utilization of the tangent-linear observation operator (Equation 4.1) during the minimization by the application of the Jacobians matrix $\mathbf{K}$:

$$\mathbf{H}(\delta\mathbf{x}) = \mathbf{K}\delta\mathbf{x}. \tag{4.4}$$

The Jacobian matrix contains the partial derivatives of the radiances with respect to the analysis control vector elements. The approach used for deriving the Jacobians in the presence of radiance-affecting clouds is given below. Furthermore, the adjoint of the operator was replaced by the utilization of the transpose of $\mathbf{K}$. Technically speaking, the Jacobian solution is computationally less expensive, because only a simple mathemati-

cal multiplication of the actual state vector increments with the Jacobians is needed at each iteration step to calculate the response of the radiances due to that state vector increment. The same applies to the response of the state vector values due to changes in radiance space, which can be calculated by the multiplication of radiance increments with the transposed of the Jacobian matrix. On the other hand, the storage of the Jacobians throughout the minimization of the cost function becomes significantly memory demanding, in particular if thousands of observations are assimilated. However, this is accepted in the HIRLAM assimilation system since it is outweighted by avoiding the computational cost of the direct utilization of the TL and AD routines of the observation operator. Furthermore, both solutions are mathematically equivalent considering the present form of the cost function.

In this framework, the assimilation and forecast model is run on the model domain as described in Stengel et al. (2009) with a spatial model resolution of 22 km. During the minimization of the cost function, the spatial resolution is reduced to 66 km in the first minimization (first outer-loop) and 44 km in the second. The assimilation window is specified with 6 h The background error statistics were derived as described in Parrish and Derber (1992) using 36 h and 12 h forecasts covering three summer months, and using a statistical balance operator (Berre, 1997; Derber and Bouttier, 1999). The choice of shorter forecast length pairs compared to the proposed 48 h/24 h forecasts was done due to the growing influence of the boundary conditions in a limited area model with time. Further, the statistics based on 48 h/24 h forecasts are likely to overestimate the correlation length scales at 6 h forecast length (background fields), because the length scales of forecast error covariances increase with increasing forecast lengths (Bengtsson, 1971). The reader is referred to Huang et al. (2002) and Gustafsson (2006) for further details of the HIRLAM 4D-Var system.

The set-up of the HIRLAM forecast model is identical to the version used in Stengel et al. (2009). The main features are here shortly summarized. The HIRLAM forecast model contains a semi-Lagrangian advection scheme, and physical parametrisations for radiation (Savijärvi, 1990) and for convection and large-scale condensation processes (Rasch and Kristjánsson, 1998; Kain, 2004). It further comprises a moist conserved turbulence scheme (Cuxart et al., 2000), and the ISBA (Interaction Soil Biosphere Atmosphere) land surface scheme (Noilhan and Mahfouf, 1996). The maximal forecast length is 48 h for which the lateral boundary information is provided by forecasts of the European Centre for Medium-Range Weather Forecasts (ECMWF) model with a 3 h interval.

4.2.2 IR Jacobians in the presence of clouds

Clear-sky Jacobians are usually calculated either by using differences in modelled brightness temperatures responding to small changes in each control vector element, or by

employing the adjoint of the RT with small increments in brightness temperature space as input. Due to the generally strong sensitivity of IR radiation to cloud particles, the Jacobians of the control vector parameters differ from their clear-sky equivalents in the presence of cloudiness if this is included in the atmospheric state provided to the RT model. The additional occurring Jacobians of any cloud parameter in these case are usually discarded, which is simple due to the fact that these parameters are not in the control vector. An exception is the usage of cloud-top pressure and cloud fraction as local extensions of the control vector (McNally, 2009). Corresponding Jacobians are used to alter these cloud parameters during the minimization of the cost function.

In our study, the diagnosed profiles of cloudiness (LWC, IWC, and CC) are used as temporary variables within the observation operator. They constrain the RT calculation in the non-linear and adjoint observation operator. Jacobians of LWC, IWC, and CC are output of the AD of the RT model and are different from zero on vertical levels diagnosed to contain clouds. In the AD of the observation operator the AD of the SIMPHYS is employed subsequently to the AD of the RT model. Thus, the Jacobians of the temporary cloud parameters can be mapped onto the Jacobians of the control vector parameters such as temperature and moisture. With this methodology the derived Jacobians of the control vector parameters implicitly account for their interaction to the mentioned cloud parameter. This provides a suitable instrument to properly adjust the atmospheric state, as defined by the analysis control vector towards cloud-affected radiance observations during the analysis process. Examples of such Jacobians can be found in Stengel et al. (2010).

A limitation of the assimilation strategy used is that it relies on the cloudiness modelled by SIMPHYS, which for some cases might deviate significantly from the actual atmospheric condition. For the derivation of the Jacobians this means that no sensitivity to cloud variables are present at those levels for which the modelled cloudiness is zero. A further problematic issue occurs for overcast conditions, where the modelled sensitivity of the radiances with respect to changes of the geometrical thickness of clouds, i.e. to changes of the vertical position of cloud top and cloud base, is constrained by the discrete vertical resolution of the NWP model. In general, the best representativeness of the derived Jacobians in the presence of clouds can be expected under broken cloud conditions in which the cloud cover acts as smoothing factor avoiding jumps in the sensitivities due to non-linearities in the cloud processes. These jumps could for example occur in overcast scenes when the discrete vertical resolution of the model limits a proper description of the sensitivities of the radiances with respect to changes in cloud top height. The Jacobians for different cloud conditions are exemplarily shown in Stengel et al. (2010).

To limit the errors in modelling clouds, they are critically verified by comparison to the observed cloudiness leading to a rejection of those radiance observations for which the

modelled and observed cloud cover deviates too much, which is described in section 4.3 in more detail. Thus, the provided Jacobians can be assumed to be properly generated. Furthermore, the Jacobians are re-calculated at the beginning of each inner-loop minimization, which accounts for the occuring deviation of the radiances sensitivities due to the new first guess of the atmospheric state.

4.3 Description of assimilation and forecast experiments

4.3.1 Satellite data selection

Three of SEVIRI's IR channels, namely WV062, WV073 and IR134, which are spectrally located around 6.2 μm, 7.3 μm and 13.4 μm were selected. WV062 and WV073 are mainly sensitive to mid and upper-tropospheric moisture. IR134 is mainly sensitive to temperature throughout the troposphere and to radiation emitted by the surface. Additionally, IR134 is slightly sensitive to lower tropospheric moisture. Examples of their temperature Jacobians can be found in Stengel et al. (2009). The radiances observations in these channels were classified with respect to the cloud conditions in each pixel into three observation types: CLS for clear-sky conditions, LLC in the presence of low-level clouds (not radiance affecting), and CLD for conditions with radiance-affecting clouds. All observation types are defined as a 5-by-5 pixel box representation. The cloud characteristics, namely cloud top pressure (CTP) and cloud fraction, are based on Le Gleau and Derrien (2002), which was developed in connection with the EUMETSAT Satellite Application Facility on Nowcasting and Very Short Range Forecasting. Cloud fraction is indirectly derived by considering the binary cloud information in all pixels with respect to the total number of pixels in a pixel box.

CLS observations are found in boxes with cloud fraction of 0. LLC observations are identified as in Stengel et al. (2009) in cloudy pixels for which at least one channel is not affected by the clouds, i.e. at least 95% of the integrated temperature Jacobian has to be above the satellite-derived CTP. CLD observations are found in all remaining cloudy pixels for which the cloud fraction is either between 0.1 and 0.9 (broken cloud) or equal to 1 (overcast). Cases with cloud fraction greater than 0.9 and lower than 1 are discarded due to expected distinctive violation of the linearity assumption. This needs to be done, because the present, incremental form of the cost function in the HIRLAM assimilation system assumes linearity in the vicinity of the background. Significant deviations from the linearity assumption leads to a degraded analysis, due to the incresing invality of the Jacobians with increasing non-linearity In all remaining cloudy pixels, CLD observations are defined as in Stengel et al. (2010) with the exception that also slightly cloud-affected observations (with a simulated effect of the cloud lower than 0.5 K) were included in

Table 4.1: Bias correction values (y^{bc}) and observation error standard deviation (σ^o) for assimilated satellite observations. The values depend on the cloudy conditions in each scene.

	Clear sky		Broken clouds *High*		Broken clouds *Low*		Overcast *High*		Overcast *Low*	
	y^{bc}	σ^o	y^{bc}	σ^o	y^{bc}	σ^o	y^{bc}	σ^o	y^{bc}	σ^o
WV062	0.0	2.0	-1.6	1.7	0.0	2.0	-0.4	2.7	0.0	2.0
WV073	0.0	2.0	-1.8	2.6	-1.0	1.9	0.3	6.3	1.8	4.2
IR134	0.0	1.5	-1.2	4.1	0.1	2.3	0.2	7.9	1.5	3.4

this group of observations in this study. The cloud fraction criteria, which are applied to separate between broken clouds and overcast, had to be fulfilled by both the modelled and the observed cloudiness. Observations in cases for which one of both failed this test were rejected to limit uncertainties of the cloudiness introduced by SIMPHYS. Also, observations were rejected for which either the SIMPHYS simulation or the observations had cloudiness, while the other had not.

4.3.2 Experiment definitions

Three different experiments were conducted covering a period from 3 June 2006 until 31 July 2006 with 4D-Var analyses performed every 6 h window. The conventional observations, which comprise surface station (SYNOP), radiosonde, and pilot-balloon reports, as well as measurements from ships, aircraft and buoys, were used in all three experiments. Experiment names and assimilated observations are as follows:

- CNTRL: Conventional observations only
- SEV_CLEAR: Conventional, and CLS and LLC observations
- SEV_ALLSKY: Conventional, and CLS, LLC and CLD observations

The satellite observations in SEV_CLEAR and SEV_ALLSKY were included with a temporal resolution of 1 h. Constant bias corrections for each observation were applied depending firstly on the cloud amount in the pixel, and secondly, if identified as cloudy, on the vertical position of the clouds. All values were inferred from a passive monitoring of observation minus background departures from 8 sequential 4D-Var cycles prior to the time period of the experiments. Similarly, the observation error standard deviations (σ^o) for cloudy observations were chosen with respect to these data (Stengel et al., 2010). For clear-sky observations, σ^o was set to 2.0 K for WV062 and WV073, and 1.5 K for IR134 (Stengel et al., 2009). All values are summarized in Table 4.1.

All radiance observations were checked against the background applying σ^o and the background error standard deviations in observation space (σ^b). All observations for which the innovation exceeded the limit of $\sqrt{2(\sigma^{o2} + \sigma^{b2})}$ were rejected. Subsequently,

a spatial thinning was performed reducing the spatial resolution of the satellite data to approximately 90 km. This minimizes spatial observation error correlations, which are not accounted for in the assimilation scheme. The order of priority in a thinning box, i.e. preferring one radiance observation type over another, was chosen as follows: CLD observations (highest priority), LLC observations, CLS observations (lowest priority). This also led to a slightly reduced number of CLS and LLC observations in SEV_ALLSKY compared to SEV_CLEAR, since these observations are rejected in favour of CLD observations.

It needs to be noted that the experiments CNTRL and SEV_CLEAR have similarities to the experiments CNTRL and SEVLLC discussed in Stengel et al. (2009). This is due to the fact that the new extended observation operator only affects cases with significant cloud contribution on the radiances. However, the introduction of 5x5 pixel box super-observations as well as the new background error structure functions are important changes that affect the experiment results. This motivated the re-run of these experiments in the course of this study to enable an optimal evaluation of the effect of cloud-affected satellite observations in SEV_ALLSKY which is the main aim of this study.

4.3.3 Observation statistics

CLS, LLC, and CLD observations were investigated in terms of their number, and departure from background and analysis given the chosen observation preprocessing. As one example, these data were extracted from the SEV_ALLSKY experiment are discussed here (Figure 4.1). CLS and LLC observations build the majority of the assimilated observations, each type with approx. 1000 to 4000 for WV062 and WV073 in each 6 h assimilation window. The smaller number of LLC observations for channel WV073, compared with WV062, is due to the lower peaking Jacobians in this channel. For the same reason the LLC observations of channel IR134 are fewer than in the other two channels. Further, the IR134 channel is only used above ocean surfaces which leads to an additional decrease of the numbers. The numbers of CLD observations are clearly smaller. They are in the order of 300 to 800 per assimilation window when splitting these observations into two classes with broken and overcast conditions. To give a general estimate, including CLD radiance observations in the given assimilation scheme increases the total number of observations by approx. 8 to 12 % in each channel with the highest increase percentage occuring for channel WV062. It is also important to note, that the numbers are relative constant during the experimental period of 2 months. This indicates that a relative stable observation preprocessing despite the static bias correction coefficients.

Similarly, the background minus observation (B-O) departures show a stable behaviour during the experimental period. For CLS and LLC observations the standard deviations of B-O departures in SEV_CLEAR and SEV_ALLSKY lay between 0.5 and 1.2 K with the

smallest values for IR134 and without any significant biases on average. CLD observations in SEV_ALLSKY show slightly increased B-O values of 1.5 to 2.2 K with highest values found for WV073. The observation minus analysis departures generally reveal reduced standard deviations compared with B-O, which thus highlights the successful assimilation of the cloud-affected radiance observations.

4.4 Impact on analysis fields

To investigate the impact of assimilated cloud-affected radiance observations on the analysis fields, we analysed systematic deviations of the analyses of SEV_CLEAR and SEV_ALLSKY with respect to CNTRL. Calculated mean (bias) and standard deviations for the upper-air fields are shown in Figure 4.2. These values represent the full experimental period and include cases located in regions over the Atlantic Ocean covered by SEVIRI observations with zenith angles lower than 70°.

The plots show small to moderate deviations for temperature and humidity for both SEV experiments with amplitudes decreasing with height above 850 hPa. On the one hand both SEV experiments generally do not differ much for these parameters in the mid and upper troposphere. On the other hand some clear differences are found at 850 hPa. This is also the level for which both the temperature and humidity curves indicate the greatest analysis increments for these two parameters. Furthermore, the bias profiles reveal a warming and drying above that level in SEV_ALLSKY compared with SEV_CLEAR. The drying might be partly due to the changes in temperatures due to the definition of relative humidity. For geopotential height, the standard deviation for both experiments are similar and increase with height until 300 hPa, while decreasing above this level, where also some differences between SEV_CLEAR and SEV_ALLSKY are found. The biases are negative in the lower and positive in the upper part for both SEV experiments. In SEV_ALLSKY the bias for geopotential height is slight pushed towards higher values in the upper part. The wind analyses does not show much deviation between the SEV experiments except some slight, vertically persistent increase in the standard deviation of SEV_ALLSKY.

To summarize, the analyses of both SEV experiments show statistical deviations from corresponding fields of CNTRL due to the assimilated satellite observations. It is also shown, that additionally assimilated cloud-affected observations further modify analysed temperature and moisture in the lower troposphere and for geopotential height in the upper troposphere. This underlines the potential of these observations to create additional analysis increments after the variational analysis procedure.

A similar investigation for land cases, co-located to assimilated radiosonde sites show much smaller deviations between the experiments (not shown) indicating the constraining

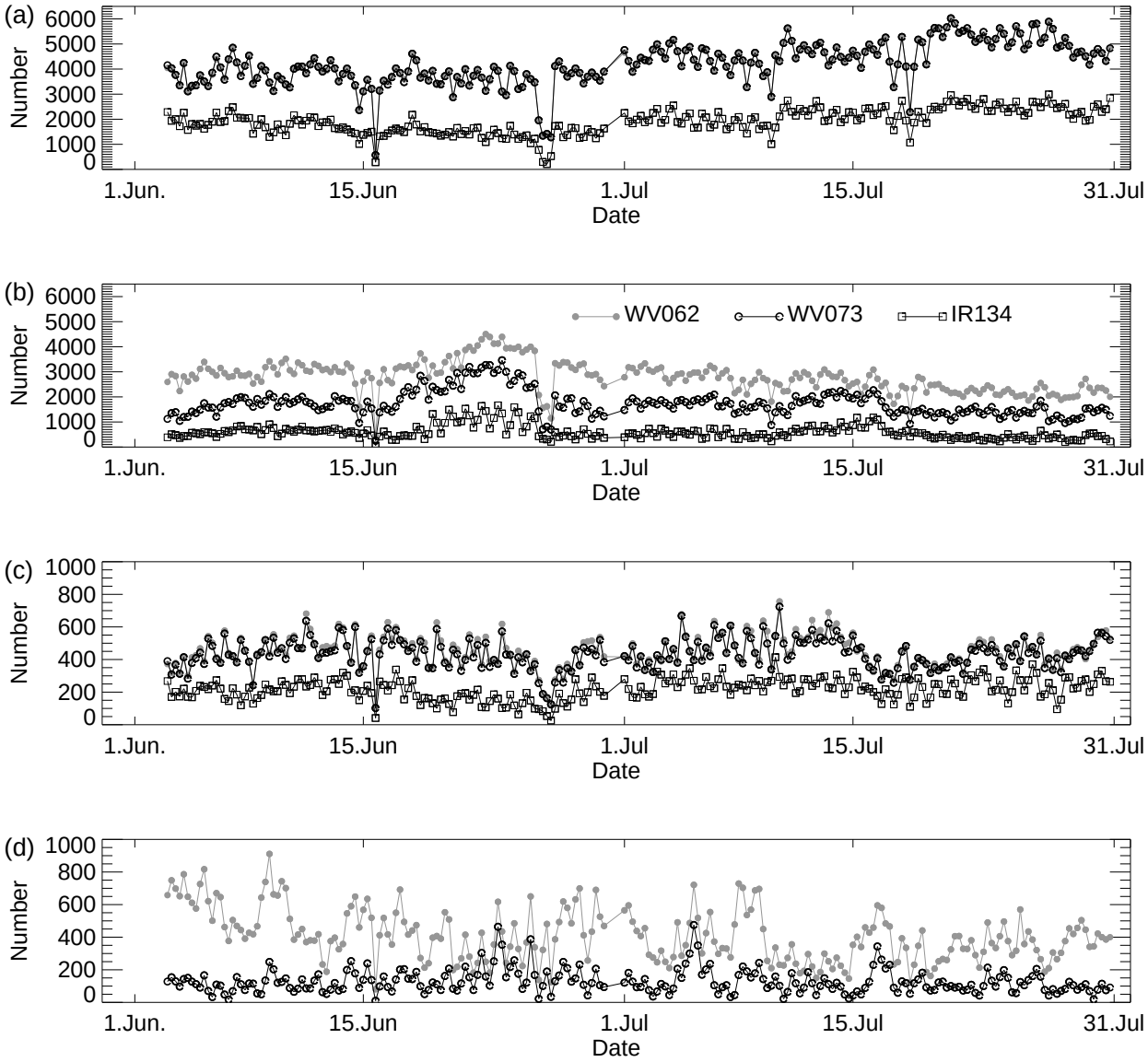

Figure 4.1: Number of assimilated radiance observations in SEV_ALLSKY with following types: (a) CLS, (b) LLC, (c) CLD (broken clouds), and (d) CLD (overcast).

force of assimilated sondes on the analysis and/or smaller innovations indicating increased background accuracy over land than over ocean. However, some impact over land is still noticeable as for example shown in Figure 4.3 and 4.4 where the analysis departures (00 h forecast length) of both SEV experiments relative to CNTRL are reported. These plots also exhibit the statistically significant analysis modifications at all shown vertical levels for temperature, humidity and wind speed. However, the absolute increase in the departure of the analysis to radiosondes is rather small, as for example visible in Figure 4.5 for relative humidity at 500 hPa. Generally, the increased departure to radiosondes in the SEV* experiments is explainable by the smaller relative weight of the radiosondes observations during the minimization of the cost function compared to CNTRL, since in the latter less observations are assimilated. This also prevents the comparison of the analysis with radiosondes to serve as a measure of the analysis quality. Furthermore, no other reliable and independent observations are available to enable an objective evaluation of the actual model state accuracy at analysis time, because all available observations passing the quality check are assimilated. A reduction in the number of these assimilated observations, for example of radiosondes, to enable such an objective analysis evaluation is questionable, since the interplay of observations of various observation types in particular leads to the best estimate of the atmospheric state. For this reason, a very common approach is followed, which assesses the analysis accuracy indirectly by the evaluation of the model forecasts. In contrast to the analysis, radiosondes become more and more reliable reference measurements with increasing forecast lengths, since the absolute model error increases significantly. Further, radiosonde can be considered increasingly independent from the NWP model with increasing forecast length. Thus, the evaluation of the forecast accuracy can be assessed through comparison to radiosondes valid at the same time. This is described for all performed experiments in the next section.

4.5 Impact on forecast accuracy

The change in forecast quality for both SEVIRI experiments was assessed by comparing their forecast errors, which were derived against radiosonde observations, to the corresponding values of the CNTRL run. RMSE and bias values were calculated every 12 h for forecast lengths of 00, 12, 24, 36, and 48 h starting from the analyses at 0000 and 1200 UTC. The normalized deviations of the values of SEV_CLEAR and SEV_ALLSKY against CNTRL were averaged over the full experimental time period and plotted as function of pressure level and forecast length (Figure 4.3 and 4.4). Both figures also show the levels and forecast lengths for which the normalized error deviation exceeds the 99 % confidence level, which was calculated using a standard two-sided t-test.

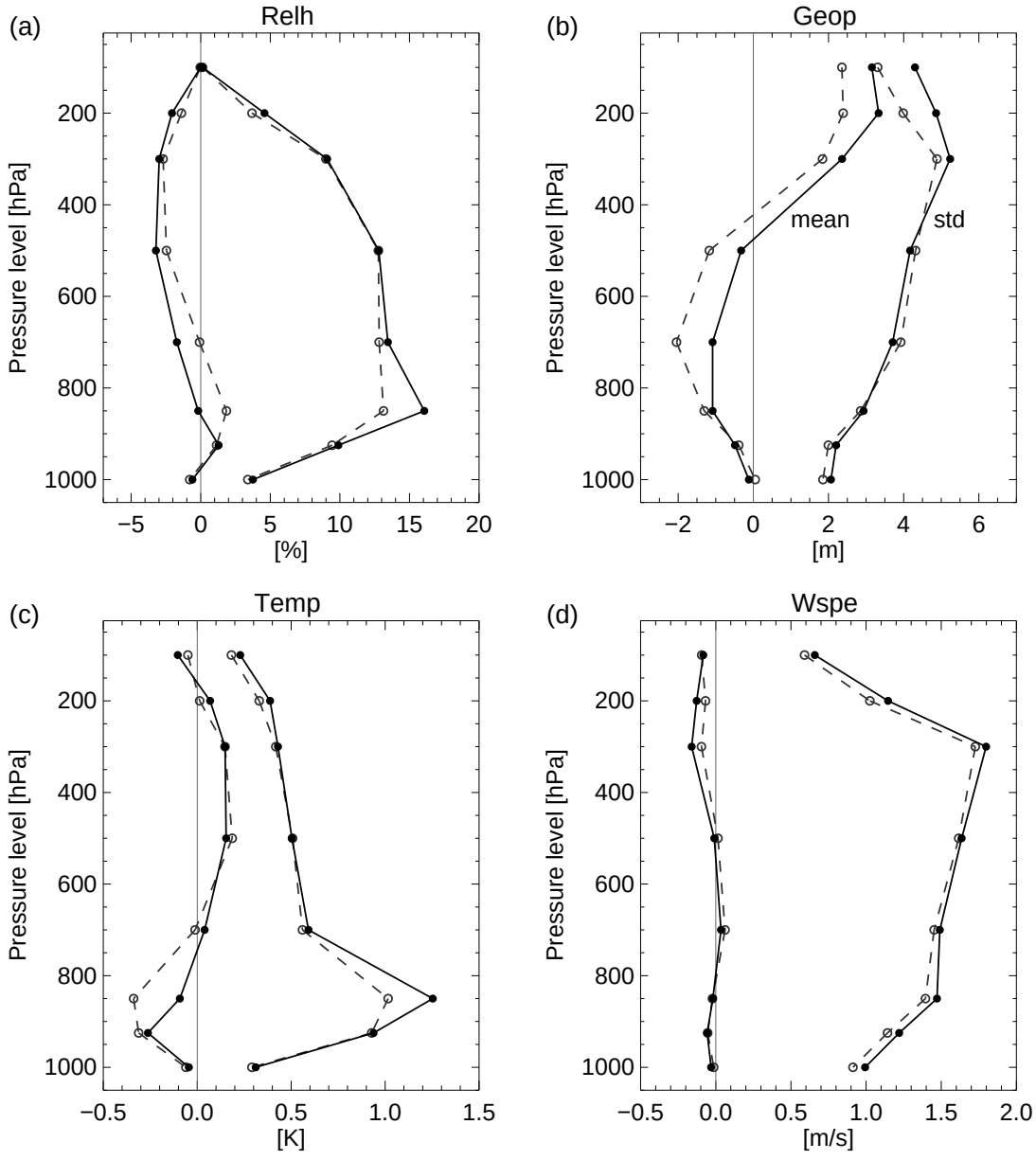

Figure 4.2: Mean and standard deviations (std) of analysis differences for SEV_CLEAR (dashed line) and SEV_ALLSKY (solid line) with respect to CNTRL for (a) relative humidity, (b) geopotential height, (c) temperature, and (d) wind speed sampled over ocean regions with SEVIRI coverage.

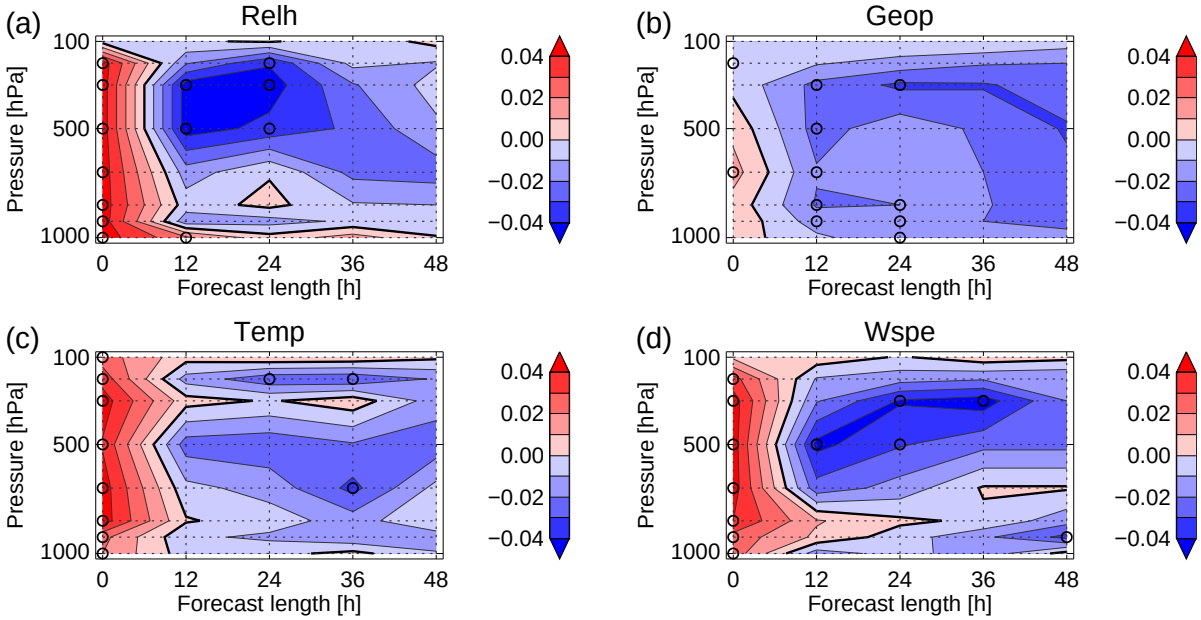

Figure 4.3: Contour plot of normalized mean forecast error deviation in SEV_CLEAR against CNTRL for (a) relative humidity, (b) geopotential height, (c) temperature, and (d) wind speed. Negative values imply an error reduction. The values were calculated at analysis time (00 h) and for forecast lengths of 12, 24, 36, and 48 h at vertical levels marked by the dashed horizontal lines. The circles mark forecast lengths and vertical levels for which the error reduction exceeds the 99 % confidence level.

4.5.1 SEV_CLEAR

As mentioned above at forecast lengths of 00 h (time of analysis) the NWP fields are drawn away from radiosondes, in particular for temperature and moisture with up to 5% (Figure 4.3). The actual SEV_CLEAR forecast is generally characterized by improvements compared to CNTRL. This is visible for all parameters at all heights and forecast lengths investigated. A few exceptions with slight degradation of the forecast scores are found. For moisture, largest improvements of the RMSE of approx. 4 % are found above 500 hPa at forecast lengths of 12 to 24 h with decreasing amplitude afterwards. Only a small reduction of the forecats accuracy is found in the lower troposphere. For temperature, the forecast skill increased by up to approx. 3 % at 600 hPa at 36 h. The impact on geopotential height is generally positive and increasing with forecast lengths. The maximum error reduction against CNTRL is found at longer forecast lengths and mid to upper troposphere between 500 and 300 hPa which amounts to approx. 4 % reduction. Wind forecast accuracy is very similar showing positive impacts on at nearly all forecast lengths and vertical levels.

The significance analysis, also shown in the Figure 4.3, exhibits many forecast lengths and levels for which the impact was found to be statistically significant with respect to the 99 % confidence level.

4.5.2 SEV_ALLSKY

Generally speaking, the normalized forecast error deviations for SEV_ALLSKY (Figure 4.4) are very similar compared with the SEV_CLEAR results (Figure 4.3). However, some small differing features are found, which on the one hand reveal further improvements in the upper troposphere for moisture and for geopotential height in the entire troposphere, and for temperature in the middle troposphere. On the other hand, some small degradation is visible in particular in the lower troposphere for temperature and moisture compared with the SEV_CLEAR results. When considering the 99 % confidence levels, as measure of reliability for forecast results, clearly more levels and forecast lengths are found for which the confidence level is exceeded by the error reduction.

To further investigate the particular impact of the additional assimilated cloud-affected radiances, we also analysed the the normalized forecast error deviation of SEV_ALLSKY with respect to SEV_CLEAR summarized over all forecast lengths (Figure 4.6).

The values shown support the argumentation above. Cloud-affected radiances lead to generally improvements with the maximum of relative error reduction of 0.5 to 1 % in the mid and upper troposphere. As also mentioned above and noticable in Figure 4.6, some degredation of the forecast accuracy is found around 850 hPa for temperature and humidity. A similar but smaller feature in the lower troposphere is found for wind. While the wind speed scores are nearly neutral, wind direction is clearly characterized by large improvements up to almost 3 % around 700 hPa and in the upper troposphere. This slight negative impact in lower tropospheric layers might be explained by characteristic temperature and moisture features, which might occur in, above, and below cloud layers. The used structure functions on the other hands are derived from a wide range of atmospheric conditions, and for this reason far from being ideal in cloudy cases, because sharp features in atmospheric variables are smoothed out by averaging. For our studies, this means that the assimilated radiance signal in mapped onto a too broad vertical atmospheric layer, possibly causing the unrealistic analysis increments within and below clouds. This finding motivates further research on flow-dependend background errors and their spatial correlations, to provide structure functions better applicable for cloudy scenes.

4.6 Summary and conclusions

In this article we assessed the impact of cloud-affected satellite radiance observations, measured by SEVIRI, on 4D-Var analysis and forecast of the limited-area NWP model HIRLAM. Building on the work of Stengel et al. (2010), cloud-affected radiances were included using an extended observation operator which includes a simplified physics for handling the cloud processes. After some further modifications this framework was used

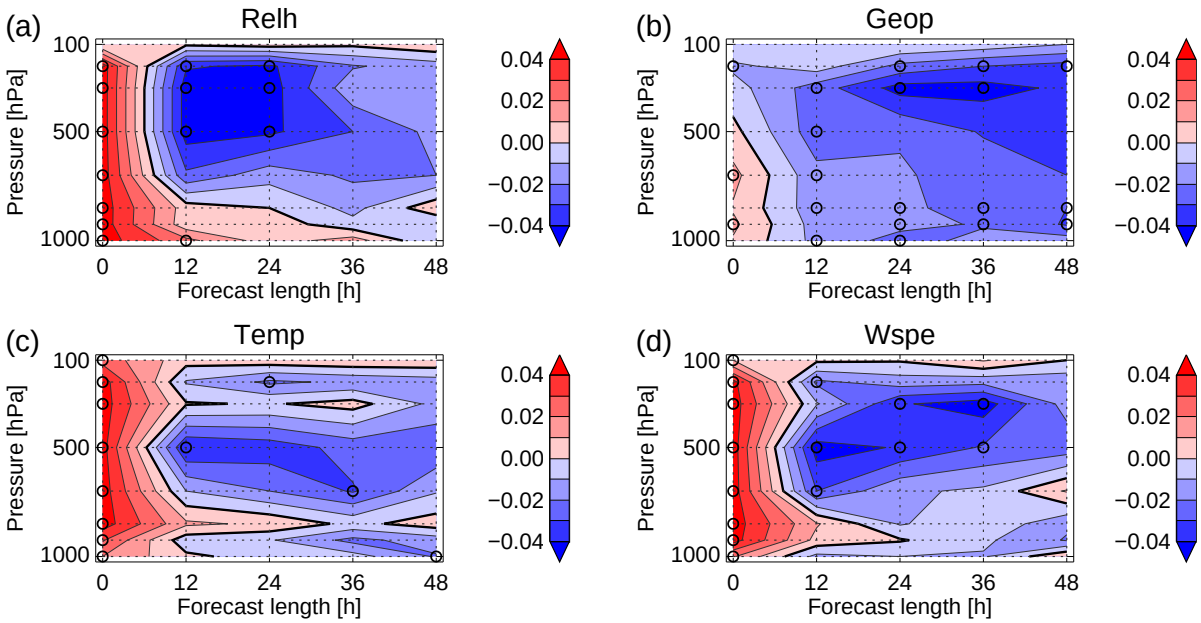

Figure 4.4: As figure 3, but for SEV_ALLSKY against CNTRL.

to conduct data assimilation and forecast experiments covering a two month period. The impact on forecast accuracy was evaluated by comparing the forecast errors when assimilating cloud-affected radiances with reference experiments.

Confirming earlier studies, IR satellite observations do overall improve the accuracy of the HIRLAM forecast. Largest improvements are found in the upper troposphere from 500 hPa to 200 hPa with normalized error reductions of up to 4 %. The assimilation of cloud-affected radiances further reduces the forecast errors at these heights by additional approx. 1 % for geopotential height and humidity, and approx. 3 % for wind direction. Slightly negative impact was identified for temperature, moisture, and wind in the lower troposphere, while most level are characterized by a positive impact of cloud-affected radiances.

The assimilated cloud-affected radiances, as treated in the given framework, do significantly alter the performed variational analysis and lead subsequently to mainly improved forecasts. However, the small degradation found for the forecast accuracy in the lower troposphere, compared to the results when not using cloud-affected observations, highlight some still existing problems in the assimilation. One reasons for this might be the relatively wide structure functions of the background errors which, in particular in cases of relatively opaque clouds, might lead to a too strong vertical spreading of the cloudy radiance signal below the cloud, while the signal in these cases only contains information about the uppermost cloud layers and the atmosphere above. Also, often occurring jumps in, for example, temperature and moisture profiles at cloud top and base, are therefore

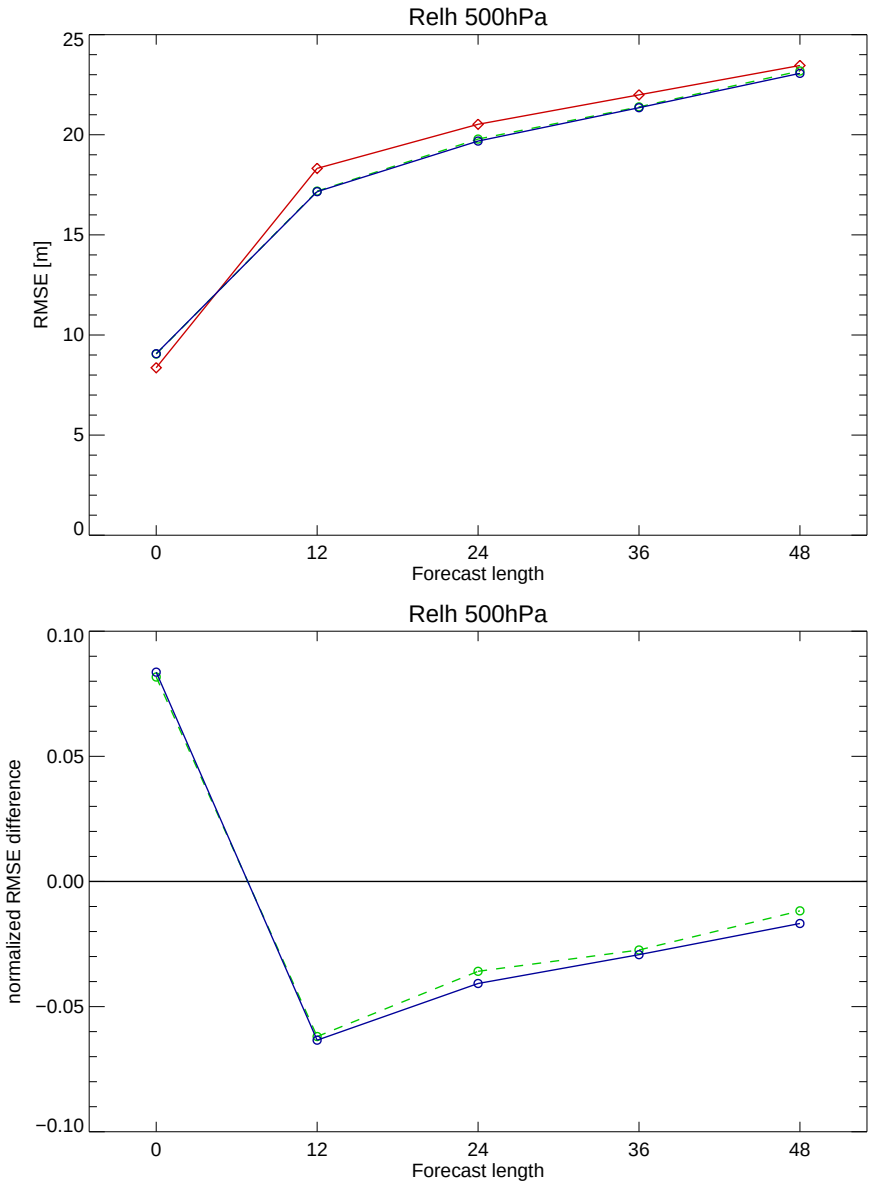

Figure 4.5: Upper panel: Absolute departure of model 500 hPa relative humidity from radiosonde measurements for all three model runs: CNTRL (red solid line), SEV_CLEAR (green dashed line), and SEV_ALLSKY (blue solid line). The values are shown for the analysis time (00h) and forecast lengths of 12, 24, 36, and 48 hours. Lower panel: Relative departure of 500 hPa relative humidity departures of SEV_CLEAR (green dashed line), and SEV_ALLSKY (blue solid line) with respect to CNTRL.

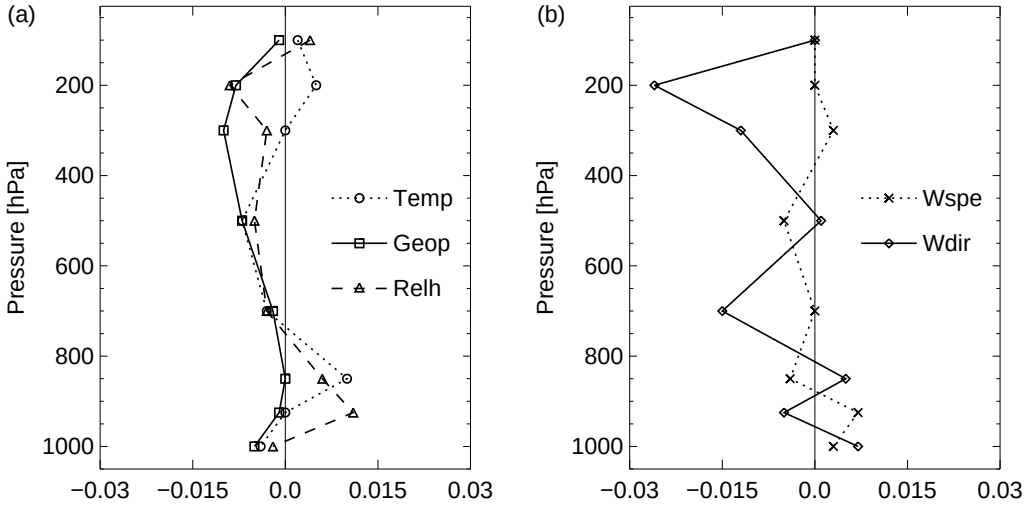

Figure 4.6: Normalized forecast error deviation of SEV_ALLSKY with respect to SEV_CLEAR for (a) temperature (Temp), relative humidity (Relh) and geopotential height (Geop), and (b) wind speed (Wspe) and wind direction (Wdir).

not accounted for. Similarly, the currently used background error structure functions, which also do not optimally account for the horizontal inhomogeneity of cloud fields, might lead to too large near-homogeneous analysis increments. This strengthens the usage of super-observations or of observations with a high spatial resolution, instead of only thinned observations, and this in conjunction with background errors and their structure functions adjusted to cloudy situations. Furthermore, the choice of observation errors and assimilation parameters should in the future be further evaluated to fully exploit the benefit of cloud-affected radiance observations. Also, an enhanced radiances bias correction as proposed in Harris and Kelly (2001) or Auligné et al. (2007) should be considered, in particular with cloud properties, such as cloud cover or cloud top pressure, as predictors. Finally, the application of this assimilation approach in global models will reveal the full potential of these observations on a global scale.

4.7 acknowledgment

This work was supported by the Swedish National Space Board (Contract DNR 105/08:2). It built on the fruitful work started under the Research Fellowship Program of the European Organisation for the Exploitation of Meteorological Satellites (EUMETSAT). Also, the authors would like to thank Nils Gustafsson and Per Dahlgren for their advices. The comments of the anonymous referees are appreciated.

5 Summary and Outlook

This work presents a comprehensive investigation of the impact of geostationary satellite observations on the accuracy of the analysis and forecast of the limited-area NWP model HIRLAM. For this, infrared measurements of the SEVIRI instrument have been processed to be assimilated in the HIRLAM variational data assimilation scheme. Beyond the assimilation of clear-sky satellites radiances, this work further presents a novel approach to expand this by the assimilation of cloudy radiances and its practical application. The inclusion of clear-sky and cloudy radiances in the HIRLAM assimilation schemes is motivated by the fact that they can lead to a more accurate description of the atmospheric state potentially leading to increased accuracy in numerical weather prediction.

In the first part of the work, the impact of SEVIRI radiances in clear-sky and low-level cloud regimes was investigated. Here, the HIRLAM model was modified to include corresponding brightness temperatures (TB) as additional observation type. A sophisticated observation screening procedure was developed to identify those channels unaffected by low-level clouds when occurring. Then, the biases between the observed and simulated TBs were monitored and analysed revealing a small, relative stable bias in the WV062 channel which was corrected by a fixed bias correction offset. The TBs for the channels WV073 and IR134 showed no significant persisting bias. However, a small diurnal variation of the bias in WV062 and WV073 was found, which exhibits a diurnal dependence of the NWP model or cloud mask quality. In extended assimilation and forecast experiments it was investigated both, the changes in the atmospheric analysis fields introduced by the new assimilated observations, and the changes in the accuracy of the subsequent forecast. Corresponding results clearly revealed that the assimilation of the spatio-temporal highly resolved geostationary satellite observations can potentially improve the accuracy of a limited area NWP model. This was in particular shown by the upper-air forecast of geopotential height and moisture, being improved by up to 5 %, and precipitation forecast.

In the second part of this work the focus was placed onto cloud-affected radiances which are usually rejected from assimilation. This undertaking was supported by the utilization of a 4D-Var system which, together with the high spatial resolution of SEVIRI enables the capture of the spatiotemporal highly variable clouds. The assimilation of

these observations is assumed to be very informative to the NWP system due to the weather-active character of these regions. The assimilation procedure implemented uses a simplified moist physics scheme to diagnose the cloudiness internally in the observation operator. In extended tests the new operator was verified with respect to (1) its forward-modelling performance, where observed and modelled cloudy radiances were compared, (2) its capability to identify cases for which the linearity assumption, i.e. the linear response of the modelled radiances with respect to changes in the input control vector variables, in the vicinity of the cloudy background state does not hold, and (3) the practical performance in a complete 4D-Var system.

It was found that the new observation operator clearly improves the simulations of the cloudy satellite observations leading to reasonable departures from their observational equivalents and near-Gaussian shaped deviation statistics. Smallest standard deviations were found for the two water vapour channels under broken cloud conditions.

By considering the modelled cloudiness within the operator, it was shown that cases with too complicated atmospheric conditions, which potentially cause moderate to strong non-linearities, can be identified. This potentially enables a rejection of certain channels in each pixel in the pre-processing of the radiances prior to the actual minimization of the cost function.

Further, one full 4D-Var experiment revealed the successful assimilation of cloud-affected radiances with realistic analysis increments created in regions of clouds which were left empty when assimilating clear-sky radiances only. The departure of the analysis to the observations was clearly smaller than for the background, which again proved the successfulness of this technique. Also, the analysis was found to be improved in terms of upper-tropospheric biases compared to a control experiment when using not-assimilated radiosondes as reference.

As the last part of this work the built framework for cloudy radiance assimilation was subjected to a comprehensive verification using extensive assimilation and forecast experiments. Here, the impact of assimilated cloud-affected radiances on-top of already assimilated clear-sky radiances and conventional observations was assessed. The monitoring of deviations between observations and their modelled equivalents revealed a small bias only, with a stable behaviour during the entire experimental period. The impact on analysis and forecast quality of the HIRLAM model was determined by comparisons to reference measurements of radiosonde and SYNOP stations valid at the same time as the forecast.

It was clearly shown that cloud-affected radiances in the given assimilation framework provide additional information to the atmospheric analysis. The analyses were estimated to be closer to the true atmospheric state on averaged, since the subsequent forecasts

exhibited overall improved accuracy with respect to the used verification data. This was in particular found for geopotential height and wind throughout the troposphere, and for temperature and moisture in the mid troposphere. However, in lower tropospheric layers a slight degradation of the forecast accuracy for these two parameters was found. The scores for surface variables such as surface pressure and precipitation revealed only minor changes.

Overall, the work presented in this thesis clearly highlights the potential benefit a limited area NWP model can gain from assimilated geostationary satellite observations. The high spatial and temporal resolution of water vapour and temperature signals and cloud imagery provide a valuable source of information about the true atmospheric state. This can efficiently be captured by 4D-Var frameworks, complementing the high vertical resolution of temperature and moisture information from polar-orbiting satellites. However, continuous research is necessary to further exploit certain aspects of the assimilation of clear-sky and cloudy radiances measured by geostationary satellites and their impact on the accuracy of the numerical weather prediction. Some generic ideas are given in the following.

Outlook

Tangent-linear assumption in cloudy scenes

As investigated in section 3.4.2, the HIRLAM assimilation system, and more generally almost all NWP assimilation systems, assume a linear radiance response with respect to changes in the control vector variables within the vicinity of the background state. This assumption is needed with respect to the commonly used formulations of the cost function. Significant deviations from this assumption can lead to degradations in the atmospheric analysis. While for clear-sky cases this response is usually not violated, moderate to strong non-linearities can occur when clouds are involved, in particular when the cloud-describing parameters are not fixed but variable. For example, moderate non-linearities can occur in the transition from clear to cloudy sky, or vice versa, or, more pronounced near "cloud saturation" in the vicinity of cloud cover of one. Thus, for these cases the calculated Jacobians are insufficiently representing the non-linear response of the radiances. In section 3.4.2 this problem was approached by rejecting exactly those potentially difficult cases beforehand. This approach is rather simple, since it only uses cloud cover as indicator, which might unnecessarily often lead to a rejection of observations, for example, if the cloud cover is close to one, but where the observation would rather lead to a decrease of the cloud amount instead of a further increase, reaching cloud saturation. To handle this more effectively two advanced solutions are proposed in the following.

One could assess the changes in cloudiness in the vicinity of the background state by applying increments to the background, which are in the order of the background errors. This would, after diagnosing the cloudiness from the perturbed state, provide some estimate of potentially occuring non-linearities for each scene. This assessment might be done already in the satellite pre-processing and prior to the data thinning procedure, since the identified scenes could be already filtered out at that stage.

Another approach could be to perform a similar test directly during the minimization of the cost function. Here, cases can be identified for which the modelled cloud cover, diagnosed from the background state plus the state vector increment at the current iteration step, for example, approach overcast. The assessment of non-linearities could even directly be done in brightness temperature space. This would have the big advantage of avoiding the definition of cloudiness threshold, since the deviation of tangent-linear and non-linear radiances responses could directly be calculated. As in variational quality control (Anderson and Järvinen, 1999) cases with significant deviations could be flagged and, then or at a later iteration step, rejected. Alternatively, the corresponding observation weight (usually given by the ratio of observation errors and background errors in observation space) could be decreased to avoid strong problems with respect to the convergence of the cost function.

However, all these approaches should be complemented by the application of multiple outer-loops which provide re-linearisation (re-calculation of the Jacobians) at the changed first guess state. Multiple outer-loops also provide the possibility to use all or certain cloudy observations in one of the later outer-loops. There, smaller deviations between the model state and the true atmospheric state can be expected.

Bias correction

The removal of systematic biases between modelled and simulated radiances, which can be caused by systematic errors in both the radiative transfer calculations and in the satellite measurements, is essential for the successful assimilation of satellite observations. An inappropriate bias correction on the other hand can lead to systematic errors in the analyses and to a degradation of the quality of the subsequent forecast. Different bias correction approaches have been discussed in the literature in the past (e.g. Harris and Kelly, 2001; Auligné et al., 2007). One of the most common approaches uses the correlation between the observation-minus-simulation deviations and the so-called predictors. These predictors are certain atmospheric parameters, to which the RT calculations are sensitive. Using an appropriate data sample, regression coefficients are calculated beforehand and then applied to the actual predictor values at observation location to correct for the radiance bias. The choice of one approach often has a significant impact on the

forecast quality. On the other hand too offensive corrections might also destroy an essential part of the information contained in the measurements. Since all studies in this work used a relatively simple correction with a fixed offset, further improvements in the results might be achievable with more advanced schemes as mentioned above.

In the few studies tackling the assimilation of cloud-affected radiances, the bias correction methodology has often only been adopted from the clear-sky radiance assimilation. But, since the radiative transfer calculation and the spatial representativeness become more complex in cloudy cases, it becomes clear that different systematic errors might occur and that further adjustments will have to be made.

When applying the bias correction approach as mentioned above, important local cloud parameters, for example, cloud fraction and cloud top pressure, should be included as additional predictors, since they significantly influence the modelled radiances. Thus, improper handling of the radiative effect of these parameters would lead to biases in observation space. In this context, the standard control vector variables, such as temperature and moisture, should also be investigated if they contain systematic deviations from truth in cloudy regions. These biases in the model fields and their contribution to the radiances biases are still under-exploited and need further consideration. These bias contributions should be separated and not be corrected within the radiance bias correction, but by tuning of the forecast model.

Background and observation errors

In variational data assimilation systems errors have to be assigned to the observations and the background (e.g. Lorenc, 2003). It is well known that model field accuracies vary spatially and temporally. However, the estimated model errors, which need to be specified for the background fields in variational data assimilation, are in most models spatially uniform. This approach is of course very inefficient, since it seems to be obvious that these errors are different for different weather regimes. In the recent past, some work has started to overcome these shortcomings and to investigate flow-dependent background error specifications (e.g. Riishøjgaard, 1998; Buehner, 2005). Such approach leads to a flow-depended balance between the background fields and observations, which should ideally also include scene-depended observation error specifications. The need for such a flow-dependence of the background errors is in particular needed for cloudy and rainy scenes, where the forecast errors are misrepresented in the current operational formulations of background error covariances matrices (Montmerle et al., 2010).

A scene-dependence of observations error specifications, which include radiance measurement and radiance simulation errors, is also desirable since there is a scene-dependent quality of the radiative transfer calculations in the observation operator. This can lead to biases, as mentioned above, but also to increased absolute simulation errors. The perfor-

mance of observation operators is certainly better for clear-sky regions. Cloudy cases are characterized by additional uncertainties in the description of the absorption of liquid and ice cloud particles. At visible and microwave frequencies these cases can also be characterized by significant scattering of radiation in clouds, which is to the first extend negligible in the infrared. Further, the signal-to-noise characteristics of the satellite instrument can be signal dependent, which means that the actual error of the measurements, as the complementing part of the observation error, can be function of the measurement itself.

Another important issue is the error correlation between different observations in neighbouring pixels. These error correlations exist firstly due to the fact that the errors in the background profiles, and therefore the corresponding radiance simulation errors, are spatially correlated. Secondly, the satellite measurements in neighbouring pixels might also not be completely independent due to the instrument scan characteristics.

For the time being, the specification of the these correlations is circumvented in almost all NWP models by a thinning of the observations (e.g. Dando et al., 2007) to remove neighbouring pixels with possible error correlations. The observation thinning is often also applied to reduce the total number of observations. On the other hand, observation thinning in general might be suboptimal since many small-scale features, which are detected in the higher resolved satellite observations, are missed. An alternative strategy is called *super-obbing*, which stands for the definition of super-observations usually created by averaging neighboured pixels. This might also reduce the spatial error correlations in the observations. It is generally assumed to be very difficult to determine realistic values for these errors.

Additional error correlations in the observations occur among the instrument channels themself (e.g. Garand et al., 2007). These errors can originate from instrument characteristics. Error correlations in the radiance simulations should also be investigated, because these errors are usually also included in the observation error term in the cost function. As example, different channels are influenced by similar or even the same physical processes in the atmosphere, e.g. the measurements in the SEVIRI's channels WV062 and WV073 are influenced by water vapour absorption and emission along the line of sight path. Errors in the modelling of this effect in the RT model will affect the simulated radiances in both channels, which would lead to inter-channel error correlations.

In general, disregarding of observation error correlations, thus assuming all observations to be independent, lead to a suboptimal analysis. This also motivates further research to fully exploit the capabilities of spatially highly resolved satellite radiances with constantly rising spatial and spectral resolution.

Final remarks

Ultimately, the most effective approach for the non-trivial task of assimilating cloud-affected radiances in NWP frameworks is the inclusion of cloud parameters in the 3/4D-Var analysis control vector. This includes the determination of these parameters during the minimization of the cost function equally to the other atmospheric parameters included in the control vector. However, this ultimate approach is not likely to be realized in an operational NWP system within the next years due to various reasons. That's why approaches as presented in this study are implemented in NWP systems, since they on the one hand circumvent some of the difficulties, but on the other hand already enable the utilization of cloud-affected radiance observations. They valuably contribute to this particular field of research and lead to further improvements in numerical weather prediction.

References

Anderson, E., Järvinen, H., 1999. Variational quality control. Q. J. R. Meteorol. Soc. 125 (554), 697–722.

Andersson, E., Hólm, E., Bauer, P., Beljaars, A., Kelly, G. A., McNally, A. P., Simmons, A. J., Thépaut, J.-N., Tompkins, A. M., 2007. Analysis and forecast impact of the main humidity observing systems. Q. J. R. Meteorol. Soc. 133, 1473–1485.

Andersson, E., Pailleux, J., Thépaut, J.-N., Eyre, J. R., McNally, A. P., Kelly, G. A., Courtier, P., 1994. Use of cloud-cleared radiances in three/four-dimensional variational data asimilation. Q. J. R. Meteorol. Soc. 120, 627–653.

Auligné, T., McNally, A., Dee, D., 2007. Adaptive bias correction for satellite data in a numerical weather prediction system. Q. J. R. Meteorol. Soc. 133 (624), 631–642.

Barker, D., Huang, W., Guo, Y., Bourgeois, A., Xiao, Q., 2004. A three-dimensional variational data assimilation system for MM5: Implementation and initial results. Mon. Weather Rev. 132, 897–914.

Bauer, P., Geer, A., Lopez, P., Salmond, D., 2010. Direct 4D-Var assimilation of all-sky radiances. Part I: Implementation. Quarterly Journal of the Royal Meteorological Society 136 (652), 1868–1885.

Bengtsson, L., 1971. An experiment in the assimilation of data in dynamical analysis. Tellus 23 (4-5), 328–336.

Berre, L., 1997. Non-separable structure functions for the HIRLAM 3DVAR. HIRLAM Technical Report 30, 40 pp.

Buehner, M., 2005. Ensemble-derived stationary and flow-dependent background-error covariances: Evaluation in a quasi-operational NWP setting. Q. J. R. Meteorol. Soc. 131 (607), 1013–1043.

Chevallier, F., Bauer, P., Mahfouf, J., Morcrette, J., 2002. Variational retrieval of cloud profile from ATOVS observations. Q. J. R. Meteorol. Soc. 128 (585), 2511–2525.

Chevallier, F., Lopez, P., Tompkins, A., Janisková, M., Moreau, E., 2004. The capability of 4D-Var systems to assimilate cloud-affected satellite infrared radiances. Q. J. R. Meteorol. Soc. 130 (598), 917–932.

Courtier, P., Andersson, E., Heckley, W., Vasiljevic, D., Hamrud, M., Hollingsworth, A., Rabier, F., Fisher, M., Pailleux, J., 1998. The ECMWF implementation of three-dimensional variational assimilation (3D-Var). I: Formulation. Q. J. R. Meteorol. Soc. 124 (550), 1783–1807.

Cuxart, J., Bougeault, P., Redelsperger, J., 2000. A turbulence scheme allowing for mesoscale and large-eddy simulations. Q. J. R. Meteorol. Soc. 126 (562), 1–30.

Dando, M., Thorpe, A., Eyre, J., 2007. The optimal density of atmospheric sounder observations in the Met Office NWP system. Q. J. R. Meteorol. Soc. 133 (629), 1933–1943.

Derber, J., Bouttier, F., 1999. A reformulation of the background error covariance in the ECMWF global data assimilation system. Tellus 51A, 195–221.

Derrien, M., Le Gléau, H., 2005. MSG/SEVIRI cloud mask and type from SAFNWC. International Journal of Remote Sensing 26 (21), 4707–4732.

Eyre, J. R., 1991. A fast radiative transfer model for satellite sounding systems. ECMWF Tech. Memo. 176.

Fischer, C., Montmerle, T., Berre, L., Auger, L., Ştefănescu, S., 2005. An overview of the variational assimilation in the ALADIN/France numerical weather-prediction system. Q. J. R. Meteorol. Soc. 131 (613), 3477–3492.

Garand, L., Heilliette, S., Buehner, M., 2007. Interchannel error correlation associated with AIRS radiance observations: Inference and impact in data assimilation. Journal of Applied Meteorology and Climatology 46 (6), 714–725.

Gauthier, P., Charette, C., Fillion, L., Koclas, P., Laroche, S., 1999. Implementation of a 3D variational data assimilation system at the Canadian Meteorological Centre. Part I: The global analysis. Atmosphere Ocean 37 (2), 103–156.

Gauthier, P., Tanguay, M., Laroche, S., Pellerin, S., Morneau, J., 2007. Extension of 3dvar to 4dvar: Implementation of 4dvar at the meteorological service of canada. Monthly Weather Review 135 (6), 2339–2354.

Gauthier, P., Thépaut, J., 2001. Impact of the digital filter as a weak constraint in the pre-operational 4DVAR assimilation system of Météo-France. Mon. Weather Rev. 129 (8), 2089–2102.

Geer, A., Bauer, P., Lopez, P., 2010. Direct 4D-Var assimilation of all-sky radiances. Part II: Assessment. Quarterly Journal of the Royal Meteorological Society 136 (652), 1886–1905.

Gustafsson, N., 1992. Use of a digital filter as weak constraint in variational data assimilation. Proceedings ECMWF Workshop on Variational Assimilation, with special emphasis on three-dimensional aspects, 327–338. Available from: ECMWF, Shineld Park, Reading, Berks. RG2 9AX, UK.

Gustafsson, N., 2006. Status and performance of HIRLAM 4D-Var. HIRLAM Newsletter 51, 8 pp.

Gustafsson, N., Berre, L., Hornquist, S., Huang, X., Lindskog, M., 2001. Three-dimensional variational data assimilation for a limited area model. Part I: General formulation and the background error constraint. Tellus 53A, 425–446.

Harris, B., Kelly, G., 2001. A satellite radiance-bias correction scheme for data assimilation. Q. J. R. Meteorol. Soc. 127 (574), 1453–1468.

Holm, E., Andersson, E., Beljaars, A., Lopez, P., Mahfouf, J.-F., Simmons, A., Thepaut, J.-N., 2002. Assimilation and modelling of the hydrological cycle: ECMWF's status and plans. ECMWF Tech. Memo. 383.

Huang, X., Xiao, Q., Barker, D., Zhang, X., Michalakes, J., Huang, W., Henderson, T., Bray, J., Chen, Y., Ma, Z., et al., 2009. Four-dimensional variational data assimilation for WRF: Formulation and preliminary results. Mon. Weather Rev. 137, 299–314.

Huang, X., Yang, X., Gustafsson, N., Mogensen, K., Lindskog, M., 2002. Four-dimensional variational data assimilation for a limited area model. HIRLAM Technical Report 57, 44 pp.

Kain, J., 2004. The Kain–Fritsch convective parameterization: an update. J. Appl. Meteorol. 43 (1), 170–181.

Kelly, G., Thépaut, J.-N., 2007. Evaluation of the impact of the space component of the Global Observing System through Observing System Experiments. Proceedings of Seminar on Recent developments in the use of satellite observations in numerical weather prediction, 327–348. Available from: ECMWF, Shineld Park, Reading, Berks. RG2 9AX, UK.

Köpken, C., Kelly, G., Thépaut, J.-N., 2004. Assimilation of Meteosat radiances data within the 4D-Var system at ECMWF: Assimilation experiments and forecast impact. Q. J. R. Meteorol. Soc. 130, 2277–2292.

Le Gleau, H., Derrien, M., 2002. User manual for the PGE01-02-03 of the SAFNWC/MSG: Scientific part. EUMETSAT documentation SAF, NWC/IOP/MFL/SCI/SUM/01, Available from: Centre de Meteorologie Spatiale, Meteo–France, Toulouse, France.

Lindskog, M., Gustafsson, N., Navascúes, B., Mogensen, K., Huang, X., 2001. Three-dimensional variational data assimilation for a limited area model. Part II: Observation handling and assimilation experiments. Tellus 53A, 447–468.

Lopez, P., Moreau, E., 2005. A convection scheme for data assimilation: Description and initial tests. Q. J. R. Meteorol. Soc. 131 (606), 409–436.

Lorenc, A., 2003. Modelling of error covariances by 4D-Var data assimilation. Q. J. R. Meteorol. Soc. 129 (595), 3167–3182.

Lorenc, A., Ballard, S., Bell, R., Ingleby, N., Andrews, P., Barker, D., Bray, J., Clayton, A., Dalby, T., Li, D., et al., 2000. The Met. Office global three-dimensional variational data assimilation scheme. Q. J. R. Meteorol. Soc. 126 (570), 2991–3012.

Mahfouf, J., Rabier, F., 2000. The ECMWF operational implementation of four-dimensional variational assimilation. II: Experimental results with improved physics. Q. J. R. Meteorol. Soc. 126 (564), 1171–1190.

McNally, A., 2002. A note on the occurrence of cloud in meteorologically sensitive areas and the implications for advanced infrared sounders. Q. J. R. Meteorol. Soc. 128 (585), 2551–2556.

McNally, A., 2009. The direct assimilation of cloud-affected satellite infrared radiances in the ECMWF 4D-Var. Q. J. R. Meteorol. Soc. 135 (642), 1214–1229.

Montmerle, T., Michel, Y., Ménétrier, B., 2010. Modelling of background error covariances for the analysis of clouds and precipitation. ECMWF-JCSDA Workshop on Assimilating Satellite Observations of Clouds and Precipitation, 15-17 June 2010, Available from: ECMWF, Shineld Park, Reading, Berks. RG2 9AX, UK, www.ecmwf.int.

Montmerle, T., Rabier, F., Fischer, C., 2007. Relative impact of polar-orbiting and geostationary satellite radiances in the Aladin/France numerical weather prediction system. Q. J. R. Meteorol. Soc. 133, 655–671.

Munro, R., Köpken, C., Kelly, G., Thépaut, J.-N., Saunders, R., 2004. Assimilation of Meteosat radiances data within the 4D-Var system at ECMWF: Data quality monitoring, bias correction and single-cycle experiments. Q. J. R. Meteorol. Soc. 130, 2293–2313.

Noilhan, J., Mahfouf, J., 1996. The ISBA land surface parameterisation scheme. Global and Planetary Change 13, 145–159.

Pangaud, T., Fourrie, N., Guidard, V., Dahoui, M., Rabier, F., 2009. Assimilation of AIRS Radiances Affected by Mid-to Low-Level Clouds. Mon. Weather Rev. 137 (12), 4276–4292.

Parrish, D., Derber, J., 1992. The National Meteorological Center's spectral statistical-interpolation analysis system. Mon. Weather Rev. 120, 1747–1763.

Pavelin, E., English, S., Eyre, J., 2008. The assimilation of cloud-affected infrared satellite radiances for numerical weather prediction. Q. J. R. Meteorol. Soc. 134 (632), 737–749.

Petty, G., 2004. A first course in atmospheric radiation. Sun Dog Books.

Rabier, F., Järvinen, H., Klinker, E., Mahfouf, J., Simmons, A., 2000. The ECMWF operational implementation of four-dimensional variational assimilation. I: Experimental results with simplified physics. Q. J. R. Meteorol. Soc. 126 (564), 1143–1170.

Rasch, P., Kristjánsson, J., 1998. A comparison of the CCM3 model climate using diagnosed and predicted condensate parameterizations. J. Climate 11 (7), 1587–1614.

Rawlins, F., Ballard, S., Bovis, K., Clayton, A., Li, D., Inverarity, G., Lorenc, A., Payne, T., 2007. The Met Office global four-dimensional variational data assimilation scheme. Q. J. R. Meteorol. Soc. 133 (623), 347–362.

Reuter, M., 2005. Identification of cloudy and clear sky areas in MSG SEVIRI images by analyzing spectral and temporal information, dissertation - Free University Berlin, available at: http://userpage.fu-berlin.de/geoiss/en/publications/dissertations.html.

Riishøjgaard, L., 1998. A direct way of specifying flow-dependent background error correlations for meteorological analysis systems. Tellus A 50 (1), 42–57.

Saunders, R., Brunel, P., 2005. RTTOV-8-5 Users Guide - Version 1.8. Eumetsat/ECMWF SAF Programme, Document ID NWPSAF-MO-UD-008. Available from: NWP SAF Helpdesk, Met Office, FitzRoy Road, Exeter, EX1 3PB, UK.

Saunders, R., Matricardi, M., Brunel, P., 1999. An improved fast radiative transfer model for assimilation of satellite radiance observations. Q. J. R. Meteorol. Soc. 125, 1407–1425.

Saunders, R., Matricardi, M., Brunel, P., English, S., Bauer, P., O'Keefe, U., Francis, P., Rayer, P., 2005. RTTOV-8 science and validation report. Eumetsat/ECMWF SAF Programme, Document ID NWPSAF-MO- TV-007. Available from: NWP SAF Helpdesk, Met Office, FitzRoy Road, Exeter, EX1 3PB, UK.

Savijärvi, H., 1990. Fast radiation parameterization schemes for mesoscale and short-range forecast models. J. Appl. Meteorol. 29 (6), 437–447.

Schmetz, J., Pili, P., Tjemkes, S., Just, D., Kerkmann, J., Rota, S., Ratier, A., 2002. An introduction to Meteosat Second Generation (MSG). Bull. Amer. Meteor. Soc. 83, 977–992.

Stengel, M., 2005. Fernerkundung atmosphärischen Wasserdampfes mit SEVIRI, Diploma thesis - Free University Berlin, available at: http://userpage.fu-berlin.de/geoiss/en/publications/theses.html.

Stengel, M., Lindskog, M., Undén, P., Gustafsson, N., Bennartz, R., 2010. An extended observation operator in HIRLAM 4D-VAR for the assimilation of cloud-affected satellite radiances. Q. J. R. Meteorol. Soc. 136 (649), 1064–1074.

Stengel, M., Undén, P., Lindskog, M., Dahlgren, P., Gustafsson, N., Bennartz, R., OCT 2009. Assimilation of SEVIRI infrared radiances with HIRLAM 4D-Var. Q. J. R. Meteorol. Soc. 135 (645, Part B Sp. Iss. SI), 2100–2109.

Szyndel, M. D. E., Kelly, G., Thépaut, J.-N., 2005. Evaluation of potential benefit of assimilation of SEVIRI water vapour radiance data from Meteosat-8 into global numerical weather prediction analyses. Atmos. Sci. Let. 6, 105–111.

Takeuchi, Y., Tsuyuki, T., 2002. The operational 3D-Var assimilation system of JMA for the Global Spectrum Model and the Typhoon Model. CAS/JSC WGNE Research Activities in Atmospheric and Oceanic Modelling 32, 0159–0160.

Tompkins, A., Janisková, M., 2004. A cloud scheme for data assimilation: Description and initial tests. Q. J. R. Meteorol. Soc. 130 (602), 2495–2517.

Undén, P., Rontu, L., Jarvinen, H., Lynch, P., Calvo, J., 2002a. HIRLAM-5 scientific documentation. SMHI Norrkoping, Sweden.

Undén, P., Rontu, L., Järvinen, H., Lynch, P., Calvo, J., Cats, G., Cuxart, J., Eerola, K., Fortelius, C., Garcia-Moya, J., et al., 2002b. HIRLAM-5 Scientific Documentation, HIRLAM-5 Project. Tech. rep., Available from: SMHI, S-601767 Norrkoping, Sweden.

Wyser, K., 1998. The effective radius in ice clouds. Journal of Climate 11 (7), 1793–1802.

Zou, X., Liu, H., Derber, J., Sela, J., Treadon, R., Navon, I., Wang, B., 2001. Four-dimensional variational data assimilation with a diabatic version of the NCEP global spectral model: System development and preliminary results. Q. J. R. Meteorol. Soc. 127 (573), 1095–1122.

List of Figures

List of Tables

Acknowledgements

This work has been made possible by the scientific help and support of numerous people.

First of all I would like to thank Prof. Dr. Jürgen Fischer for the opportunity to research on this exciting topic and to include the major scientific results and findings in this dissertation. Prof. Fischer and his colleagues at the Institute for Space Sciences create an unique working environment, which is always characterized by scientific expertise and support, and the possibility for personal and professional growth.

Further, I thank very much the current and former staff of the Meteorological Analysis and Prediction unit of the Swedish Meteorological and Hydrological Institute (SMHI) in Norrköping, Sweden, in particular Per Undén (head of section), Magnus Lindskog, Per Dahlgren and Nils Gustafsson. During my stay at SMHI, which was enabled by the financial support of the EUMETSAT Research Fellowship program, I was given freedom and support to exploit new scientific fields and approaches, always accompanied by countless fruitful discussions. The findings of this work were published in articles in international journals and build the core of this dissertation.

Many parts of this work were also accompanied by feedback, suggestions and advice of Prof. Dr. Ralf Bennartz (University of Wisconsin, Madison, Wisconsin).

However, my biggest thanks go to my parents Elke and Uwe Stengel. Their support during my studies of meteorology, my stays in the USA and Sweden, and during the preparation of this thesis is deeply appreciated.

Curriculum Vitae

For reasons of data protection,
the curriculum vitae is not included in the online version

For reasons of data protection,
the curriculum vitae is not included in the online version

For reasons of data protection,
the curriculum vitae is not included in the online version